

**Diego Rodrigo Villafani Caballero**

**Embedded OTDR Monitoring  
Systems for Next Generation  
Optical Access Networks**

**TESE DE DOUTORADO**

**DEPARTAMENTO DE ENGENHARIA ELÉTRICA**  
Programa de Pós-graduação em  
Engenharia Elétrica



**Diego Rodrigo Villafani Caballero**

**Embedded OTDR Monitoring Systems for  
Next Generation Optical Access Networks**

**Tese de Doutorado**

Thesis presented to the Programa de Pós-graduação em Engenharia Elétrica of PUC-Rio in partial fulfillment of the requirements for the degree of Doutor em Engenharia Elétrica.

Advisor: Prof. Jean Pierre von der Weid

Rio de Janeiro  
September 2017



**Diego Rodrigo Villafani Caballero**

**Embedded OTDR Monitoring Systems for  
Next Generation Optical Access Networks**

Thesis presented to the Programa de Pós-graduação em Engenharia Elétrica of PUC-Rio in partial fulfillment of the requirements for the degree of Doutor em Engenharia Elétrica. Approved by the undersigned Examination Committee.

**Prof. Jean Pierre von der Weid**

Advisor

Departamento de Engenharia Elétrica – PUC-Rio

**Prof. Guilherme Penello Temporão**

Centro de Estudos em Telecomunicações – PUC-Rio

**Prof. Luis Ernesto Ynoquio Herrera**

Centro de Estudos em Telecomunicações – PUC-Rio

**Prof. Andrew Henry Cordes**

Centro de Estudos em Telecomunicações – PUC-Rio

**Prof. Rogerio Passy**

MLS Wireless

**Prof. Ricardo Marques Ribeiro**

UFF

**Prof. Giancarlo Vilela de Faria**

Ouro Negro SA

**Prof. Márcio da Silveira Carvalho**

Vice Dean of Graduate Studies

Centro Técnico Científico – PUC-Rio

Rio de Janeiro, September the 1st, 2017

All rights reserved.

### **Diego Rodrigo Villafani Caballero**

Diego Rodrigo Villafani Caballero was born in Sucre, Bolivia, in 1989. He graduated from the Bolivian Catholic University, in Telecommunications Engineering in 2010. Later, he received his MSc. degree in Electrical Engineering from the Pontifical Catholic University of Rio de Janeiro in 2013. His present areas of interest are Optical Communications, Optical access Networks, Radio over Fibre systems and 5G transport. He is a member and an active participant of the Optoelectronics Laboratory at PUC-Rio.

Bibliographic data

Villafani Caballero, D. R.

Embedded OTDR Monitoring Systems for Next Generation Optical Access Networks / Diego Rodrigo Villafani Caballero; advisor: Jean Pierre von der Weid. – Rio de Janeiro: PUC-Rio, Departamento de Engenharia Elétrica, 2017.

v., 87 f: il. color. ; 30 cm

Tese (doutorado) - Pontifícia Universidade Católica do Rio de Janeiro, Departamento de Engenharia Elétrica.

Inclui bibliografia

1. Engenharia Elétrica – Teses. 2. Engenharia de Telecomunicações – Teses. 3. Reflectômetro óptico no domínio do tempo;. 4. Monitoramento de fibra óptica;. 5. Multiplexação de subportadora;. 6. Rádio sobre fibra;. 7. Redes ópticas passivas;. 8. Multiplexação por divisão de comprimento de onda;. 9. OTDR incorporado;. 10. Redes de acesso de nova geração;. 11. Fronthaul móvel;. 12. Redes de Transporte 5G;. 13. Monitoramento da camada física..

I. von der Weid, J. P.. II. Pontifícia Universidade Católica do Rio de Janeiro. Departamento de Engenharia Elétrica. III. Título.

CDD: 620.11

To my parents, Jaime Villafani and Lourdes Caballero, for their love, support  
and encouragement.

## Acknowledgments

I would like to thank my mentor Prof. Jean Pierre von der Weid for his guidance, encouragement and leadership. He is an exceptional adviser who helped me to shape my life as an Engineer.

To my advisors at The Royal Institute of Technology in Stockholm, Sweden. Prof. Lena Wosinska and Prof. Jiajia Chen, thank you for the opportunity and guidance during my time at KTH.

To Dr. Patryk Urban, for the discussions, guidance and friendship during my time at Ericsson Research and onward.

To my friend and colleague Dr. Luis Ynoquio for the constant discussions related to optical communications and optoelectronics.

To all the professors and employees of PUC-Rio for their coaching and support.

To my girlfriend, friends and family for their encouragement and support.

To CNPq, PUC-Rio and Ericsson Telecomunicações S.A., for their financial support.

## Abstract

Villafani Caballero, Diego Rodrigo; von der Weid, Jean Pierre (Advisor). **Embedded OTDR Monitoring Systems for Next Generation Optical Access Networks**. Rio de Janeiro, 2017. 87p. Tese de Doutorado – Departamento de Engenharia Elétrica, Pontifícia Universidade Católica do Rio de Janeiro.

In order to support the requirements for 5th generation mobile networks (5G), optical communication systems will be used in the access part of the network. This is because the evolution of radio access networks includes the centralization of the most critical equipment in order to deploy low power mobile access points, like distributed antenna systems and small cells. The emerging services call for the deployment of radio over fibre technologies with emphasis on bandwidth efficiency, energy efficiency and high reliability. Within this scope, an efficient monitoring of the physical layer would become essential for the operation of these networks. The monitoring system should provide in-service, cost efficient and centralized fault localization with minimum impact on data transmission. This thesis proposes several transceiver-embedded optical time domain reflectometry monitoring systems. The monitoring systems are tested over different data transmission systems and network architectures, where one architecture was simulated and several others experimentally validated.

## Keywords

Optical Time Domain Reflectometer; Optical Fibre Monitoring; Sub-carrier Multiplexing; Radio over Fibre; Passive Optical Networks; Wavelength Division Multiplexing; Embedded OTDR; Next Generation Optical Access Networks; Mobile Fronthaul; 5G Transport Networks; Physical Layer Monitoring.

## Resumo

Villafani Caballero, Diego Rodrigo; von der Weid, Jean Pierre. **Sistemas Integrados de Monitoramento por OTDR para Redes de Acesso Óptico de Próxima Geração**. Rio de Janeiro, 2017. 87p. Tese de Doutorado – Departamento de Engenharia Elétrica, Pontifícia Universidade Católica do Rio de Janeiro.

Para suportar os requisitos das redes móveis de 5a geração (5G), os sistemas de comunicação óptica serão usados nas redes de acesso. Isso ocorre porque a evolução das RAN (*Radio Access Networks*) incluem a centralização do equipamento mais crítico para implantar pontos de acesso móveis de baixa potência, como DAS (*Distributed Antenna Systems*) e *Small Cells*. Os serviços emergentes solicitam a implantação de tecnologias de rádio sobre fibra com ênfase na eficiência de largura de banda, eficiência energética e alta confiabilidade. Neste âmbito, um monitoramento eficiente da camada física é imperativo para a operação dessas redes. O sistema de monitoramento deve fornecer uma localização de falhas em serviço, econômico, centralizado e com impacto mínimo para a transmissão de dados. Esta tese propõe vários sistemas de monitoramento incorporado no transceptor utilizando reflectometria óptica no domínio do tempo. Os sistemas de monitoramento são testados em diferentes sistemas de transmissão de dados e arquiteturas de rede, onde é apresentada uma validação simulada e outras experimentais.

## Palavras-chave

Reflectômetro óptico no domínio do tempo; Monitoramento de fibra óptica; Multiplexação de subportadora; Rádio sobre fibra; Redes ópticas passivas; Multiplexação por divisão de comprimento de onda; OTDR incorporado; Redes de acesso de nova geração; Fronthaul móvel; Redes de Transporte 5G; Monitoramento da camada física.

## Table of contents

1	Background and Introduction	16
2	Optical Access Networks	19
2.1	Passive Optical Networks (PON)	19
2.1.1	TDM-PON	20
2.1.2	WDM-PON	21
2.1.3	Hybrid-PON (HPON)	22
3	Radio over Fibre	24
3.1	Digital Radio over Fibre	26
3.2	Analogue Radio over Fibre	28
3.3	Subcarrier Multiplexing	29
4	Optical Fibre Monitoring Systems	32
4.1	Optical Time Domain Reflectometer	32
4.1.1	OTDR fundamentals	32
4.1.2	Performance Parameters	34
4.1.2.1	Measurement Range.	34
4.1.2.2	Dynamic Range.	34
4.1.2.3	Dead Zones.	35
4.1.2.4	Spatial Resolution.	36
4.1.2.5	Tradeoff Between Dynamic Range and Resolution.	36
4.1.3	Monitoring Systems in Optical Access Networks	37
4.1.3.1	Monitoring Techniques for WDM-PON.	38
4.1.3.2	Embedded Monitoring Techniques.	39
5	Simulation of a SCM/WDM-PON with in-service baseband embedded OTDR monitoring	41
5.1	VPI Simulator	41
5.2	Proposed System	43
5.3	Simulation results	44
5.4	Dynamic Range Estimation	50
6	Experimental Demonstrations	52
6.1	Baseband Embedded OTDR with Baseband Data Signals	52
6.2	Baseband Embedded OTDR with Subcarrier Multiplexed ASK Digital Signal	55
6.2.1	Fibre Monitoring Results and Impact on Data Transmission	56
6.3	Baseband Embedded OTDR with Subcarrier Multiplexed LTE Signal	59
6.3.1	Fibre Monitoring Results and Impact on Data Transmission	60
6.4	Baseband Embedded OTDR with Subcarrier Multiplexing LTE-A Signal, Electrical Combination and Direct Modulation	63
6.4.1	Fibre Monitoring Results and Impact on Data Transmission	65

6.5	Embedded Multiplexed AMCC and OTDR signal for Analogue Radio over Fibre Systems	67
6.5.1	Fibre Monitoring Results and Impact on Data Transmission	70
7	Conclusions	76
	Bibliography	79

## List of figures

Figure 2.1	TDM-PON basic architecture.	20
Figure 2.2	WDM-PON basic architecture.	21
Figure 2.3	TWDM-PON basic architecture.	22
Figure 3.1	Distributed RAN and Centralized RAN.	24
Figure 3.2	Basic concept of a RoF system.	26
Figure 3.3	Digitalized RoF system.	27
Figure 3.4	Analogue RoF system.	28
Figure 3.5	Subcarrier Multiplexing in Radio over Fibre Systems.	30
Figure 4.1	Generic OTDR block diagram.	33
Figure 4.2	Typical OTDR trace with principal events [40] (Pg. 438).	34
Figure 4.3	Dynamic Range and Measurement Range [40] (Pg. 442).	35
Figure 4.4	Attenuation and Event Dead Zone [40] (Pg. 443).	36
Figure 4.5	Tradeoff between Dynamic Range and Resolution [40] (Pg. 445).	37
Figure 5.1	Universe, Galaxy and Star in VPI simulator.	42
Figure 5.2	(a) SCM/WDM-PON system. (b) OLT Setup with in-service baseband embedded OTDR monitoring and (c) ONU scheme.	43
Figure 5.3	Transmission Spectrum in the C-band.	45
Figure 5.4	MZM Power transfer function and modulation indexes.	46
Figure 5.5	SER vs ROP for different $m_{OTDR}$ with $m_{Signal}=0.3$ .	47
Figure 5.6	Power penalty for different $m_{OTDR}$ values at chosen SER levels.	48
Figure 5.7	(a) SER versus different $m_{OTDR}$ values for different pulse lengths and (b) OTDR peak pulse power versus different $m_{OTDR}$ values.	48
Figure 5.8	64QAM constellation for 100 ns, 200 ns pulse lengths with $m_{OTDR}=1.2$ and no OTDR.	49
Figure 6.1	Baseband Embedded OTDR with superimposed baseband data signal.	53
Figure 6.2	Normalized Transfer Function of the Amplitude Modulator.	53
Figure 6.3	OTDR Trace and BER with Superimposed signals.	54
Figure 6.4	Baseband Embedded OTDR with subcarrier multiplexed digital signal.	55
Figure 6.5	OTDR signal (Red) and Digital data signal (Black) received at the OFN PD.	56
Figure 6.6	OTDR trace with In-service monitoring in the baseband and subcarrier digital signal in 2 GHz.	57

Figure 6.7 Bit error rate for an ASK modulation signal at different received optical powers with and without link monitoring combined in the same polarization mode and orthogonal polarization mode.	58
Figure 6.8 Baseband Embedded OTDR with subcarrier multiplexing LTE signal.	59
Figure 6.9 OTDR and LTE frequency spectrum.	60
Figure 6.10 In-service embedded OTDR fault localization.	61
Figure 6.11 Noise Floor Comparison with in-service and offline monitoring.	61
Figure 6.12 Measured Error Vector Magnitude rms value for different Received Optical Powers with and without link supervision.	62
Figure 6.13 Effect of different optical combination schemes on the 64QAM OFN received signal constellation. a) Orthogonal polarization modes; b) Same polarization modes.	63
Figure 6.14 Experimental set-up and electrical frequency spectrum.	64
Figure 6.15 Measured EVM for QPSK, 16QAM and 64QAM under different system conditions. The data transmission power is set to a) -4 dBm and b) -8dBm. The required EVM percentages are shown for each modulation format.	65
Figure 6.16 OTDR traces for different OTDR peak currents and Transmission Powers. The data transmission power is set to a) -4 dBm and b) -8 dBm. In a), the higher transmission power forces a higher minimum ODTR peak current (200 mA) for the return pulse to be seen. In b) only 100 mA is required.	66
Figure 6.17 Offline BE-OTDR trace with induced loss and fault localization.	67
Figure 6.18 Embedded Multiplexed AMCC and OTDR signal for a-RoF.	68
Figure 6.19 Outputs of the FPGA. a) shows the output of port A, the AMCC 128 kbps signal, while b) shows the output of port B, the OTDR trigger pulses. Both plots are zoomed to the 17 ms gap between AMCC signals where the 15.88 ms of OTDR triggers reside.	69
Figure 6.20 AMCC Bit Error Rate measurement with different OTDR peak currents.	71
Figure 6.21 Error Vector Magnitude for different bias currents and OTDR peak currents.	71
Figure 6.22 Error Vector Magnitude for different bias currents with and without AMCC signal.	72
Figure 6.23 Different OTDR traces for different OTDR peak current pulses and different laser bias currents.	73
Figure 6.24 OTDR traces for a 4.3 dB induced loss.	74

## List of Abbreviations

10GEPON – 10 Gigabit Ethernet Passive Optical Network  
3GPP – Third Generation Partnership Project  
5G – 5th Generation Mobile Networks  
5G PPP – 5G Public Private Partnership  
64QAM – 64 Quadrature Amplitude Modulator  
A/D – Analogue to Digital  
ADC – Analogue to Digital Converter  
AM – Amplitude Modulator  
AMCC – Auxiliary Management and Control Channel  
APD – Avalanche Photodiode  
a-RoF – Analogue Radio over Fibre  
AWG – Arrayed Waveguide Grating  
BBU – Baseband Unit  
BER – Bit Error Rate  
BER-r – Bit Error Rate Receiver  
BER-t – Bit Error Rate Transmitter  
BPF – Band Pass Filter  
BS – Base Station  
BS – Beam Splitter  
BSG – Binary Signal Generator  
CA – Carrier Aggregation  
CAPEX – Capital Expenditure  
CNR – Carrier to Noise Ratio  
CO – Central Office  
CoMP – Coordinated Multi-Point  
CPRI – Common Public Radio Interface  
CRN – Coherent Rayleigh Noise  
CW – Constant Wave  
D/A – Digital to Analogue  
D2D – Device to Device  
DAC – Digital to Analogue Converter  
DAS – Distributed Antenna Systems  
DR – Dynamic Range

d-RoF – Digital Radio over Fibre  
DU – Digital Unit  
DWDM – Dense Wavelength Division Multiplexing  
EA – Electrical Amplifier  
EPG – Electrical Pulse Generator  
EPON – Ethernet Passive Optical Network  
EVM – Error Vector Magnitude  
FM – Frequency Modulation  
FPGA – Field Programmable Gate Array  
FSK – Frequency Shift Keying  
FUT – Fibre Under Test  
GEPON – Gigabit Ethernet Passive Optical Network  
GPON – Gigabit-capable Passive Optical Network  
HPF – High Pass Filter  
HPON – Hybrid Passive Optical Networks  
IEEE – Institute of Electrical and Electronics Engineers  
IF – Intermediate Frequency  
IFFT – Inverse Fast Fourier Transform  
IMT 2020 – International Mobile Telecommunications 2020  
IoT – Internet of Things  
ITU-T – International Telecommunication Union  
LD – Laser Diode  
LO – Local Oscillator  
LTE – Long Term Evolution  
LTE-A Long Term Evolution Advanced  
MFH – Mobile Fronthaul  
M-MIMO – Massive Multiple Input Multiple Output  
MZM – Mach-Zehnder Modulator  
NEP – Noise Equivalent Power  
NGOAN – Next Generation Optical Access Networks  
NG-PON2 – Next Generation Passive Optical Networks 2  
NRZ – Non Return to Zero  
OAM – Operation Administration Management  
OBSAI – Open Base Station Architecture Initiative  
OC – Optical Circulator  
ODN – Optical Distribution Network  
OFDM – Orthogonal Frequency Division Multiplexing  
OFDR – Optical Frequency Domain Reflectometry  
OFN – Optical Frontend Node

OLT – Optical Line Terminal  
ONT – Optical Network Terminal  
ONU – Optical Network Unit  
OPEX – Operational Expenditure  
OTDR – Optical Time Domain Reflectometry  
OTM – Optical Transceiver Monitoring  
PBS – Polarization Beam Splitter  
PD – Photodetector  
PON – Passive Optical Networks  
PRBS – Pseudo Random Binary Sequence  
PSK – Phase Shift Keying  
PtMP – Point to Multipoint  
PtP – Point to Point  
QAM – Quadrature Amplitude Modulation  
RAN – Radio Access Network  
RAT – Radio Access Technologies  
RAU – Radio Access Unit  
REP – Received Electrical Power  
RF – Radio Frequency  
RH – Radio Heads  
RIN – Relative Intensity Noise  
RMS – Root Mean Square  
RN – Remote Node  
RoF – Radio over Fibre  
ROP – Received Optical Power  
RPG – Rectangular Pulse Generator  
RRU – Remote Radio Unit  
RU – Radio Unit  
SCM – Subcarrier Multiplexing  
SCM-PON – Subcarrier Multiplexing Passive Optical Network  
SER – Symbol Error Rate  
SNR – Signal to Noise Ratio  
SOA – Semiconductor Optical Amplifier  
TDM – Time Division Multiplexing  
TDMA – Time Division Multiple Access  
TDM-PON – Time Division Multiplexing Passive Optical Network  
TIA – Transimpedance Amplifier  
TL-OTDR – Tunable Laser Optical Time Domain Reflectometer  
TLS – Tunable Laser Source

T-PC-OTDR – Tunable Photon Counting Optical Time Domain Reflectometer

TWDM – Time and Wavelength Division Multiplexing

VEA – Variable Electrical Attenuator

VOA – Variable Optical Attenuator

VSA – Vector Signal Analyzer

VSG – Vector Signal Generator

WDM – Wavelength Division Multiplexing

WDM-PON – Wavelength Division Multiplexing Passive Optical Network

XG-PON – 10 Gigabit-capable Passive Optical Network

xMBB – Extreme Mobile Broadband

# 1

## Background and Introduction

Advances in technology and a shift in human behaviour are driving and shaping the 5th Generation Mobile Networks (5G). People's need to use broadband communication services anytime and everywhere, in addition to the advent of new systems like the Internet of Things (IoT) are pushing the next big step of telecommunication networks to define a general consensus of what 5G should be able to achieve.

Even if no standards have been defined yet, many research forums and projects have been established worldwide with the aim of setting out a common definition, possible targets, and underlying technologies for 5G. Among the many forums and projects related to 5G networks are, the International Mobile Telecommunication 2020 (IMT 2020), the 5G Forum Korea, the 5G Public Private Partnership (5G PPP), the METIS and METIS II.

Recently, the METIS and METIS II projects, which are considered an official model of the European 5G networks [1], have defined a 5G system and concept that consists of three generic 5G services and four main enablers [2]. The idea of defining new generic services, and enablers for these services, brings different challenges to different segments of the network depending on the characteristics of each of them. For example, one of the services proposed, called Extreme Mobile BroadBand (xMBB), aims to provide low latency communication and data rates going to the range of Gbps to the final user. This service will be the main contributor to the challenges of the access and transport network segments. Within this scope, different service enablers, such as the Dynamic Radio Access Network (Dynamic RAN) are proposed. Furthermore, these new enablers will need to use different technologies, like Device to Device communication (D2D), in order to provide local traffic offloading and not saturate the core network [3].

The RAN architecture is directly related to the transport and access connections between the different mobile access points, that can be macro or small-cells and the aggregation and core networks. In this case, considering the large amounts of bandwidth demanded in 5G ( $\sim 800$  MHz), optical fibre communication systems are undoubtedly great candidates to support the requirements of 5G in the access networks [4].

As a proposed solution, Passive Optical Network (PON) architectures are currently the best candidates to form the Optical Distribution Network (ODN) and have received a lot of attention from research and industry groups. Within this scope, Wavelength Division Multiplexing Passive Optical Networks (WDM-PON) are reliable candidates to provide scalability, energy efficiency and high data rates to the network [5]. Therefore, chapter 2 of this thesis describes the concept of PON and the different combinations and standardizations of these architectures including WDM-PON.

The RAN architecture, mentioned before, should provide solutions to the transportation of different Radio Access Technologies (RAT) to the core or aggregation part of the network. Within this scope, the concept of Centralized RAN has been considered for deployment in different test cases, e.g. in dense urban areas where several RAT can share the Central Office (CO) and the ODN. This concept has proven to reduce the Operational Expenditure (OPEX) costs and energy consumption of the network. Furthermore, different technologies can be used over Centralized RANs. The two main technologies can be classified as Analogue Radio over Fibre (a-RoF) and Digital Radio over Fibre (d-RoF). Hence, chapter 3 of this thesis presents the different motivations for using the Centralized RAN concept and later presents a review of RoF technologies, where we focus attention on the main differences, strengths and weaknesses, between d-RoF and a-RoF.

The operation of an optical access network with high reliability, stability and cost efficiency is becoming a big challenge. This is because a single feeder fibre can carry several wavelengths as in the case of WDM-PON. Within this scope, one of the essential aspects of the operation of these networks is the physical layer monitoring, which should provide in-service, detailed and rapid evaluation of the ODN, while imposing minor additional costs and preserving high data signal quality. Therefore, chapter 4 lays out the different optical access monitoring systems, where Optical Time Domain Reflectometry (OTDR) is the main focus. Later, the chapter provides an overview of different monitoring systems applied to WDM-PON. Furthermore, embedded monitoring systems are presented and discussed.

Chapters 5 and 6 show the main results and contributions of the thesis. In chapter 5, an a-RoF system and a WDM-PON architecture with in-service Baseband Embedded OTDR monitoring is proposed and simulated. The performance of the proposed system is investigated and the results will be shown to verify the feasibility. Moreover, the results show, that with proper configuration, the in-service baseband monitoring signals have negligible impact on data transmission. All the work performed in chapter 5

is validated by using the VPI Photonics simulation software.

Chapter 6 describes the experimental validation of the systems, where several configurations are proposed and demonstrated in the laboratory. Here, we perform experimental demonstrations of subcarrier multiplexing-PON (SCM-PON) systems with Baseband Embedded OTDR monitoring. The impact of the monitoring systems over the transmitted data is measured for different formats and configurations. Moreover, the performance of the monitoring system is measured, and the results are shown to be efficient in fault detection and in-service monitoring.

Chapter 7 presents the conclusions of this thesis.

Optical transmission technologies are able to provide high data rates over long distances in an energy-efficient way. As a consequence, fibre-based solutions are seen as worthy and long term candidates for 5G transport networks [5]. Taking into account that 5G will combine the use of different Radio Access Technologies (RAT), Massive Multiple Input Multiple Output (M-MIMO) systems, and ultra-dense deployments of small cells [6], different optical architectures will be needed to enable a cost-efficient, energy-efficient and outstanding transportation of radio signals in different scenarios. Within this scope, the use of Passive Optical Network (PON) architectures combined with different multiplexing techniques such as Wavelength Division Multiplexing (WDM), Time Division Multiplexing (TDM) and Subcarrier Multiplexing (SCM) will be the main enablers to create a cost-efficient Optical Distribution Network (ODN). This chapter presents an overview of optical access networks that can be used in the transportation between different types of access points and the core/aggregation part of the network.

## 2.1

### **Passive Optical Networks (PON)**

Passive Optical Networks are promising candidates for the optical access networks due to their simplicity, transparency and low power consumption. PON solutions do not use any active elements in the ODN to regenerate, amplify or distribute the optical signal, therefore, they are optically transparent to any protocol. The system is based on a Point-to-Multipoint (PtMP) architecture, where the Central Office (CO) contains one or more Optical Line Terminals (OLT) and is connected to a Remote Node (RN) by means of a feeder fibre. In the RN, a passive element distributes the optical signal to different distribution fibres that are connected to the Optical Network Units (ONU) or Optical Network Terminals (ONT). ONT is an International Telecommunication Union (ITU-T) term that describes a single-tenant ONU connected and served by the distribution fibre. In the case of multiple-tenant units, the ONU may distribute the services to the individual units, using technologies like Ethernet over twisted pair or others. In this thesis the terms are used

interchangeably.

PONs can be divided into several subclasses, according to the end-to-end transmission protocol and the multiple access techniques used for sharing the common resources (e.g. the feeder fibre). The next subsections present an overview of the different PON subclasses.

### 2.1.1 TDM-PON

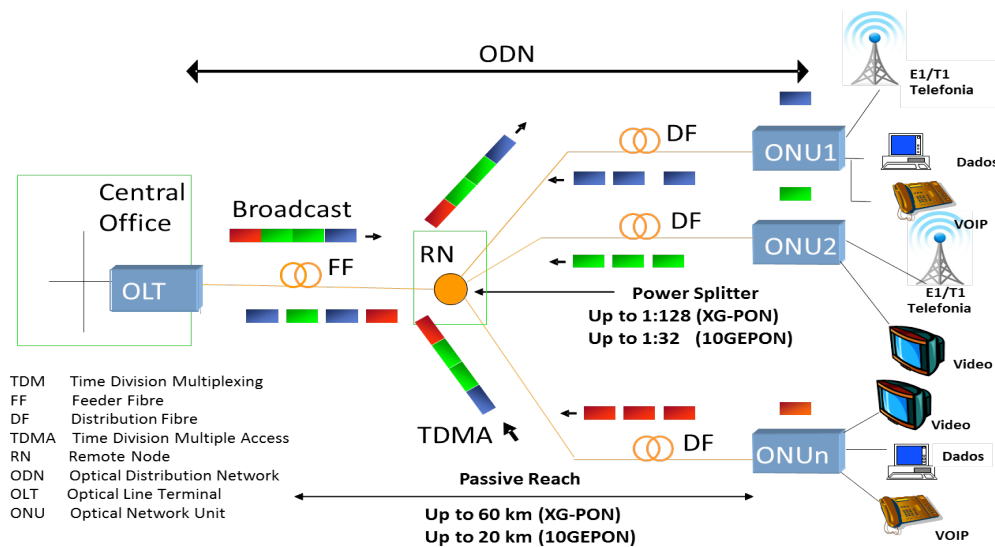


Figure 2.1: TDM-PON basic architecture.

Figure 2.1 shows the basic architecture of a TDM-PON. This technique uses Time Division Multiple Access (TDMA) to multiplex the signals in the upstream and downstream directions. In the downstream direction the data is broadcasted to all ONUs using one or more power splitters at the ODN. In the upstream direction the data is sent by each ONU in a pre-defined time-slot, which needs to be coordinated by the protocol of the system to avoid collisions. Two standard groups, the ITU-T and the Institute of Electrical and Electronics Engineers (IEEE), developed different standards with different industry organizations. The two standards using TDMA are the Gigabit-capable PON (GPON) developed by the ITU [7] and the Ethernet PON (EPON or GEAPON) developed by the IEEE [8]. Both of them have several similarities in terms of the optical infrastructure, but are very different in execution and protocol management. GPON is mostly deployed in North America and some

parts of Europe, while Asia-Pacific countries like Japan and China have mostly deployed GEAPON/EPON systems [9].

The difficulty with TDM-PON is that the downstream bit rate is shared among all the ONUs. For example, if the bit rate in a GPON network is 2.5 Gbps, and it is shared among 32 users, as in the standard, the bit rate per user will be around 80 Mbps. An extension of the standards improves the maximum bit rate in XG-PON [10] and 10GEAPON [11] to 10 Gbps in the downstream direction. The split ratios are also improved to 1:128 and 1:32 users respectively.

### 2.1.2 WDM-PON

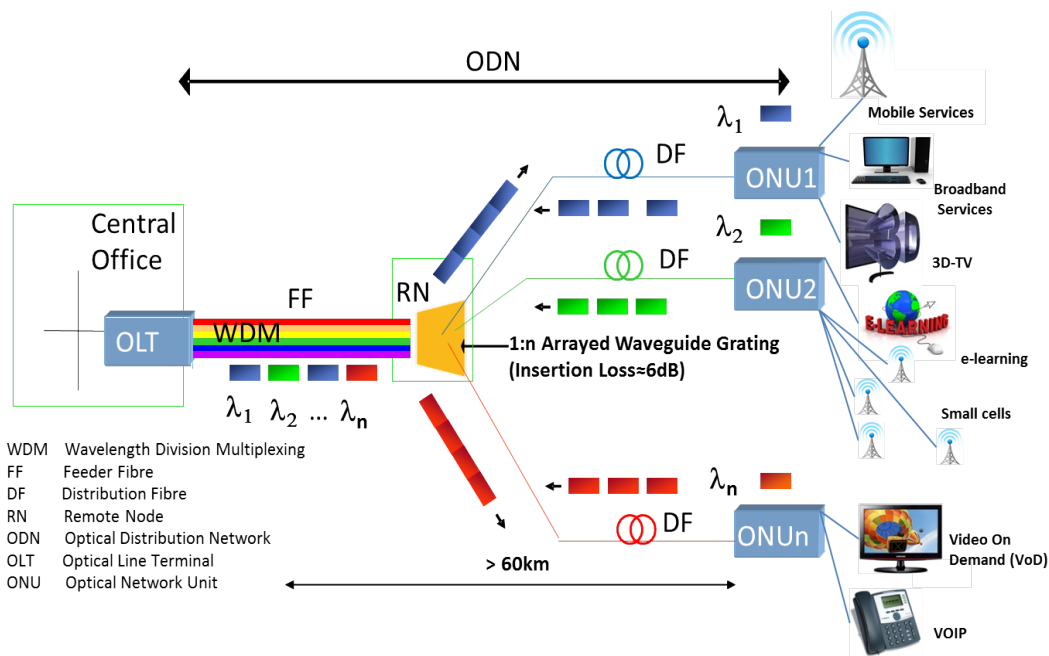


Figure 2.2: WDM-PON basic architecture.

Figure 2.2 shows the basic architecture of a WDM-PON. It uses either power splitters or wavelength multiplexers/demultiplexers (e.g. Arrayed Waveguide Grating, AWG) in the RN. In the case of using a power splitter, the insertion loss of the equipment increases depending on the splitting ratio (e.g. 1:8 ~9db; 1:32 ~15dB). In contrast, an AWG has a much lower insertion loss (e.g. 1:32 ~6dB), providing an increase of the passive reach of the network. In WDM-PON, each ONU is served by a specific wavelength. Therefore, it is possible to provide an individual bit rate for each ONU. Moreover, the security can be improved in comparison to TDM-PON because all the optical signal is not broadcasted to all the ONUs. WDM-PON has a Point-to-Point (PtP)

connection in the wavelength perspective, whereas the fibre topology is still PtMP. In the case of a power splitter, each ONU needs to be equipped with an optical filter (fixed or tuneable) in order to select their own dedicated wavelength. This second type of system is called "broadcast and select WDM-PON" and loses the security characteristic of typical WDM-PON system.

WDM-PON is limited by the number of available wavelengths that can be transmitted through the fibre. Specifically, the number of channels depends on the channel spacing, e.g. 100 GHz channel spacing has 40 channels in the 4 THz C band, hence it could be improved by reducing the channel spacing. The ITU-T standard G.694.1 provides a frequency grid for Dense WDM (DWDM) applications that varies the channel spacing from 12.5 GHz to 100 GHz [12]. This architecture is one of the strong candidates for the next generation optical access networks because of the scalability and high bit rate capacity [13].

### 2.1.3 Hybrid-PON (HPON)

PUC-Rio - Certificação Digital Nº 1321989/CA

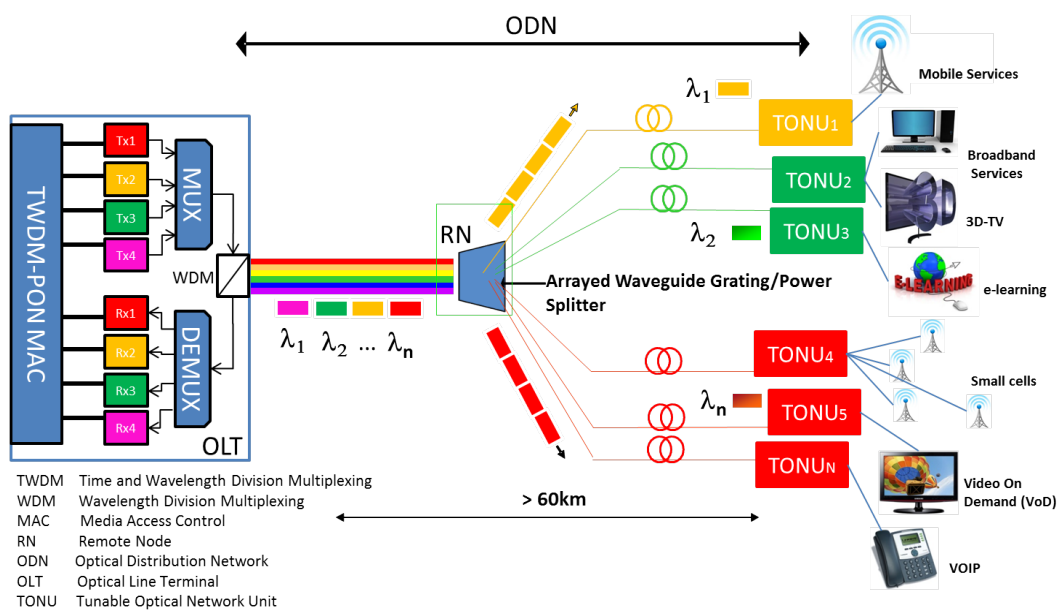


Figure 2.3: TWDM-PON basic architecture.

Hybrid PON (HPON) is the mixture of two or more multiplexing techniques, and it is not limited to the above mentioned ones. There are several other multiplexing technologies that can be used in HPONs, such as Orthogonal Frequency Division Multiplexing (OFDM) and Subcarrier Multiplexing (SCM). The use of two or more multiplexing technologies makes it possible to come up with a more powerful network architecture, needed in order to

meet the requirements of the next generation optical access networks. For example, the combination of TDM and WDM-PON technologies brings benefits such as scalability, flexibility, and maximum bit rate per user as shown in the following. The ITU-T recommendation G.989 [14], that describes the general requirements for Next Generation Passive Optical Networks 2 (NG-PON2), combines the use of Time and Wavelength Division Multiplexing (TWDM) in order to achieve at least 40 Gbps of aggregated capacity per feeder fibre and split ratios of at least 1:256. In addition, this recommendation gives examples of different services offered in the TWDM-PON, such as enterprise connectivity and mobile backhauling of Radio Frequency (RF) signals. Figure 2.3 shows a basic H-PON architecture using TWDM-PON.

With respect to mobile backhauling, using protocols like the Common Public Radio Interface (CPRI) is the most common practice nowadays. This protocol uses Analogue to Digital and Digital to Analogue Converters (ADC/DAC) to transport the RF signal in a digitalized form. It supports bit rates up to 9.83 Gbps between the Baseband Unit (BBU) and Remote Radio Unit (RRU), reaching the requirements of 4G systems, but in order to achieve the requirements of 5G, higher bit rates and/or other technologies like Analogue Radio over Fibre (a-RoF) will be needed.

For the purpose of transporting the different RF signals from the access point to the core network, the idea of using a PON is of great interest, since the architecture will bring savings in terms of Capital Expenditure (CAPEX) and Operational Expenditure (OPEX) [15]. In the case of mobile back/front-hauling, the optical access network architecture can also be shared with other types of services offered to the residential and business customers, such as broadband internet. In this case, Base Stations (BS) are located in the ONUs where the antennas are co-located. The technologies used to transport RF signals over optical fibres are known as Radio over Fibre (RoF) and they are studied in chapter 3.

### 3 Radio over Fibre

The use of optical fibre links to transmit Radio Frequency (RF) signals was first demonstrated in 1984 [16]. However, the optical equipment and infrastructure were overly expensive for their deployment at that time. Nowadays, different companies offers an assortment of cost effective products and methods for cellular coverage applications using optical fibre links [17, 18]. These services and products are installed in different scenarios such as inside buildings, public places and dense urban areas and achieve the required performance with acceptable costs. The savings in costs originate from the centralizing of the RF equipment in a Central Office (CO) that reduces the equipment in the Radio Unit (RU) sites. This chapter first describes the motivation of centralized Radio Access Networks (RANs), later continues with focus on the concept of Analogue Radio over Fibre (a-RoF) systems, as well as its differences with the more common Digital Radio over Fibre (d-RoF) system.

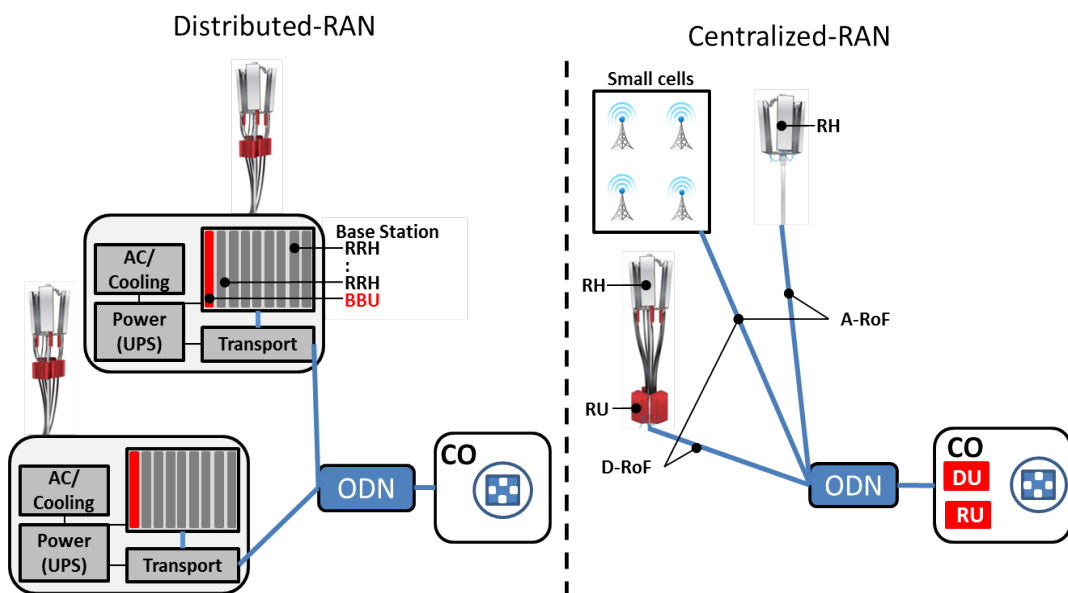


Figure 3.1: Distributed RAN and Centralized RAN.

The idea of using centralized processing in RANs instead of distributed RANs, as shown in Fig. 3.1, is of great interest in the deployment of 5G net-

works. This is due to three important drivers; network operational advantages, reduction of energy consumption and radio performance [19].

The first driver comes from the network operational teams, who recognize Centralized RAN as a site engineering solution to increased roll-out difficulties, especially in dense urban areas. Indeed, as the Digital Unit (DU) and sometimes the RU are moved to a CO, only the RUs and Radio Heads (RH) are left on the antenna site, reducing the installation footprint. The separation of the RU depends on the RoF system that is used (d-RoF or a-RoF). These aspects are expected to bring cost benefits apart from time savings in installation and repair. Moreover, adding new Radio Access Technologies (RATs) and small cells to the big picture, this deployment becomes of great interest for network operators and service providers.

A second driver is the reduction of energy consumption, made possible by the Centralized RAN. A detailed analysis is provided in [20], based on existing infrastructures with already available RAN equipment. The analysis demonstrates that 40-50 percent of energy savings can be achieved with respect to traditional macro cell installation with backhaul. The biggest gains come from an RU installation close to the antenna, that avoids power dissipation in coaxial feeders. Furthermore, the fact that cooling or air conditioning is no longer needed at the antenna site further reduces the energy consumption. Even higher power savings should come with phase two of Centralized RAN deployments, where DU pools will be capable of dynamically allocating processing resources according to the traffic load.

A third driver is related to radio performance. Very low latency between DUs enables better performance in handling mobility and improved uplink coverage. Furthermore, the Centralized RAN architecture enables the implementation of Coordinated Multi-Point (CoMP). This Long Term Evolution Advanced (LTE-A) feature is expected to provide higher capacity and improved cell-edge performance, due to coordination between adjacent cells. Then, in the case of heterogeneous networks, including macro and small cells, the sharing of the DU between small cells and parent macro cell (in the same coverage area) will allow better interference management.

As the Distributed RAN moves towards pooling of resources, enabling technologies should be capable of transporting the RF signals from the CO to the remote locations without degradation of the data signal and with minimal cost. Within this scope, RoF systems are the best candidates to be used. The fundamental concept of RoF systems is that they comprises the transport of analogue radio signals through an optical fibre link, and also that the radio signals are not affected by frequency interference from the proximate

radiocommunication signals [21]. Figure 3.2 shows the basic concept of a RoF system.

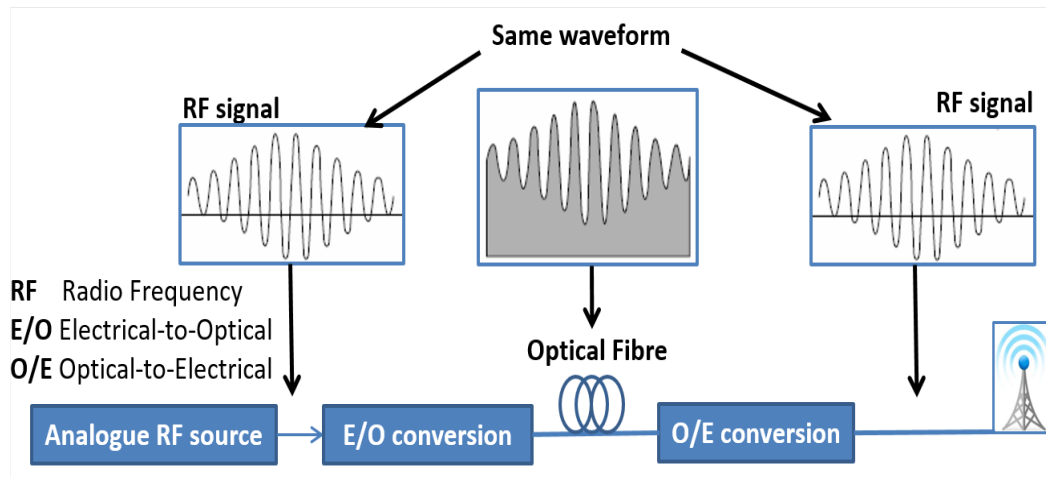


Figure 3.2: Basic concept of a RoF system.

From a technical point of view, the transportation of the RF signals over the fibre link can be done in several ways and the different methods have been proposed and studied in the literature [22, 23, 24]. The two main categories in which RoF technology can be classified are Digital RoF and Analogue RoF.

### 3.1 Digital Radio over Fibre

Digital RoF, as its name implies, is a method for transporting RF signals in a digitalized form. Figure 3.3 illustrates the general and fundamental architecture for transmitting digital radio signals.

The digital RF source illustrated in Fig. 3.3 can comprise three different schemes. In the first and second schemes, an Analogue-to-Digital (A/D) conversion is necessary inside this block, since the RF signal waveform is sampled and digitized. The difference between the first and second cases is that, in the first one, the RF waveform is sampled in an Intermediate Frequency (IF), downconverting the original frequency band to a lower frequency, which reduces the bandwidth and speed requirements of the digitizers. However, in this case, additional RF equipment is required in the remote unit for upconversion of the RF signal. In the second case, the RF waveform is sampled in the original frequency band, which requires the use of high-speed A/D converters, but reduces the equipment at the remote unit since the upconversion is not necessary. In the third scheme, the A/D conversion is avoided, since the digitized data is obtained from the Inverse Fast Fourier Transform (IFFT), of

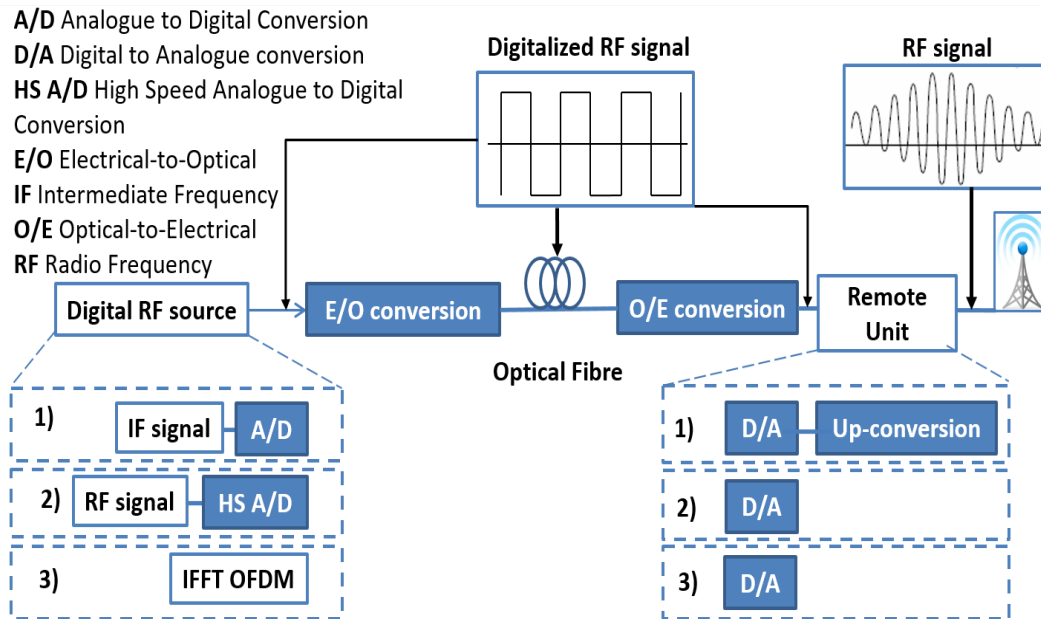


Figure 3.3: Digitalized RoF system.

the Orthogonal Frequency Division Multiplexing (OFDM) modulation, which directly provides the time-domain samples [25].

Although there has been some improvement in A/D conversion with, for example, the bandpass sampling method [26, 27], the issue with d-RoF is still the high bit rate generated after the digitalization. For example, for a 40 MHz bandwidth wireless signal, we might expect a sampling rate of 100 MHz (perhaps more, for an oversampled system), which for 10-bits per sample (perhaps required for higher-level QAM and OFDM) would result in a bit rate of at least 1 Gbps [25]. On the other hand, several research groups have demonstrated, that the d-RoF system is more robust against physical layer impairments from the optical link, while the performance of a-RoF is subject to optical channel conditions [24, 30, 31].

To conclude, at the cost of significantly increased bandwidth and the addition of high-speed A/D and D/A converters, the digital RF/IF-over-Fibre approach provides a defined level of immunity to the Signal to Noise Ratio (SNR) degradation inherent in the purely a-RoF approaches. A digitized approach, using Centralized RAN and remote radio heads, is being adopted for WiMAX and 3GPP/LTE wireless systems in industry standards such as the Common Public Radio Interface (CPRI) and the Open Base Station Architecture Initiative (OBSAI) [28, 29]. However future radio access technologies in 5G transport and access networks are looking for new standardization alternatives [1].

### 3.2

#### Analogue Radio over Fibre

Analogue RoF is probably the most straightforward radio signal distribution technology because the wireless signals modulate the optical carrier directly, without the necessity of any A/D conversion or upper layer intervention. Furthermore, the signal can be directly transmitted to the remote antenna, where it is filtered, amplified and distributed. Two different configurations of a-RoF are typically seen in the literature, RF over fibre and IF over fibre. Figure 3.4 shows the basic configuration of an a-RoF systems.

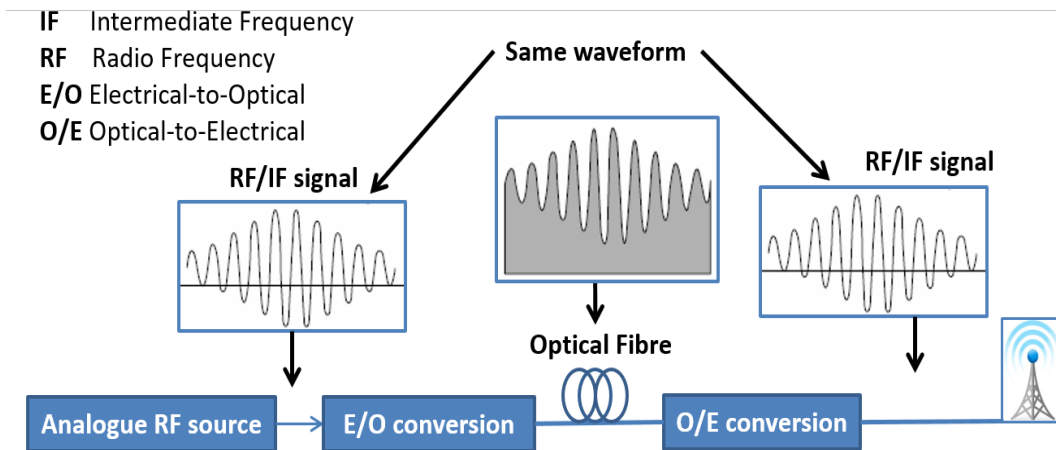


Figure 3.4: Analogue RoF system.

In the RF over fibre method, the RF signal is used to modulate a laser transmitter or an external modulator located in the CO. The output is transported over the optical fibre and detected by a photodiode receiver in the remote location. After some amplification and filtering in order to select the desired RF channel (in case of multiple RF channels), the RF signal can feed the antenna and be transmitted wirelessly.

In the alternative method, known as IF over fibre, the RF signal is downconverted to a lower frequency by means of a local oscillator and a frequency mixer. The signal is filtered and used to modulate the optical carrier. After detection at the photodiode receiver, the IF signal is upconverted to the desired RF by means of another local oscillator and frequency mixer. Subsequently, the signal is amplified, filtered and sent to the antenna for wireless transmission. At the expense of additional RF components, this approach has the advantages of using laser transmitters and photodiodes that operate at lower frequencies. Furthermore, it reduces the effects of fibre impairments, most notably those of chromatic dispersion that significantly affect the higher frequencies [25].

Unlike d-RoF, a-RoF signals may be subject to physical layer impairments and this is the main reason why it has not yet been standardized [32]. This is important as several studies point out that a-RoF needs to be standardized in order to meet the requirements of 5G and future network deployments [1, 23, 33].

A-RoF systems can provide low-latency, low-cost and energy efficient transmission of future mobile signals. According to the study performed in [32], Capital Expenditure (CAPEX) and Operational Expenditure (OPEX) cost ratios between d-RoF and a-RoF are systematically in favor of a-RoF because of the high bit rates required by d-RoF links. The digitalization process and the data rate requirements are explained in detail in ICIRRUS,2015 [19]. As an example of the requirements, by using the CPRI protocol and a typical configuration of a Radio Access Unit (RAU), transmitting a 20 MHz bandwidth Long Term Evolution (LTE) signal in a single sector with a MIMO 2x2, the bit rate requirement is 2.4576 Gbps. Moreover, for 5G configurations the requirements will increase exponentially. For example, considering the use of 3 sectors, 8x8 MIMO and 100 MHz bandwidth, the bitrate required will be up to 150 Gbps [34].

In conclusion, a-RoF systems present several advantages in comparison with d-RoF. The first advantage is that the system is bandwidth efficient, since generally wireless systems use modulation techniques that are more bandwidth efficient. For example, IEEE 802.11n WiFi networks transmits at over 100 Mbps by using channel bandwidths of less than 40 MHz, that would be the bandwidth required in an a-RoF link carrying such a signal. In contrast, a 100 Mbps Ethernet link based on digital signals, uses a channel bandwidth of over 125MHz [35]. A second advantage of using a-RoF is that it allows the centralization of the higher layers and signal processing functions in the CO, enabling the use of simplified antenna systems and reducing the costs related to the maintenance of the network. A third advantage is that the physical layer is transparent to modulation and signal formats. This is desired in 5G networks since the different RATs can share the ODN without the need of higher layer intervention, providing a simplified and cost-efficient distribution of the mobile signals.

### 3.3

#### Subcarrier Multiplexing

Subcarrier Multiplexing (SCM) enables the transportation of different RF signals over the same optical carrier. The RF signal, now referred to as subcarrier, can be multiplexed with other subcarriers by means of an

electrical multiplexer, and subsequently they can modulate an optical carrier. Subcarriers can be modulated by using analogue (AM, FM, etc.) or digital (e.g., PSK, FSK, QAM) techniques [36].

The aim of SCM is to allow the sharing of bandwidth between different operators and services. These signals at different frequencies can be easily combined to form a SCM in a RoF system. Figure 3.5 depicts the basic architecture of SCM combining analogue and digital signals in a RoF system.

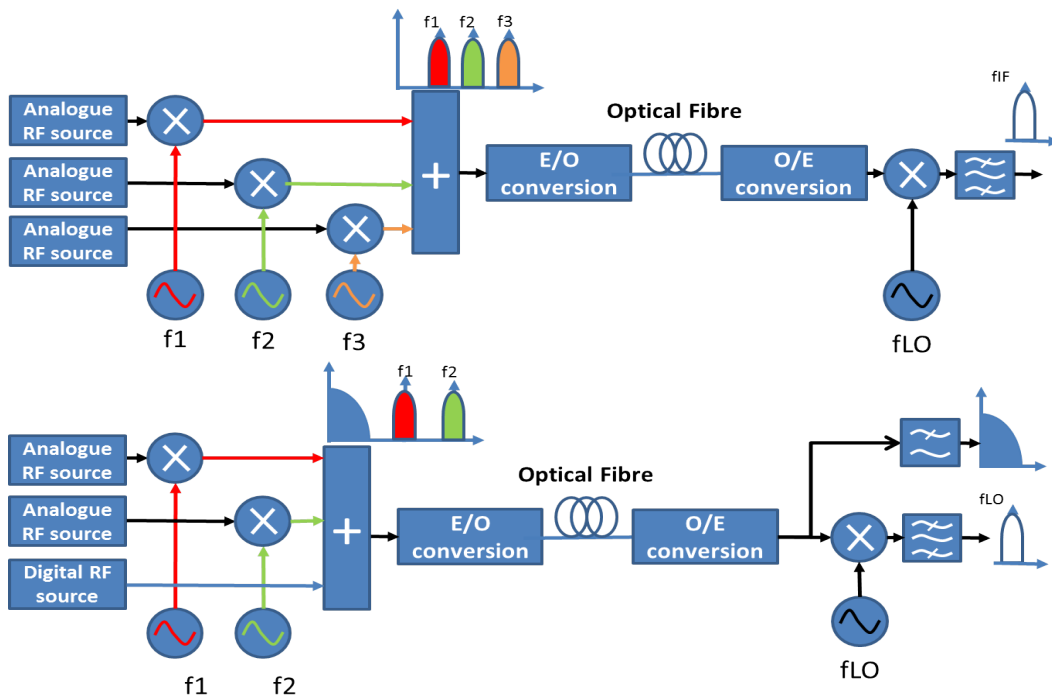


Figure 3.5: Subcarrier Multiplexing in Radio over Fibre Systems.

In Fig. 3.5, each of the analogue sources can represent a different RAT or any RF signal, and these RF signals can be upconverted or downconverted in order to occupy different frequency spectra for each of them. Note that the analogue source can also modulate the optical lightwave directly if it is already allocated in the desired frequency band. At the receiving end, the complete multiplexed signal is detected by the photodiode receiver and any individual RF subcarrier is demodulated, typically using RF heterodyne detection techniques to downconvert the required subcarrier to an IF. In the case of wireless and mobile systems, the RF signal will be used to modulate the antenna unit; this requires better filtering in order to follow the wireless regulations.

As wireless and mobile system carrier frequencies are typically in the GHz range, proposals have been made to use the lower frequency part of the spectrum for simultaneous transport of baseband signals [37], as shown in

Fig. 3.5. It is also possible to transport digital signals as subcarriers but the difficulty remains in the detection and recovery process. In the case of digital signals as subcarriers, the LO in the CO needs to be at the same frequency and phase as the LO in the transmitter site. To overcome this difficulty phase-locked-loop systems have been proposed in the literature [38, 39].

## 4

# Optical Fibre Monitoring Systems

The 5th Generation Mobile Networks (5G) and the deployment of small cells in dense urban areas will bring several challenges to the access networks. The use of Distributed Antenna Systems (DAS), Massive Multiple Input Multiple Output (M-MIMO) antenna configurations and large bandwidths calls for the use of optical fibre systems in the access networks. A key aspect for the success of such implementation will be monitoring and fault detection in the physical layer of the network, that should provide in-service, rapid and detailed monitoring of the Optical Distribution Network (ODN) at low-cost. This chapter shows an overview of different monitoring systems that have been proposed in the literature and can be used in optical access networks. Included is the theory of Optical Time Domain Reflectometry (OTDR) that is considered an important part of the thesis.

### 4.1

#### Optical Time Domain Reflectometer

This section is based on Derickson's Fiber Optic Test and Measurement book [40], which explains in a summarized manner the fundamental functionalities and benefits of an OTDR in order to characterize an optical fibre link. The OTDR is an instrument used for the characterization of optical fibre links. These OTDRs are designed to not only provide information about reflections, but also about attenuation properties and losses of the Fibre under Test (FUT). This is accomplished by exploiting backscatter and backreflected light returning from the FUT when probing it with a short optical pulse. The OTDR is able to measure the FUT by accessing only one of the fibre entries, which provides a centralized approach of the monitoring method.

#### 4.1.1

##### OTDR fundamentals

OTDRs launch short duration light pulses into a fibre and then measure the optical signal returned to the instrument as a function of the flight time. As the optical pulses propagate along the fibre, they encounter reflecting and scattering sites resulting in a fraction of the signal being reflected back in

the opposite direction. Rayleigh scattering and Fresnel reflections are physical causes for this behaviour. By measuring the arrival time and intensity of the returning light, the locations and magnitudes of faults can be determined and the fibre link can be characterized. Figure 4.1 shows a generic OTDR block diagram.

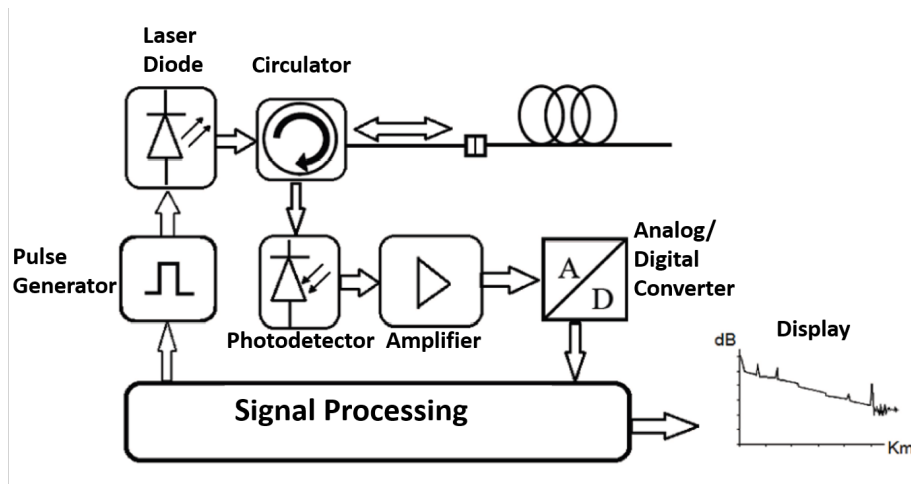


Figure 4.1: Generic OTDR block diagram.

A pulse generator triggered by the signal-processing unit is used to modulate the intensity of a lightwave. The probe signal in conventional OTDRs is a single square-pulse. Different pulse widths are used depending on the spatial resolution and sensitivity requirements of the measurement. An optical circulator is used in order to guide the optical pulse into the FUT and the returning light signal to the photodetector receiver. The last converts the received photons into current to feed a low-noise transimpedance amplifier with high linearity. The signal is next digitized in order to process the data and the FUT signature is generated. It is important to remember that the OTDR measures only the flight time of the optical pulse, and it is necessary to provide the specific optical fibre refractive index in order to calculate the correct distance. Furthermore, the backscattered light experiences a round trip propagation, consequently, the time measured by the OTDR is the double. Also the signal measured by the OTDR experiences a twofold fibre attenuation. All of these particularities are taken into account when the fibre signature is calculated. Figure 4.2 shows a typical OTDR trace with the principal events.

The vertical scale is the reflected signal level on a logarithmic scale (dB). The horizontal axis corresponds to the distance between the OTDR and a location in the FUT. The measured response typically exhibits three types of features: straight lines caused by distributed Rayleigh backscattering,

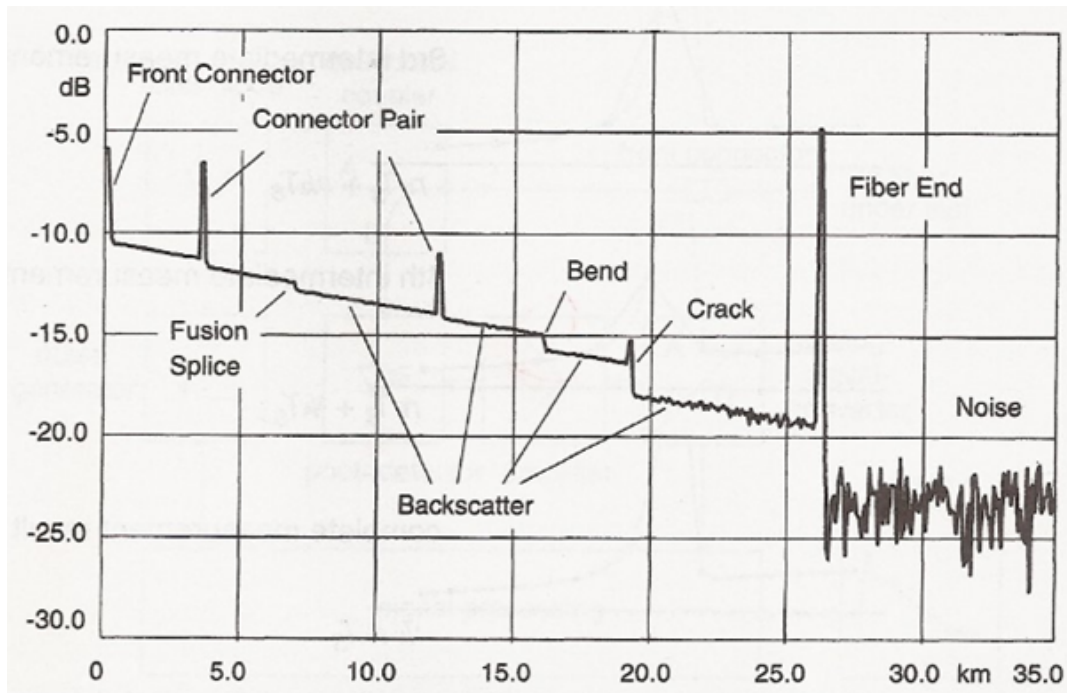


Figure 4.2: Typical OTDR trace with principal events [40] (Pg. 438).

positive spikes caused by discrete reflections, and finally steps that can either be positive or negative depending on physical fibre properties.

#### 4.1.2 Performance Parameters

The performance of an OTDR is specified by a set of parameters that describe the quality of the measurement and allow the user to understand how well the instrument fits an application's needs. The most important performance parameters are explained below.

##### 4.1.2.1 Measurement Range.

This is the maximum attenuation that can be inserted between the OTDR and an event, in such a way that, the OTDR is still able to accurately measure the event. Commonly a 0.5 dB splice is chosen as the event to be identified as is shown in Figure 4.3.

##### 4.1.2.2 Dynamic Range.

This is defined as the difference between the initial backscatter level and the noise level after 3 minutes of measurement time, expressed in decibels of

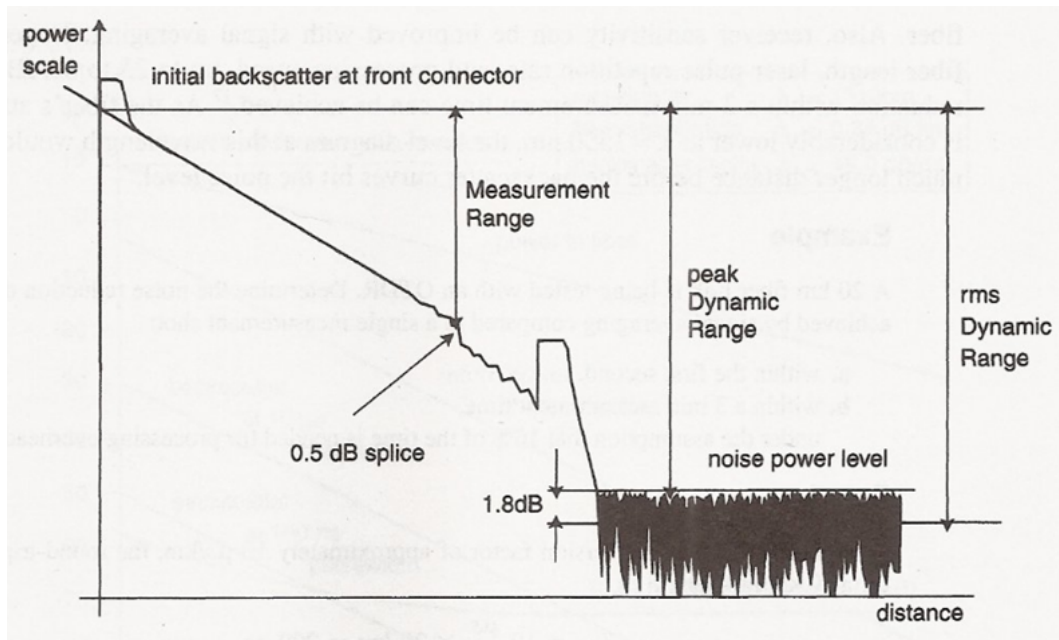


Figure 4.3: Dynamic Range and Measurement Range [40] (Pg. 442).

one-way fibre loss. The noise level can be considered as either the peak of the noise or its Root Mean Square (RMS) value. The RMS value can be estimated as 1.8 dB down from the peak noise level as it is shown on Figure 4.3.

#### 4.1.2.3

##### Dead Zones.

Fresnel reflections lead to an important OTDR parameter known as "dead zones". Dead zones occur when the reflected signal saturates the OTDR receiver. The receiver takes some time to recover after saturation, resulting in loss of information. There exist two types of dead zones: event and attenuation. The OTDR's event dead zone is the distance between the beginning of a reflection and the point 1.5 dB down from the peak on the falling edge of the reflection as indicated in Figure 4.4. The other type of dead zone, the attenuation dead zone, is defined as the distance from the start of a reflection to the point where the receiver has recovered to within a  $\pm 0.5$  dB margin around the settled backscatter trace as is also depicted in Figure 4.4. The dead zone depends on all the parameters used in the measurement including the pulse width, the receptor bandwidth and the wavelength. The purpose of specifying the dead zone is to quantify the distance over which information is lost.

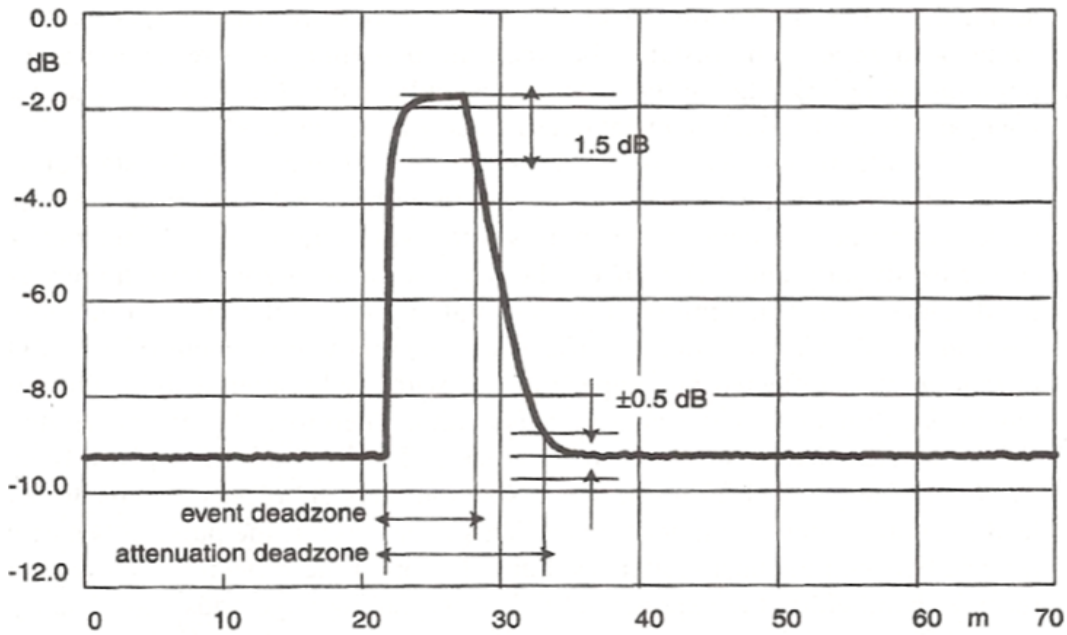


Figure 4.4: Attenuation and Event Dead Zone [40] (Pg. 443).

#### 4.1.2.4

##### Spatial Resolution.

The spatial resolution of the OTDR indicates the instrument's ability to resolve two adjacent events; where one of them might be only weakly reflective. Near-end resolution simply takes the instrument's front-panel connector reflection as the first event and characterizes how close a nonreflective event can be spaced to the instrument and accurately measured. Single-event resolution is also specified, based on an event of 1 dB or less. The single event resolution is defined as the 10 percent to 90 percent rise or fall distance. For a discrete reflection, the full width at 50 percent of the maximum is used as the resolution.

#### 4.1.2.5

##### Tradeoff Between Dynamic Range and Resolution.

A fundamental limitation for any conventional OTDR is the tradeoff between Dynamic Range (DR) and resolution. The received signal  $s(t)$  can be expressed as the convolution ( $\otimes$ ) of  $p(t)$ , the probing pulse,  $f(t)$ , the backscattering impulse response of the fibre, and  $r(t)$ , the impulse response of the receiver.

$$s(t) = p(t) \otimes f(t) \otimes r(t) \quad (4-1)$$

The achievable resolution is therefore limited by the receiver response and the geometrical width of the probe signal. For high-spatial resolution, the probe pulsewidth has to be as small as possible with a correspondingly wide receiver bandwidth. This leads to a reduced SNR. Increasing the strength of the received signal by using longer pulses and low bandwidth receivers leads to improved sensitivity with corresponding less resolution. This tradeoff of pulse width and sensitivity is shown in Fig. 4.5. Two reflective events spaced about 100 m apart have been measured with a pulsewidth of 1  $\mu$ s as well as 100 ns. For the same noise level (not shown in Fig. 4.5) we can observe that the signal coming from the 1  $\mu$ s pulse is higher than for the 100 ns pulse. Also, the upper trace shows a smoother backscatter than the lower one, the drawback of insufficient spatial resolution is evident.

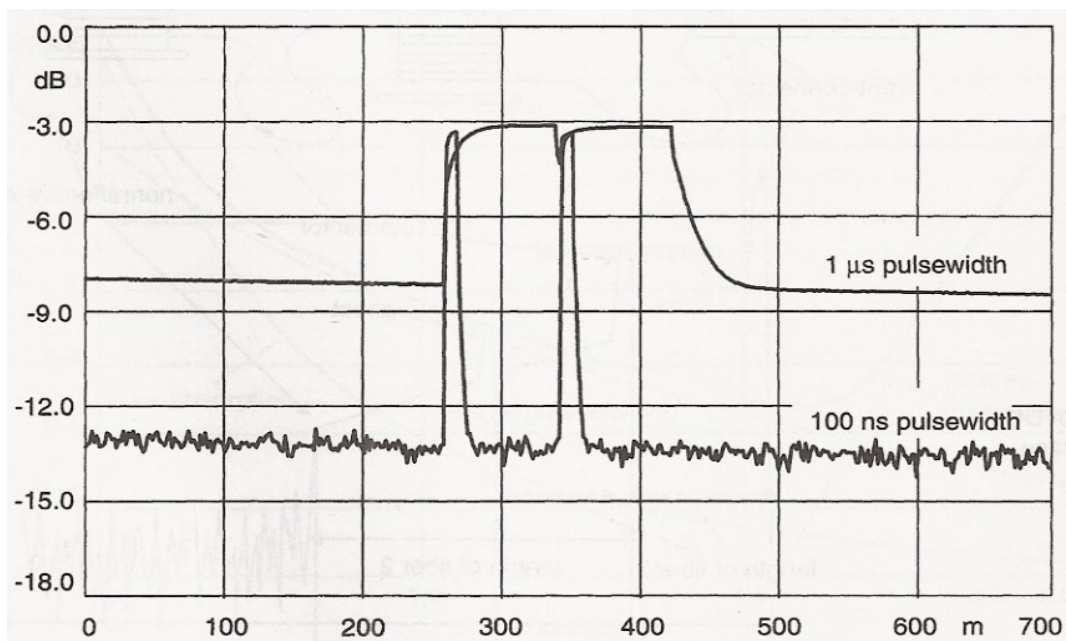


Figure 4.5: Tradeoff between Dynamic Range and Resolution [40] (Pg. 445).

### 4.1.3 Monitoring Systems in Optical Access Networks

As discussed by Esmail & Fathallah [41] and Urban et al. [42], an efficient monitoring system needs to fulfill the following requirements: 1) be able to quickly detect and localize faults in a cost-efficient way, 2) provide high resolution in distance measurement, 3) be centralized in the Central Office (CO), 4) monitor the network automatically and remotely, 5) avoid/eliminate impact on data transmission, and 6) be scalable towards different network architectures.

Many solutions to monitor Next Generation Optical Access Networks (NGOAN) have been proposed up to date, most of them focused in WDM-PON architectures where the monitoring signal is usually carried on a different wavelength than that of the data wavelength. Some other monitoring systems propose embedded monitoring techniques that will be able to reuse the laser source and reduce the cost of the network. This section provides a quick overview of the monitoring systems that can be used in NGOAN, other references like [43, 44] contain a more detail summarize of the work done in this subject.

#### 4.1.3.1

##### **Monitoring Techniques for WDM-PON.**

In order to monitor WDM-PON architectures, a Tunable Laser OTDR (TL-OTDR) was developed and experimentally validated by Ren et al. [45]. With the integration of optical filters at the fibre ends in the Optical Distribution Network (ODN), the TL-OTDR proposed would be suitable for in-line monitoring of WDM-PON links with a spatial resolution reaching 0.5 m and a wavelength shifting speed of less than 1 s. An L-band tunable laser was used as a laser source of the OTDR which permits the transmission of data in the C-band but reduces the number of available channels in the network.

Another method, proposed by Urban et al. [46], combines the Optical Transceiver Monitoring (OTM) and OTDR techniques to measure and localize failures in power splitter and wavelength splitter based PONs. This method is non-invasive to data traffic flow and requires no additional equipment on the Optical Network Terminal (ONT) side. However, the method requires upgrades in the Central Office (CO) and/or Remote Nodes (RN) and uses the U-Band for monitoring the ODN.

Amaral et al. [47] evaluate the performance of a Tunable Photon-Counting OTDR (T-PC-OTDR) in a WDM-PON with an Arrayed Waveguide Grating (AWG) in the RN proving 32 dB of DR without impact on data signal quality. The system provides a 6 m spatial resolution with an automatic detection based on signal processing methods. However, the method uses a single photon avalanche detector and an FPGA that will increase the total cost of implementation. It also uses an additional wavelength to perform the monitoring of the WDM-PON network.

### 4.1.3.2 Embedded Monitoring Techniques.

All techniques aforementioned use a dedicated source for reflectometry measurements, which increases system complexity and cost, and decreases spectrum utilization. In this regard, embedded monitoring techniques, i.e., ones using the same transceiver for both data and monitoring signals, have also been investigated.

Schmuck et al. [48] propose an integration of an OTDR monitoring equipment into existing transceivers modules. The embedded OTDR supervision solution is demonstrated using a quasi-continuous OTDR signal modulated on top of the data stream. This solution uses only 10 percent of the relative amplitude for the OTDR signal which limits its DR performance. In order to increase the network and monitoring reach, in-line Semiconductor Optical Amplifiers (SOAs) are used in the field [49]. This monitoring technique places a power penalty of 1.5 dB on the data signal. It is important to note that the data signal used in this technique is a GPON digital signal with 2.488 Gbps that in a technical view is similar to Digital Radio over Fiber (d-RoF).

As another method, Effenberger & Meng [50] propose a concept of using data patterns as the driving signal for Optical Frequency Domain Reflectometry (OFDR) for PONs. The use of algorithms that can generate the data patterns is developed and confirmed through simulation. The idea of the data pattern is that most of the energy is concentrated in a particular electronic frequency and therefore the echo received is processed using a heterodyne electronic detector circuit.

In another approach, shown by Chen et al. [51] and Vandewege et al. [52], a low-cost embedded solution is proposed for the ONU. This solution aims to provide visibility for the drop fibre section of the ODN in a power splitter configuration. Conventional OTDR systems suffer what is known as the point to multipoint problem, where the backscattered signals of all the drop fibres are aggregated in the receiver making the identification of different fibre branches a difficult task. In order to perform the monitoring of the system in a non-intrusive way the proposed system takes advantage of Time Division Multiple Access (TDMA) technology and the monitoring of each fibre branch is done while the upstream transmission is off.

As discussed in chapter 3, Analogue Radio over Fiber (a-RoF) systems are future candidates for mobile fronthaul in 5G access networks and present several benefits to the network compared to d-RoF. Mitchell [53] concludes in an impartial comparison of both technologies, that a-RoF systems are not only simpler, more cost-effective and less bandwidth demanding but also presents

flexibility and dynamic capacity for the expansion of the network. All of these factors call for a monitoring technique that can be used in a-RoF systems combined with SCM techniques and/or WDM-PON configurations.

## 5

# Simulation of a SCM/WDM-PON with in-service baseband embedded OTDR monitoring

In this chapter we simulate a Subcarrier Multiplexing and Wavelength Division Multiplexing Passive Optical Network (SCM/WDM-PON) with Analogue Radio over Fibre (a-RoF) technology for the convergence of optical and wireless access networks. The SCM/WDM-PON system includes an in-service baseband monitoring which uses an optical carrier to supervise the fibre infrastructure and several subcarriers to transmit data signals simultaneously. The performance of the proposed system is investigated where a Baseband Embedded Optical Time Domain Reflectometry (BE-OTDR) signal is applied for fibre fault monitoring. The results have verified the feasibility of the proposed system and show that with proper configuration the in-service baseband monitoring signals have negligible impact on data transmission. We used the VPI Transmission Maker version 9.2 from VPI Photonics in order to simulate the network and obtain the results.

### 5.1

#### VPI Simulator

VPI Transmission Maker has been developed for modelling all types of photonic systems and networks, including optical access networks, microwave photonic applications, Time Division Multiplexing (TDM) and WDM networks. The software combines a robust simulation scheduler with a powerful graphic interface that is able to simulate different networks including bidirectional links, ring based networks and point to multipoint architectures. The most attractive idea of using a software tool is the low-cost verification of different designs and optimization of the optical communication system.

VPI Transmission Maker can fully verify link designs at a signal level to identify further cost savings and investigate novel technologies. Some examples of link designs can be automatically imported from VPI link configurator for further detailed design and optimization. VPI TransmissionMaker is widely used as a research and development tool to evaluate novel component and system designs. Furthermore, the use of a web forum enables a direct communication with VPI experts and software developers that can help at the

moment of the system design and clarify other simulation problems [54].

VPI Transmission Maker is based on visual programming where different devices and individual elements can be interconnected in order to simulate a more complex system. A complete simulation application is called a universe and consists of interconnected modules that can be divided in different hierarchical designs. A universe is the highest level of hierarchy and does not have any external inputs or outputs. Inside a universe we can find other blocks that can be individual elements called Stars or interconnected elements encapsulated that are called galaxies. Figure 5.1 shows the different blocks in a simulation environment [57].

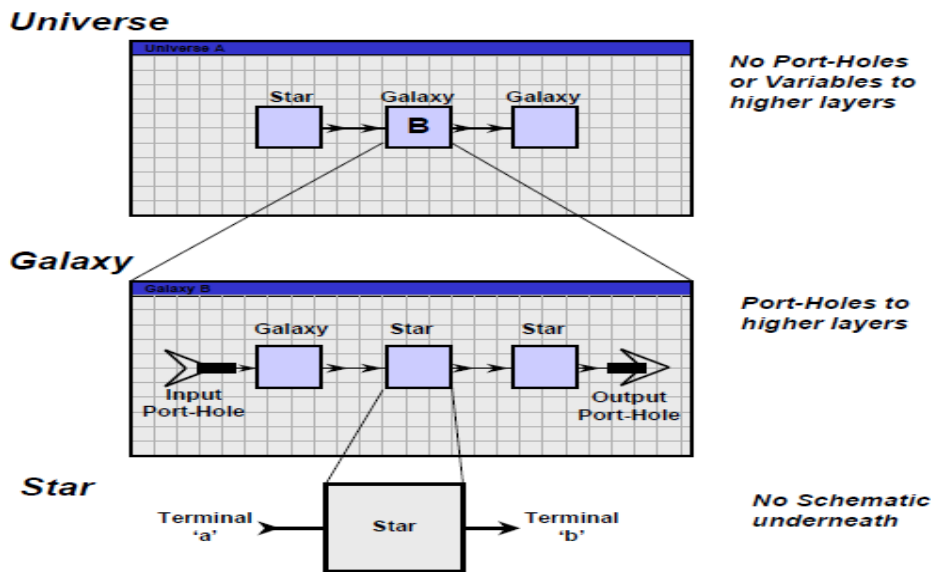


Figure 5.1: Universe, Galaxy and Star in VPI simulator.

Each of the different individual elements has its own parameters that define their behaviour. For example, for a Continuous Wave (CW) laser element, we need to define the emission frequency, the sample rate, average power and linewidth. In system modeling, the parameters of system components often depend on each other. For example, the bit rate parameter of a random bit sequence generator should match the corresponding parameter of a coder to which it is connected. Thus the bit rate should be simultaneously set depending on the symbol rate and number of bits per symbol used in some multilevel encoding schemes. All modules involved in simulation should also operate on the same time interval. Schematic parameters are used to set the values of dependent parameters. The schematic parameters are defined on the universe and galaxy levels, and can be referenced by other schematic parameters and all modules/galaxies on lower hierarchy levels [57]. Global parameters are com-

mon to all modules in a simulation schematic. Their values are important for the correct and efficient operation of the simulator.

## 5.2 Proposed System

The combination of the multiplexing techniques WDM and SCM has been presented by Shaddad et al. [55] and Yang et al. [56]. It provides efficient fibre utilization for analogue Mobile Fronthaul (MFH) and simplified radio heads, i.e., avoiding costly digital-to-analogue converters. For the purpose of providing a data-agile fibre monitoring solution for such links, we propose a concept of Baseband Embedded OTDR (BE-OTDR) combined with data subcarriers. This technique has never been proposed before and this is its the first simulation validation. It enables a single wavelength (and therefore, a single light source) to perform monitoring in parallel with SCM data transmission. The SCM/WDM-PON system is shown in Figure 5.2 where the Optical Line Terminal (OLT) sends out multiple wavelengths, each containing several subcarriers for data transmission, and baseband for the monitoring signals.

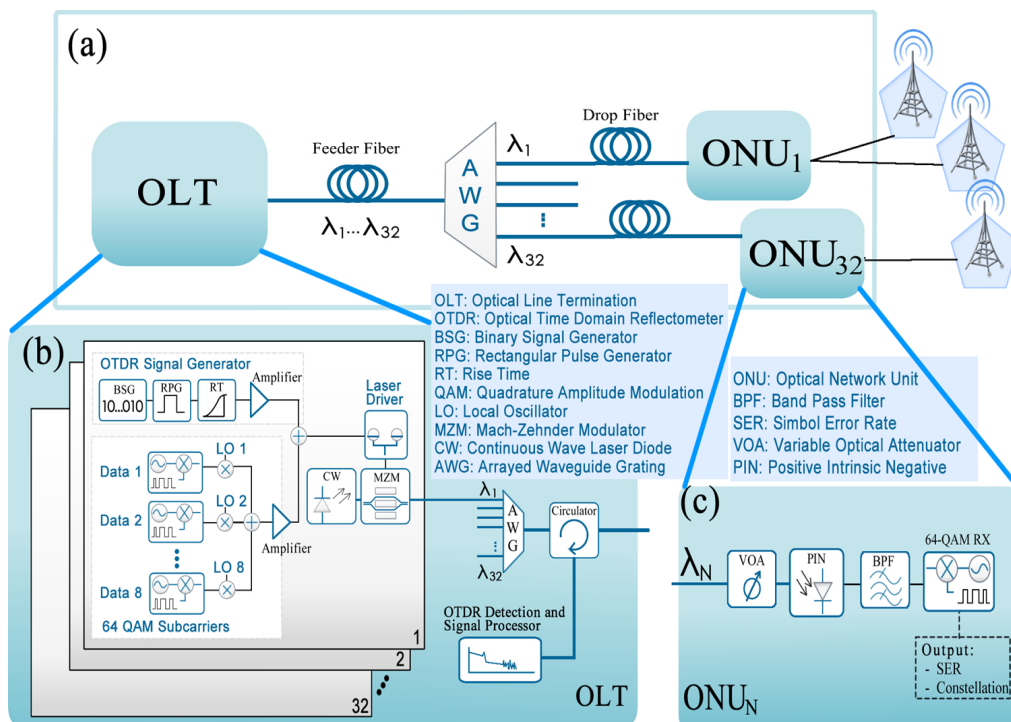


Figure 5.2: (a) SCM/WDM-PON system. (b) OLT Setup with in-service baseband embedded OTDR monitoring and (c) ONU scheme.

Figure 5.2 (b) shows the architecture of the OLT. In order to monitor each of the WDM channels to the Optical Network Unit (ONU) (where a radio head

is co-located in case of the analogue MFH), an OTDR signal has been provided in the baseband of each optical carrier. To generate this signal electrically, a Binary Signal Generator (BSG), a Rectangular Pulse Generator (RPG) and an amplifier are used. The amplifier is applied to define the modulation index of the OTDR signal ( $m_{\text{OTDR}}$ ). In order to avoid ambiguities in the OTDR trace, caused by overlapping returned pulses, the BSG has been set to generate pulses with a time interval that is the round trip time of the light, as determined by the distance from the OLT to the farthest ONU and the group velocity of light in the fibre. OTDR signals for different wavelength channels should also be coordinated in order to make sure that at any time, only one OTDR signal is reflected by one channel. This is because OTDR detection and signal processing are shared among the different channels, which avoids insertion loss introduced by an Arrayed Waveguide Grating (AWG) in the OTDR receiver path and reduces the deployment cost for monitoring equipment. The combined signal, which contains the subcarrier channels, goes through an amplifier where the modulation index of the data signal ( $m_{\text{Signal}}$ ) is defined. Subsequently, the combined OTDR pulse and the subcarrier channels modulate the optical carrier by means of a Mach-Zehnder Modulator (MZM). A CW laser is used as the carrier and an AWG is used to multiplex the various wavelengths. A circulator passes the backscattered light to the OTDR receiver. In order to avoid crosstalk from the backscattered subcarriers, filtering of the OTDR signal is needed either in the optical domain by the use of an ultra-narrow band optical filter or in the electrical domain by proper low-pass filtering.

Figure 5.2 (c) shows the ONU scheme that can be applied to the proposed SCM/WDM-PON with in-service BE-OTDR. A Band Pass Filter (BPF) is used after photodetection in order to filter out the OTDR pulses before the data receiver. For purpose of performance verification, a Variable Optical Attenuator (VOA) is used to test signal quality with different losses.

### 5.3 Simulation results

In our simulation model, the OTDR generates 100 ns pulses for a spatial resolution of around 10 m. For data transmission, each wavelength carries eight subcarrier channels spaced at 50 MHz intervals, each of which uses 64 Quadrature Amplitude Modulation (64 QAM). The bit rate for each subcarrier channel is 120 Mbps. After the local oscillator, the first subcarrier channel is up-converted to 2.4 GHz, the next one to 2.45 GHz and so on. The CW laser has a linewidth of 10 MHz and generates 10 dBm of optical output power. The other specifications of the laser, such as the Relative Intensity Noise (RIN),

are set according to the data sheet of a commercial component [58]. The AWG can multiplex the wavelengths from  $\lambda_1$  to  $\lambda_{32}$ , and has a typical insertion loss of 5 dB [59] in C band.

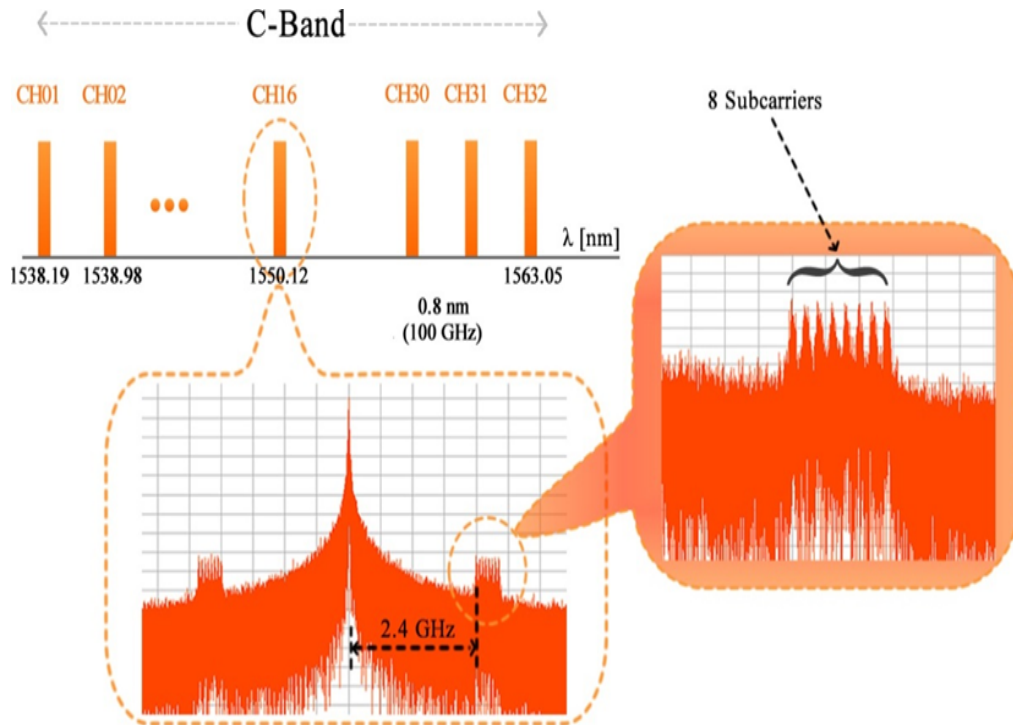


Figure 5.3: Transmission Spectrum in the C-band.

Figure 5.3 shows the optical spectrum generated in C band. 32 wavelengths in a 100 GHz comb over C band are considered. Each wavelength carries the OTDR pulse modulated in the baseband, and eight subcarrier channels for data transmission. Considering the worst case of a fully loaded system, one of the subcarriers in the middle, SC4, of wavelength channel 16, is analyzed in terms of the Symbol Error Rate (SER) of the 64 QAM data signal. Different OTDR peak power values are used in our simulation in order to identify the limit where the performance of the subcarrier channel for data traffic is affected by the monitoring signal. Two noise sources dominate our system, namely the RIN produced by our laser source and the linearity of our external modulation device. The RIN dominates the Carrier-to-Noise Ratio (CNR) in our SCM system. The Root-Mean-Square (RMS) value of the intensity noise increases quadratically with the Received Optical Power (ROP). ROP is the optical power which arrives at the detector in the ONU and, for purposes of the simulation, is controlled by the VOA. The RMS increase is because the ROP in our system is high ( $\geq 0.1$  mW) [61]. This problem can be solved by the use of a laser source with low RIN (e.g., -145 dB/Hz) and narrow linewidth (e.g., 10 MHz).

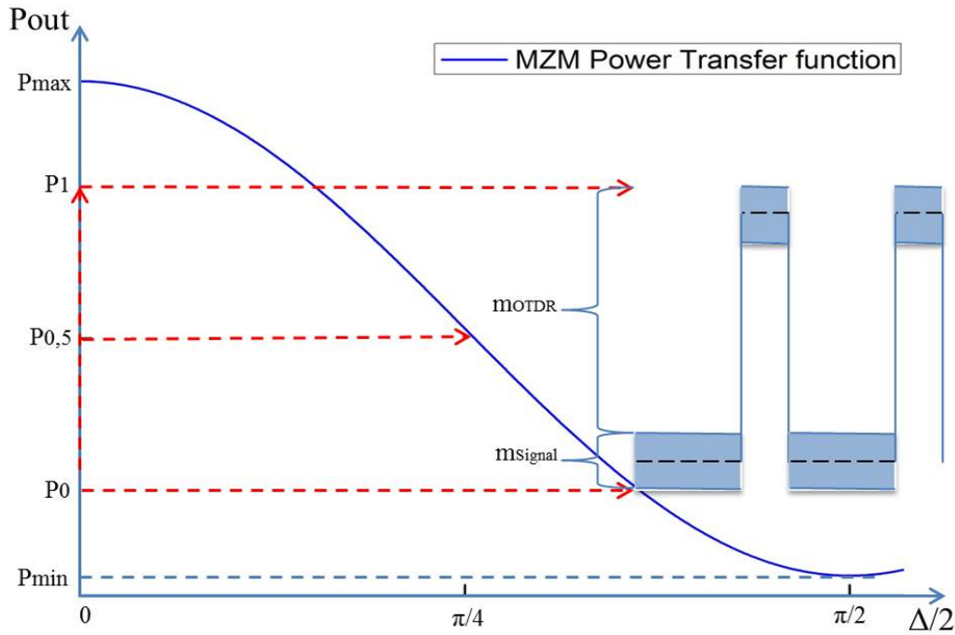


Figure 5.4: MZM Power transfer function and modulation indexes.

Figure 5.4 shows the power transfer function of the MZM device where  $\Delta$  is the phase difference between the two modulator branches. Equation (5-1) shows the MZM power transfer function:

$$P_{out} = P_{in} \cos^2(\Delta) \quad (5-1)$$

$P_{out}$  is the modulated output power and  $P_{in}$  is the optical power input from the CW laser. The MZM extinction ratio defines the difference between the maximum output power ( $P_{max}$ ) and the minimum output power ( $P_{min}$ ). It also defines the nonlinearity coefficient of the MZM, i.e., the linear region of the power transfer function. For our simulations we use an extinction ratio of 30 dB for the MZM ( $P_{max} = 10$  dBm and  $P_{min} = -20$  dBm). We define two output power levels,  $P_0 = 0.98$  mW and  $P_1 = 7.93$  mW to mark the acceptable linear region of the MZM device. This acceptable linear region was determined by the results of preliminary simulations. Modulation beyond this region is considered out of the linear region, thus the sum of the OTDR and signal peak-to-peak powers should be smaller than the linear power range  $P_1 - P_0$ . Normalizing to this power range we define  $m_{OTDR}$  as proportional to the output peak power of the OTDR pulse, whereas  $m_{Signal}$  is proportional to the maximum drive amplitude and bias current of our eight subcarrier channels. Note that the sum of  $m_{OTDR}$  and  $m_{Signal}$  is the total modulation index of our combined signal and has to be less or equal to 1 to be in the linear region of our MZM.

Hence, if the sum of the modulation indexes is more than 1, the signal is out of the linear region.

In the simulation, we consider a typical urban case [62]. OLT sends the optical signal towards the ONUs over a 5 km feeder fibre up to the RN containing an AWG that routes each of the 32 wavelengths to individual ONUs via 1 km drop fibres.

Figure 5.5 shows the SER versus the ROP for different  $m_{OTDR}$  values while keeping the  $m_{Signal}$  constant at 0.3. Note that  $m_{OTDR}=0$  is the curve without any OTDR modulation (which is considered as benchmark to identify the impact on signal quality when OTDR is introduced in optical carrier). It can be seen that the SER is affected by the nonlinearity of the MZM power transfer function. Whenever the sum of the modulation indexes is increased above the linear region, the SER of the subcarrier channel is rapidly decreased.

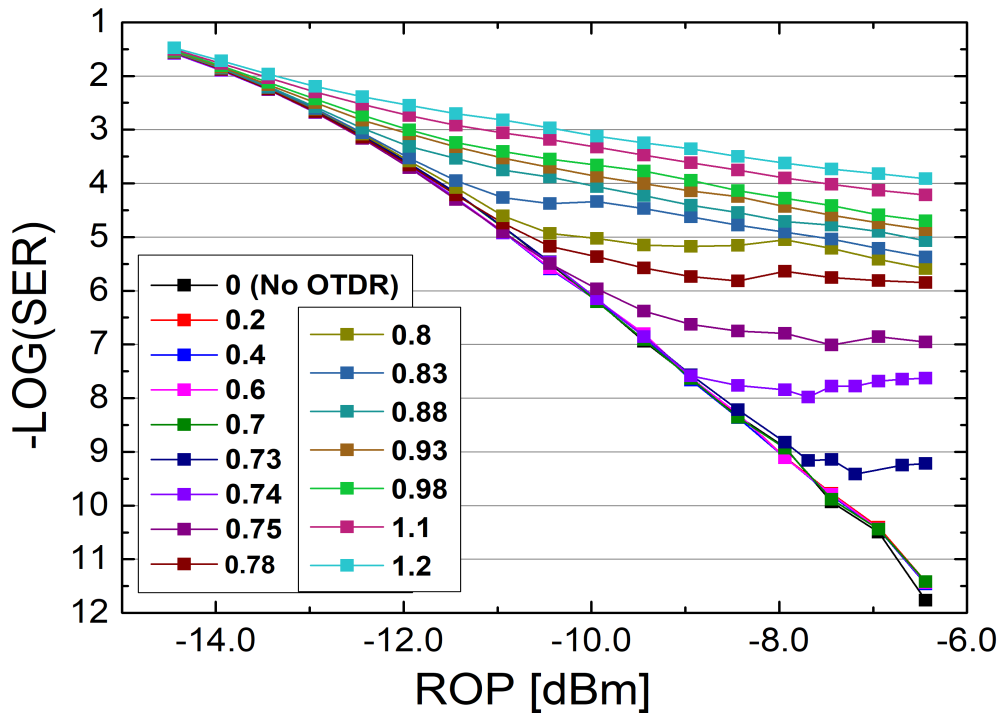


Figure 5.5: SER vs ROP for different  $m_{OTDR}$  with  $m_{Signal}=0.3$ .

From Fig. 5.5 we can observe that data points from the linear range ( $m_{OTDR} \leq 0.7$ ) are almost on top of each other at the higher ROP, their  $-\log(SER)$  values all exceed 11, on the other hand, we can observe the degradation of the  $-\log(SER)$  values after the linear region were overpassed.

Figure 5.6 shows the power penalty for different  $m_{OTDR}$  at chosen SER values. It can be observed that the SER of  $10^{-9}$  and  $10^{-6}$  are hardly to be reached after the  $m_{OTDR}$  exceeds the linear region of the MZM. Note that the

the modulation leaves the linear region when  $m_{OTDR}$  exceeds 0.7 ( $m_{Signal}$  is fixed at 0.3).

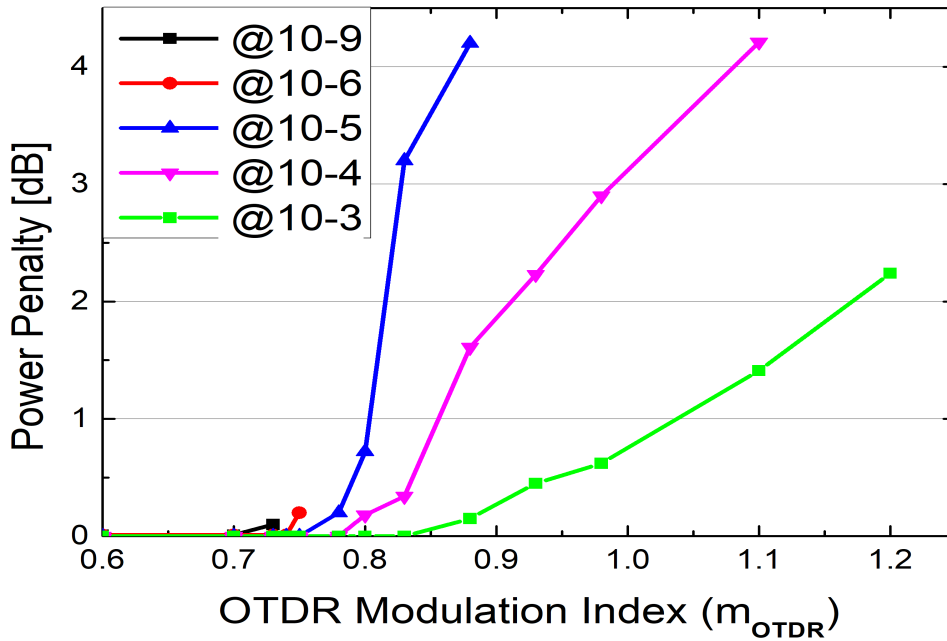


Figure 5.6: Power penalty for different  $m_{OTDR}$  values at chosen SER levels.

Figure 5.7(a) shows the SER for 2 different OTDR pulse widths as function of  $m_{OTDR}$  while the ROP is kept constant at -6.44 dBm. The OTDR peak power has been measured after filtering and is also plotted in Fig. 5.7(b).

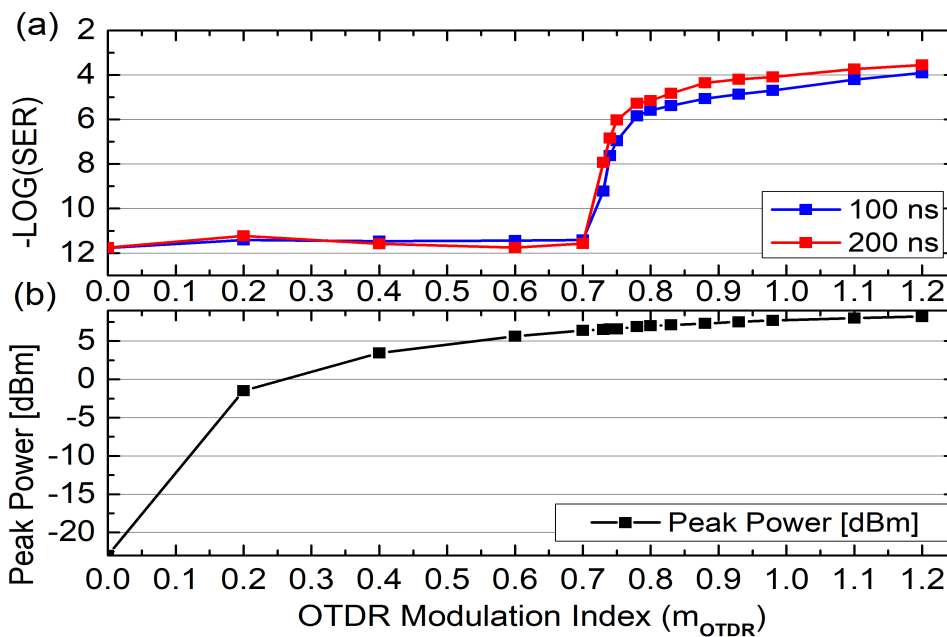


Figure 5.7: (a) SER versus different  $m_{OTDR}$  values for different pulse lengths and (b) OTDR peak pulse power versus different  $m_{OTDR}$  values.

We observe that the SER drops suddenly after a certain value of  $m_{\text{OTDR}}$  from 0.7 to 0.8 which corresponds to the MZM modulation regime with increasing nonlinearity. After this critical regime, once the extreme values of the modulation index are reached the QAM signal cannot be properly received. The large DR improvement for the OTDR can be obtained within the linearity regime of the MZM where the pulse power can be increased considerably as it is depicted in Fig. 5.7 (b). It is remarkable that after reaching the MZM nonlinearity regime, a very little increase of the OTDR pulse power, hence very little DR improvement, results in substantial data signal degradation. The detailed DR performance estimation is presented later in this section.

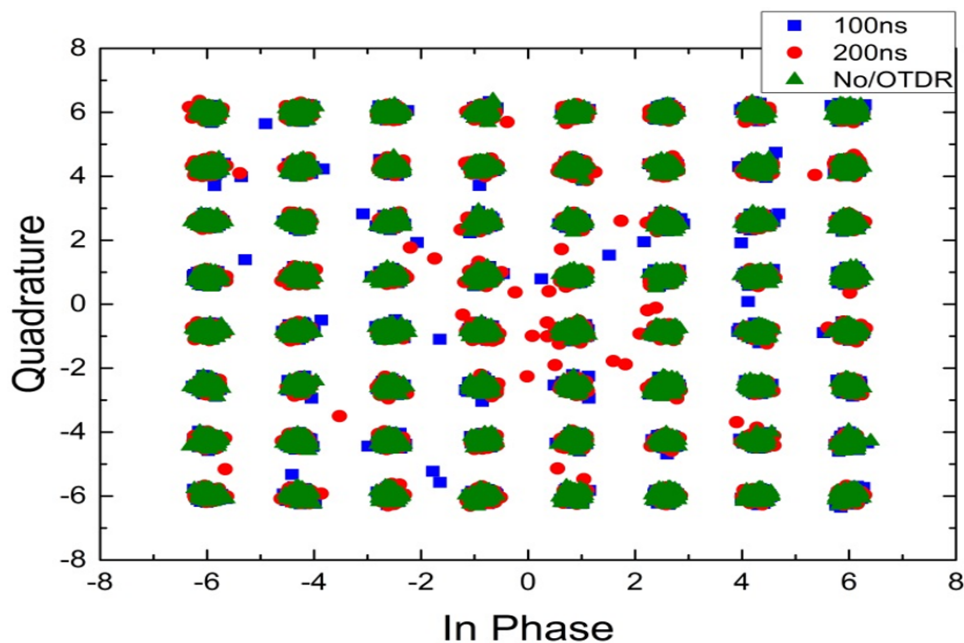


Figure 5.8: 64QAM constellation for 100 ns, 200 ns pulse lengths with  $m_{\text{OTDR}}=1.2$  and no OTDR.

Figure 5.8 shows the 64 QAM constellations for the cases with 100 ns and 200 ns OTDR pulse lengths with  $m_{\text{OTDR}}=1.2$  as well as the case without any OTDR signal. It clearly indicates the noise due to the presence of the high modulation index of the OTDR signal. We can see that the noise caused by the OTDR pulse just affects the symbols that are modulated within the nonlinear region of the MZM because they are sent together with OTDR pulses. Figure 5.8 demonstrates that the SER depends on the pulse length of the OTDR signal as is also shown in Fig. 5.7 (a).

## 5.4 Dynamic Range Estimation

In order to estimate the DR in our considered scenario we first calculate the backscattered optical power  $P_{BS}$  that reaches the OTDR receiving port by using Eq. (5-2) [63]:

$$P_{BS} = \frac{V_g \tau}{2} * P * \eta * \frac{\alpha_{SC}}{4.343} \quad (5-2)$$

Where  $V_g$  is the group velocity of light in fibre,  $\tau$  is the OTDR pulse width,  $P$  is the peak power of the transmitted light pulse,  $\eta$  is the conversion efficiency from the scattered light to that captured by the fibre and  $\alpha_{SC}$  is the attenuation coefficient due to Rayleigh scattering. The efficiency of capturing the backscattered power is calculated considering a standard single mode fibre, where  $\eta = 1.19 * 10^{-3}$ ,  $V_g = 2.04 * 10^8$  m/s and  $\alpha_{SC} = 0.2$  dB/km. As shown in the previous results, to avoid significant impact on data transmission, we have to keep  $m_{OTDR} \leq 0.7$ . Therefore, we choose the maximal allowed pulse peak power  $P = 4.5$  mW when  $m_{OTDR} = 0.7$  with the pulse width  $\tau = 100$  ns used in our system. The calculated backscattered optical power that reaches the detector is equal to -55.99 dBm.

In order to estimate the Noise Equivalent Power (NEP) of a commercial OTDR, we realize a measurement with a real OTDR [64], that is configured to send pulses of 100 ns (10 meters resolution in distance measurement) with a pulse interval of 0.1 ms. The measured values of the output peak pulse power and the DR in real time (without any average) are 19 dBm and 16 dB, respectively. By adding a 1 minute averaging time, the DR is improved to around 26 dB. With these values, we are able to estimate the NEP of the detector in the commercial OTDR that uses the same conditions as our system. The NEP can be calculated by Eq. (5-3):

$$NEP(dBm) = P_{BSOTDR}(dBm) - DR(dB) \quad (5-3)$$

Where  $P_{BSOTDR}$  (dBm) is the backscattered optical power that reaches the detector from the OTDR. According to Eq. (5-2), the measured  $P_{BSOTDR}$  would be -43.53 dBm for 19 dBm peak power. Then, we calculate the NEP to be a value of -59.53 dBm without any averaging process (DR = 16 dB) and can be improved to -69.53 dBm by utilizing a 1 minute averaging time (DR = 26 dB).

Given the NEP value of the detector and the calculated backscattered optical power that reaches the detector, we can estimate that a DR for the considered scenario is approximately 13.5 dB after a 1 minute average. It should be noted that the DR of the OTDR in the proposed system is also limited by the continuous backscattered power coming from the laser bias. The difference between the pulse peak power and the bias is 5.2 mW ( $\simeq 7$  dBm) after filtering the subcarriers. Therefore, the DR is limited to  $\simeq 7$  dB, which is obviously lower than the individual OTDR system. However, a DR of  $\simeq 7$  dB still can cover the considered scenario, i.e., a typical urban case with 5 km feeder fibre, an AWG and a 1 km drop fibre. Some improvement techniques can be used in order to increase the performance of the OTDR. Lee et al. [65] and Naseem et al. [66] used coding techniques to improve the OTDR Signal-to-Noise Ratio (SNR) without compromising the spatial resolution. Lee et al. [65] demonstrated a 9.2 dB improvement based on simplex codes. Coherent Rayleigh Noise (CRN) that causes amplitude fluctuations in a backscattered signal might be present in our system, since a narrow linewidth laser is used. However, the reduction of this type of noise has been demonstrated by Shimizu et al. [67].

## 6

# Experimental Demonstrations

The convergence of fibre and wireless in access networks is motivating the use of different technologies in order to enable the 5th Generation Mobile Networks (5G). Within this scope, the combination of Subcarrier Multiplexing (SCM) and Passive Optical Networks (PON) can provide an efficient and cost-effective solution for the transportation of different Radio Access Technologies (RAT). Moreover, in order to reduce Operational Expenditure (OPEX), a reliable monitoring technique should provide in-service, rapid and detailed evaluation of the physical layer. In this chapter, we perform several experiments to demonstrate different Mobile Fronthaul (MFH) solutions based in SCM-PON systems with Baseband Embedded Optical Time Domain Reflectometry (BE-OTDR) monitoring. The experiments are chronologically presented, and we focus our objectives on reducing the total cost of implementation and performing an accurate monitoring without degradation of data transmission. From the previous simulation, we conclude that an embedded monitoring system using an external modulator for data and monitoring signals will need to deal with the nonlinearity of the device. Therefore, in the next experiments we also focus our attention on other schemes and solutions in order to avoid the problems presented in the simulation.

### 6.1

#### Baseband Embedded OTDR with Baseband Data Signals

In order to evaluate and compare the impact of the BE-OTDR monitoring signal on the data channel, we first evaluate the monitoring system working in the same band as the data channel. Figure 6.1 shows the configuration used in our experiments.

In the experiment, we used a Bit Error Rate Transmitter and Receiver (BER-t/r) that generates and recovers the data signals. In the Central Office (CO), a Tunable Laser Source (TLS) is divided by a symmetric Beam Splitter (BS). One of the branches is directed to an electro-optical Amplitude Modulator (AM) that is driven by the BER-t; the other branch is directed to a Semiconductor Optical Amplifier (SOA) which is synchronously triggered by the output pulse of the OTDR device, generating a 100 ns wide probe pulse.

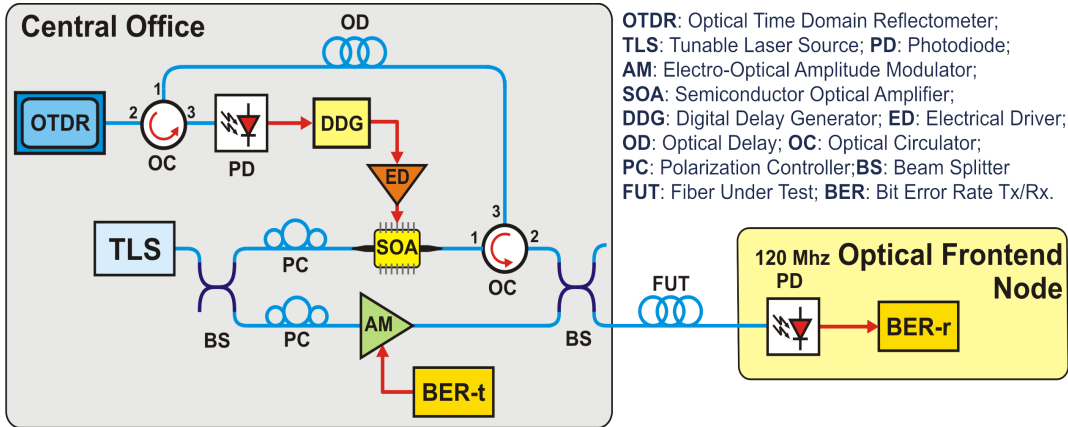


Figure 6.1: Baseband Embedded OTDR with superimposed baseband data signal.

Both branches are combined by a BS and sent to the Photodetector (PD) where the electrical signal is processed by the BER-r. The backscattered light from the Fibre Under Test (FUT) is directed back to the OTDR by two Optical Circulators (OC) and the FUT profile is traced. The bit rate transmitted is 54 Mbps since the PD at the receiver site has a bandwidth of 120 MHz and the highest bit rate is too high for this bandwidth. In order to efficiently perform the transmission of the data signals, we measured the transfer function of the AM. This measurement identifies the region where our data signal should be modulated. Figure 6.2 shows the normalized transfer function of our AM.

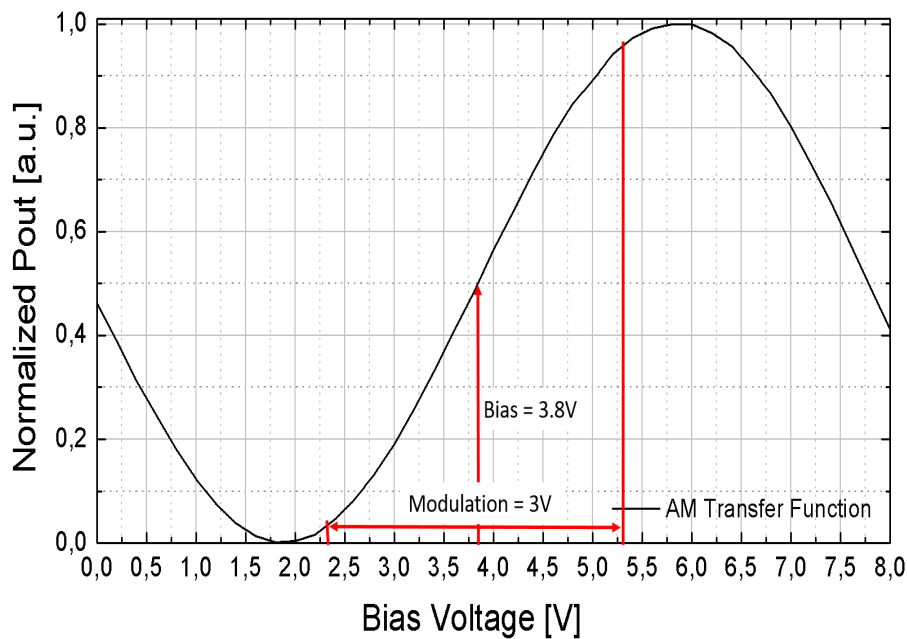


Figure 6.2: Normalized Transfer Function of the Amplitude Modulator.

In order to work in the most linear region of the AM, we use a bias voltage of 3.8 V; the signal is generated by a Pseudo Random Binary Sequence (PRBS) in the BER-t and the peak to peak amplitude of the signal is adjusted to a value of 3 V. The SOA is used as a modulator of the OTDR pulses and it has been characterized by Villafani [68]. Figure 6.3 depicts the measured OTDR trace and BER for different configurations of the data and OTDR signals.

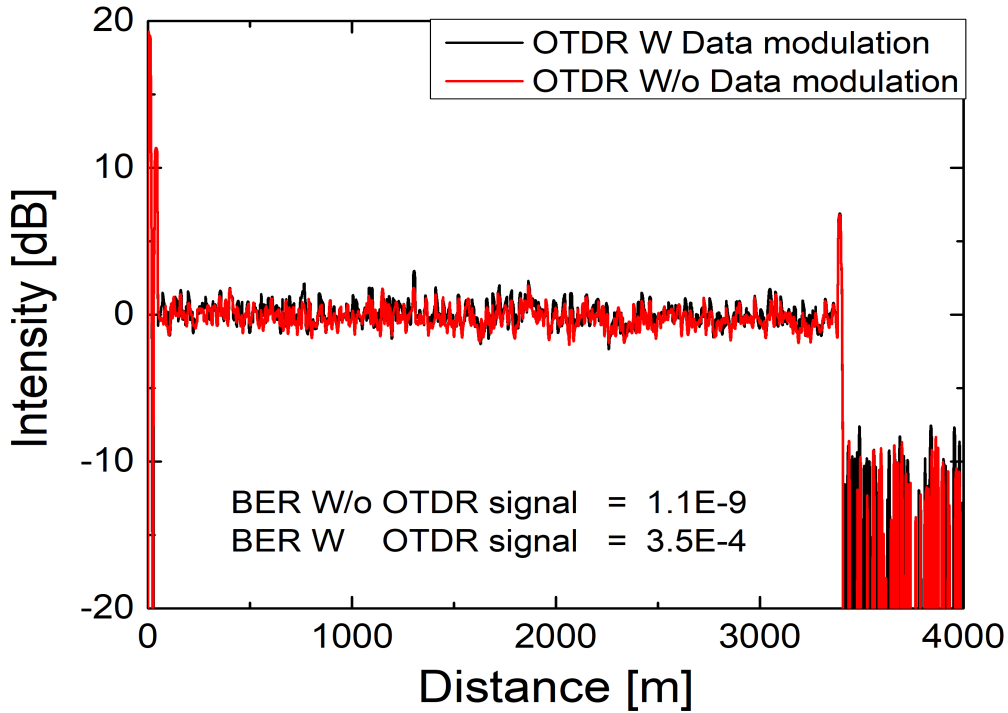


Figure 6.3: OTDR Trace and BER with Superimposed signals.

The Dynamic Range (DR) in our measurements is  $\sim 10$  dB, this because the backscattered light from the data signal is also contributing to the noise floor of the OTDR trace. In the case of an OTDR trace measurement without data modulation, it is important to note that the optical power from the bias voltage is still contributing to the backscattered light and so the noise floor of the system is still the same. Furthermore, it is interesting to note that we can estimate the BER in the system by identifying the frequency of the OTDR pulses. In our OTDR device, a 5 km distance and pulses of 100 ns were configured. During the experiment, we measured the frequency of the OTDR pulses to be a value of 10 kHz. In our OTDR device, a 5 km distance and pulses of 100 ns were configured. Additionally, at a bit rate of 54 Mbps, every bit pulse is  $\sim 20$  ns wide. If we send  $10 \cdot 10^3$  OTDR pulses per second, then,  $50 \cdot 10^3$  data pulses per second are superimposed by the OTDR signal. Considering that 50 percent of the data pulses are "0s", but will be seen as "1s" due to the presence of the OTDR signal, the BER should be  $25 \cdot 10^3 / 54 \cdot 10^6 = 4.63 \cdot 10^{-4}$  that is

approximately the measured value in our experiment ( $3.5 \cdot 10^{-4}$ ). The difference in the measured and estimated BER values can be related to the fact that the OTDR used in our measurement uses bursts of pulses and does not operate all the time, therefore the measured BER is lower than the estimated one.

## 6.2

### Baseband Embedded OTDR with Subcarrier Multiplexed ASK Digital Signal

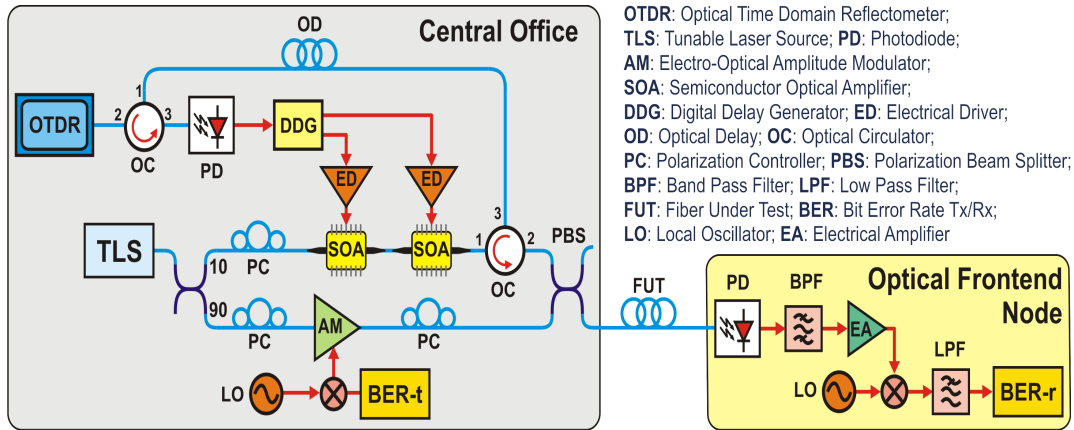


Figure 6.4: Baseband Embedded OTDR with subcarrier multiplexed digital signal.

This experiment was proposed in order to enhance the first system. The idea of using a subcarrier to transport the data channel and the baseband to monitor the signal is investigated. Figure 6.4 depicts the block diagram of our proposed setup; this takes into account both the BE-OTDR system and the Amplitude Shift Keying (ASK) digital data signal upconverted to a subcarrier channel. Notice that we made some modifications to the setup compared to Fig. 6.1. First, we used an asymmetrical BS to divide the TLS signal, and provide a higher power to the data signal. Second, we used a Polarization Beam Splitter (PBS) in order to combine the high and low power branches with orthogonal polarizations such that no coherent interference effects spoil the output optical signal (as it is shown later in the results). Third, we used a tandem configuration of two SOAs which are synchronously triggered by the detection pulse of the OTDR device and generate a 100-ns-wide high peak power probe pulse; the two SOAs are used in order to increase the peak power of the OTDR pulses since the lower power branch of the asymmetrical BS after the TLS is used. Furthermore, this configuration enhances the extinction ratio in the same way as was demonstrated by Herrera et al. [69]. Back-scattered

light from the FUT is directed back to the OTDR device by two OCs and the fibre profile is traced.

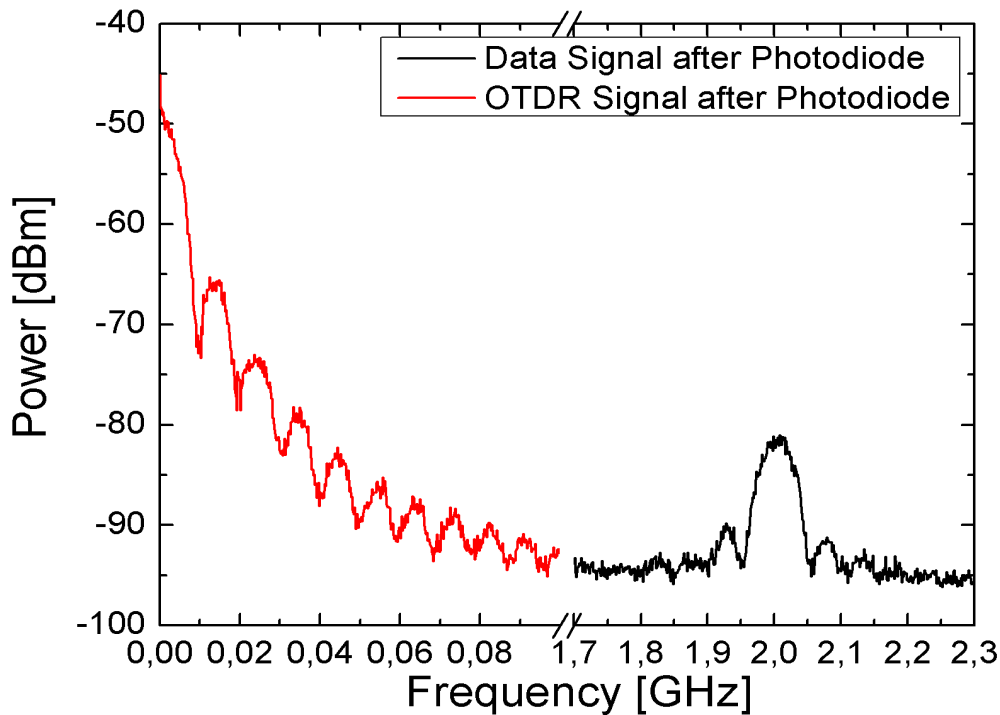


Figure 6.5: OTDR signal (Red) and Digital data signal (Black) received at the OFN PD.

Figure 6.5 depicts the electrical spectrum of the OTDR and digital data signals recovered after the PD in the Optical Frontend Node (OFN). Note that the OTDR and data signals are located in different frequencies and do not superimpose on each other. Using these different frequency bands for monitoring and data transmission enables the system to multiplex additional channels in the vicinity of 2 GHz. This is desired since the goal is often to serve different antenna sectors or different operators with different frequency channels and modulation formats.

### 6.2.1

#### Fibre Monitoring Results and Impact on Data Transmission

Figure 6.6 shows the in-service BE-OTDR monitoring results where two fibre spools, 3.38 and 12 Km respectively, are connected. A DR of  $\sim 12$  dB is achieved and the total link (15.38 Km) is successfully monitored. Although the OTDR drives a high peak power probe pulse, the major limitation on dynamic range is the increased noise floor produced by the Rayleigh backscattering data signal. As explained in the previous experiment, the bias voltage of the data signal is set to a value where the AM is working at the most linear region which

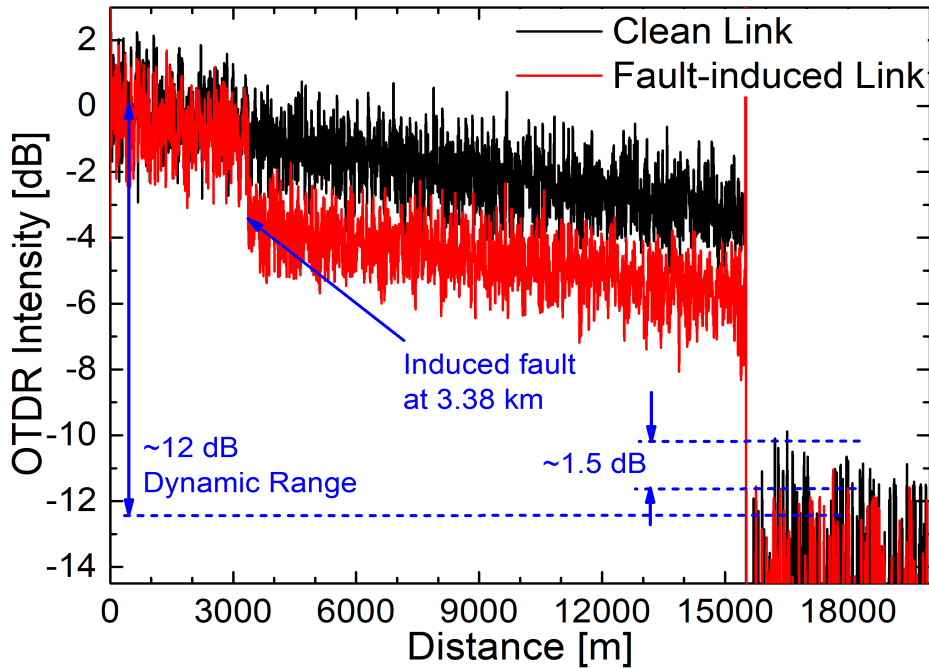


Figure 6.6: OTDR trace with In-service monitoring in the baseband and subcarrier digital signal in 2 GHz.

increases the noise floor. This occurs because the Rayleigh backscattered signal from the data channel is always present in the OTDR measurement. It is also interesting to note that after a 3 dB induced loss, the noise floor is reduced by  $\sim 1.5$  dB which confirms the influence of the data signal on the OTDR trace. It is well known that tuneable OTDR measurements suffer from the noisy contribution due to Coherent Rayleigh Noise (CRN), given that the light sources employed are highly coherent [67, 68]. This effect is also present in Fig. 6.6 and challenges the quantification of the fibre fault loss. More information about the CRN and how to mitigate this noise has been presented by Villafani [68].

In order to assess the impact on data transmission, we used a matched Band Pass Filter (BPF) at the subcarrier frequency. Subsequently, the signal was amplified and downconverted by using a frequency mixer and a Local Oscillator (LO) working in the same frequency and phase as the LO in the CO; the signal was later filtered again by a low pass filter in order to eliminate the higher frequency components. Finally, the signal was received by the BER-r and the BER is determined in the case of simultaneous data transmission and link monitoring.

Figure 6.7 shows the measured impact of the in-service monitoring over the transmitted ASK modulation format. The BER variation in case of simultaneous data transmission plus link monitoring, and when monitoring is

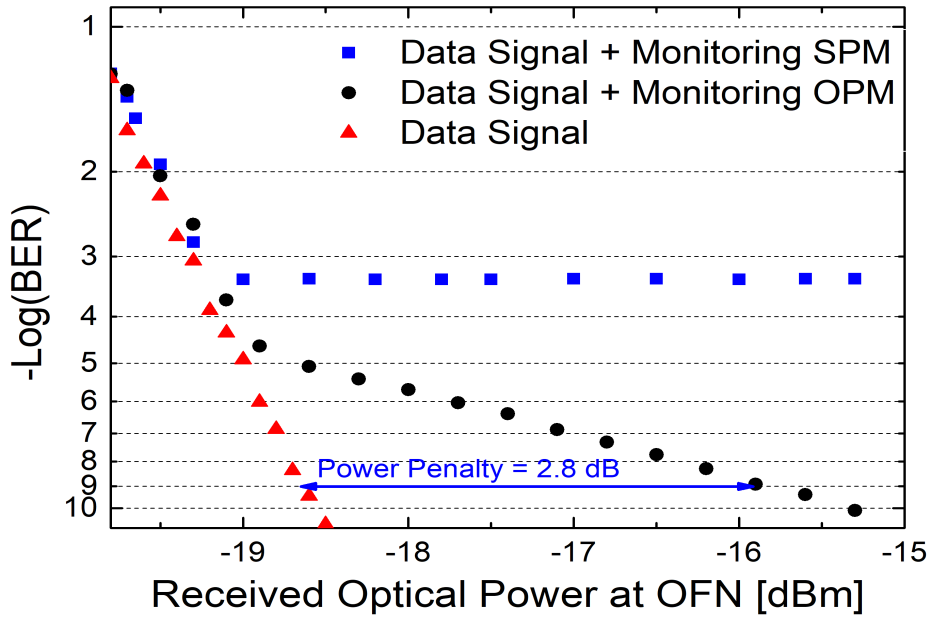


Figure 6.7: Bit error rate for an ASK modulation signal at different received optical powers with and without link monitoring combined in the same polarization mode and orthogonal polarization mode.

turned off, can be observed. In case of in-service monitoring, two curves are shown, one with the combination in orthogonal polarization modes and the other in the same polarization mode. In the case of orthogonal polarization modes, the slope of the curve changes when the received optical power (ROP) is increased, generating a 2.8 dB power penalty at a BER of  $10^{-9}$ . This noise is identified as a typical interferometric effect since it increases proportionally with the ROP. Furthermore, it is the leading source of noise after the ROP reaches -19 dBm. This interferometric effect can be considered to be caused by leakage in the PBS, where the data and monitoring signals are combined in orthogonal polarization modes. Note that the extinction ratio of the PBS is about 20 dB and a high OTDR peak pulse power is used. Therefore, since the polarization combination has been optimized for this measurement, the power penalty measured is the minimum penalty achievable when using a high peak pulse power and a PBS with this extinction ratio. In case of the combination using the same polarization mode, data and monitoring signals fully interfere and all the bits that are transmitted at the same time as the monitoring pulse are lost, giving rise to the observed BER floor at an approximate value of  $-\log(\text{BER})=3.3$ .

## 6.3

## Baseband Embedded OTDR with Subcarrier Multiplexed LTE Signal

To demonstrate the feasibility of the BE-OTDR monitoring in an a-RoF system transporting radio access technologies from the CO to the Radio Head (RH), we included in our experimental demonstration a Long Term Evolution (LTE) signal that carries a 64 Quadrature Amplitude Modulation (64-QAM) Orthogonal Frequency Domain Multiplexed (OFDM) signal with a 20 MHz bandwidth. The measurements using the LTE channel will help us to evaluate the impact on the mobile data subcarrier and the feasibility of the monitoring technique. Furthermore, we enhance our OTDR trace measurements by diminishing the CRN.

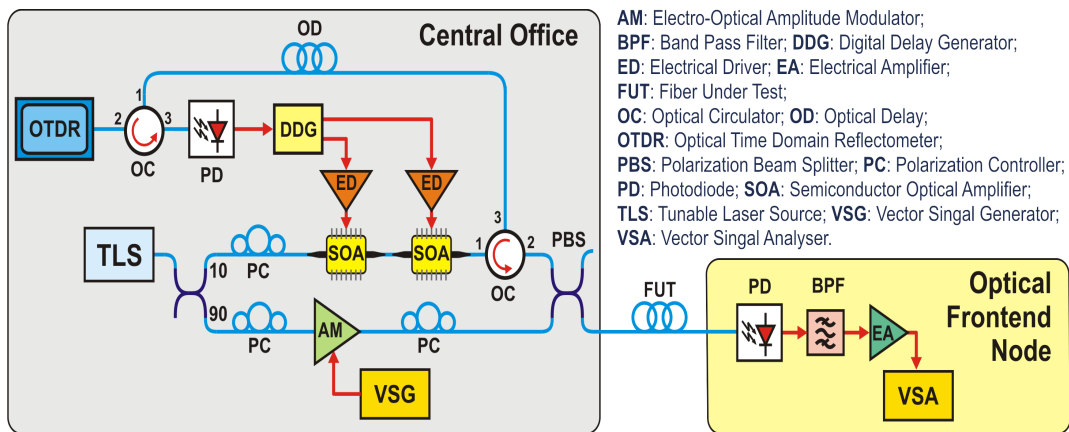


Figure 6.8: Baseband Embedded OTDR with subcarrier multiplexing LTE signal.

We depict, in Fig. 6.8, the block diagram of our proposed architecture; this takes into account both the BE-OTDR monitoring unit and the emulated SCM-PON. To demonstrate the feasibility of the experiment we used a single RF optical subcarrier channel generated in the vicinity of 2 GHz so that the a-RoF signal can indeed directly feed the RH. This subcarrier channel is provided with a 20 MHz bandwidth and carries a 64-QAM mapped LTE OFDM signal. At the CO, a commercial OTDR device was used to simplify data acquisition and signal processing whilst ensuring the embedding of the monitoring unit.

Figure 6.9 shows the frequency spectrum occupied by the BE-OTDR signal and the LTE subcarrier generated in 2.1 GHz, note that the OTDR and LTE signals are located in different frequencies and do not superimpose each other. In the case of an LTE signal, the OFN architecture is rather simple since the detected electrical signal from the photodiode feeds the RH directly. To assess the impact on data transmission, however, we make use of a matched filter at the subcarrier's frequency and measure the Error Vector

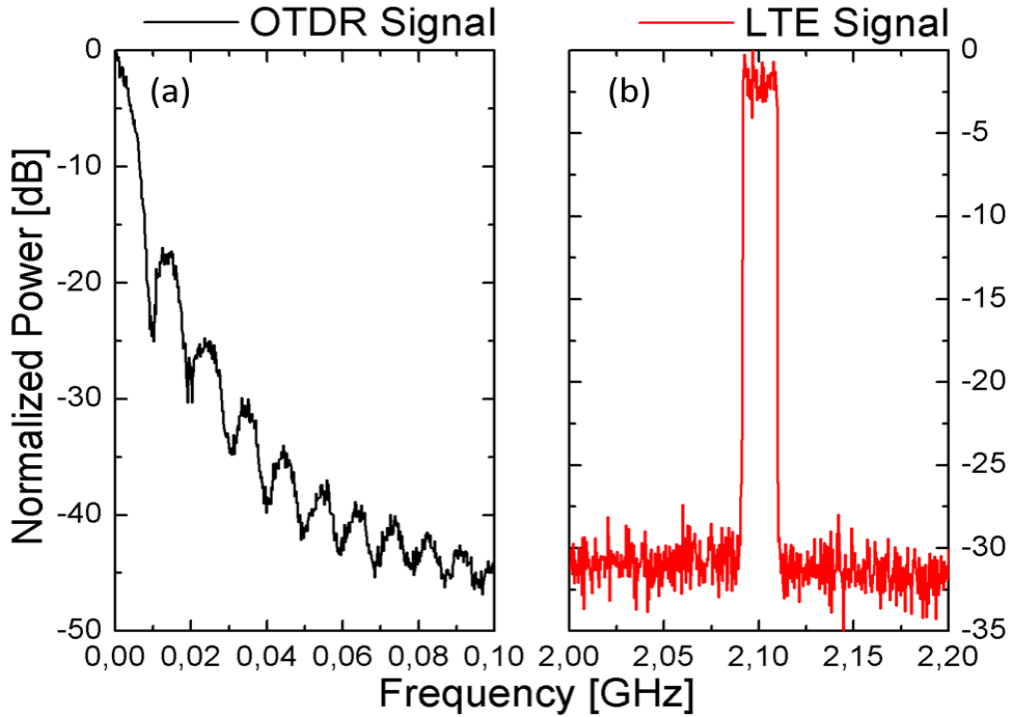


Figure 6.9: OTDR and LTE frequency spectrum.

Magnitude (EVM) in the case of simultaneous data transmission and OTDR link monitoring. To measure the EVM and the IQ constellation, a Vector Signal Generator (VSG) and a Vector Signal Analyzer (VSA) were placed at the CO and OFN, respectively.

### 6.3.1

#### Fibre Monitoring Results and Impact on Data Transmission

Figure 6.10 shows the BE-OTDR monitoring results for a 15.38-km fibre link. By inducing a 3.3 dB fault at 3.38 km, the fault localization capability of the proposed method was tested. A spatial resolution of 10-meters and an 11.5 dB DR are achieved when in-service monitoring was performed. Hence, viability of the monitoring technique is assured for SCM-PON applications. Sweeping the optical source central wavelength within the 0.8 nm-wide DWDM channel has been proposed in order to diminish the CRN of coherent OTDR measurements [70] and was employed throughout our BE-OTDR measurements. Nevertheless, the CRN contribution is higher than for usual tunable OTDRs because the optical data carrier and the OTDR signal share the same optical channel, so that the backscattered power from the optical data carrier also contributes to the overall CRN in the measurement. Note that the sweeping method was not performed in the earlier experiments and it was applied only in this section.

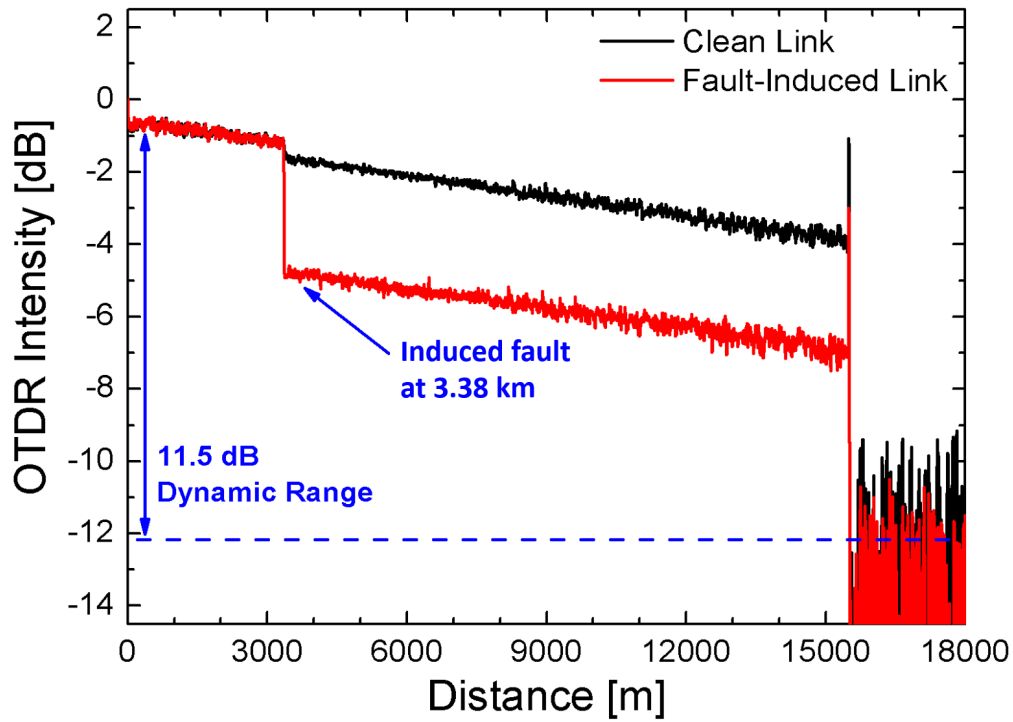


Figure 6.10: In-service embedded OTDR fault localization.

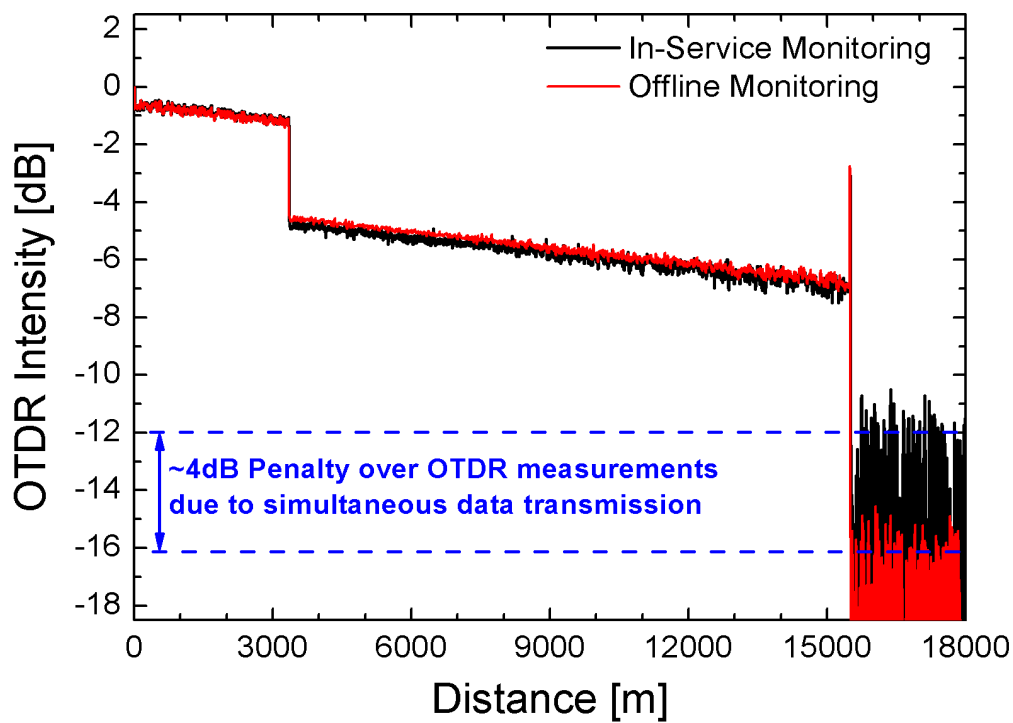


Figure 6.11: Noise Floor Comparison with in-service and offline monitoring.

As we explained in the last experiments, the limitation on the achievable DR comes from the Rayleigh backscattering contribution from the data channel which elevates the noise floor level as depicted in Fig. 6.11, where both

in-service and offline monitoring have been conducted. Note that the excessive noise is not a contribution of the data signal subcarrier, but of the optical carrier that traverses the high-power branch as discussed in the last experiments. Hence, offline monitoring, in the context of Fig. 6.11, involves disconnecting the high-power branch thus eliminating the data optical carrier rather than simply turning off the data stream exciting the electro-optic amplitude modulator.

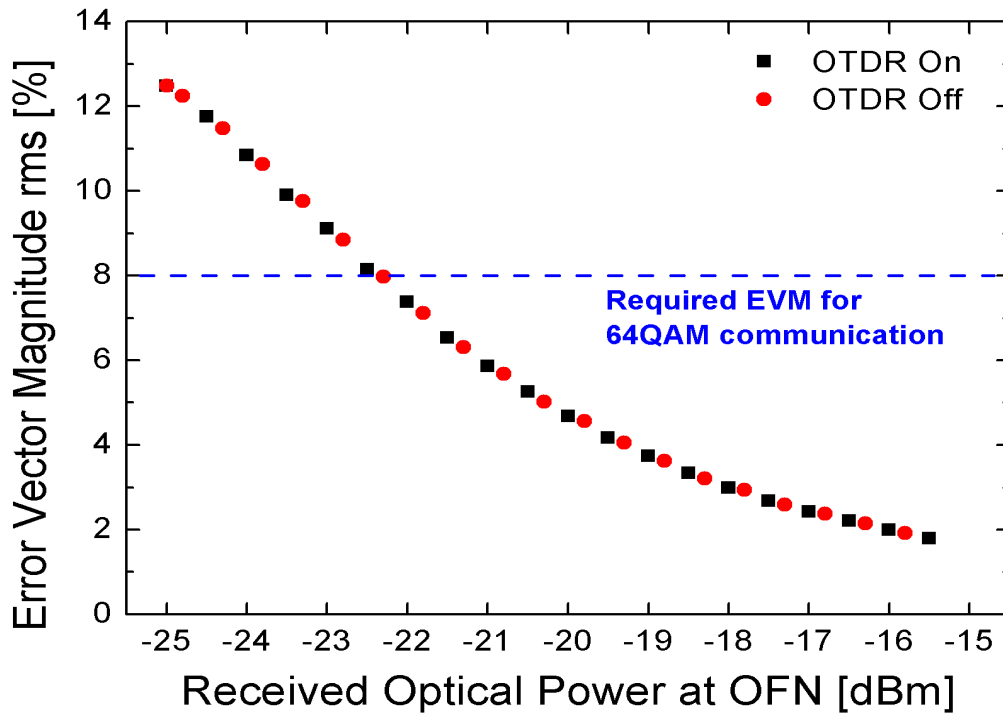


Figure 6.12: Measured Error Vector Magnitude rms value for different Received Optical Powers with and without link supervision.

As for the impact on the transmitted LTE signal, the results of the measured EVM show that negligible penalty is introduced due to in-service monitoring. Figure 6.12 depicts the EVM variation with the received data optical power at the RH measured using the conjunction of VSG and VSA. This measurement was done both for data transmission plus link monitoring and data transmission when the monitoring is turned off. Figure 6.12 also shows the required EVM of 8 percent, which is the minimum requirement of the 3rd Generation Partnership Project (3GPP) for 64-QAM modulation format [71]. The minimum ROP should be higher than -22.3 dBm in order to achieve at least 8 percent EVM.

The orthogonal polarization mode combination at the output of the BE-OTDR system is, as previously commented, mandatory to eliminate coherent effects which can render the data transmission unviable. It is interesting, therefore, to investigate the actual outcomes of the system when both monitoring

and data optical signals are combined in the same polarization mode. In view of that, we measure the LTE signal while keeping the ROP at the OFN at -16 dBm, for which the EVM is close to 2 percent as presented in Fig. 6.12. Figure 6.13 depicts the measured constellation in both cases. In (a), with the signals combined at the PBS into orthogonal polarization modes, the constellation is clean with symbols well separated. In (b), with the signals combined at a regular BS into the same polarization mode, the constellation is fuzzy with overlap between symbols. In the latter case, the data signal quality is severely affected by the monitoring signal and the measured EVM will increase dramatically (up to 12 percent for the presented results of Fig. 6.12).

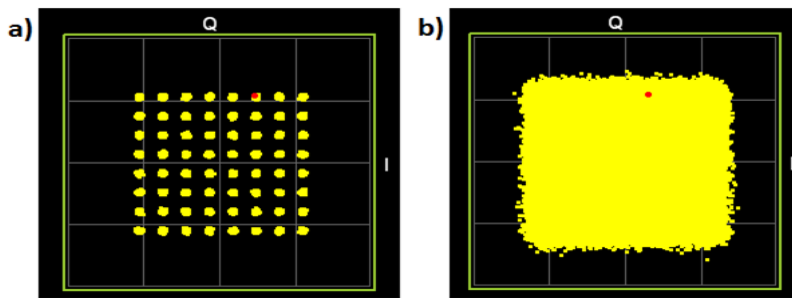


Figure 6.13: Effect of different optical combination schemes on the 64QAM OFN received signal constellation. a) Orthogonal polarization modes; b) Same polarization modes.

## 6.4

### Baseband Embedded OTDR with Subcarrier Multiplexing LTE-A Signal, Electrical Combination and Direct Modulation

In order to reduce the total cost of implementation and the number of devices utilized in our previous experiments, the electrical combination of the data and OTDR signals is proposed. We are also encouraged to use direct modulation in our experiment, since, as was demonstrated in chapter 5, the non-linearity of a Mach-Zehnder Modulator (MZM) will severely degrade the data signal after the linear region is exceeded. Furthermore, in this experiment we use 5 different mobile channels carrying different information over the same optical carrier. Figure 6.14 shows the experimental set-up of our proposed system.

A commercial OTDR device is used as a proof of concept to simplify the signal processing and data acquisition, whereas the OTDR can be replaced by: an electronic control circuit, an Avalanche Photodiode (APD) and a signal processing unit. Different OTDR peak current pulses are used in order to evaluate the system under different conditions. These pulses are generated

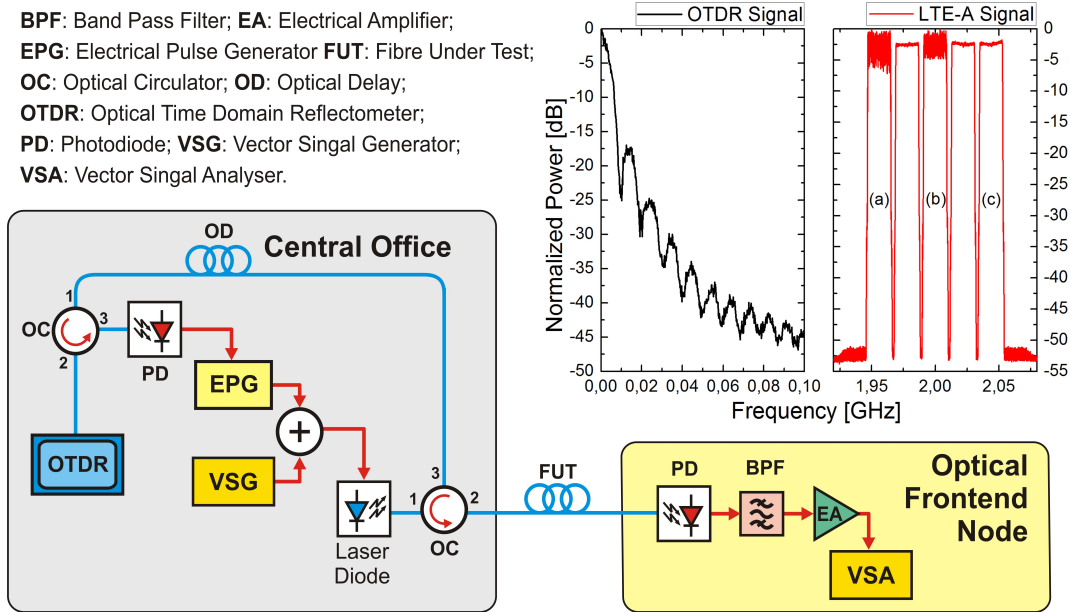


Figure 6.14: Experimental set-up and electrical frequency spectrum.

by the Electrical Pulse Generator (EPG), which is triggered by the OTDR. It is important to notice that in a configuration without the OTDR, the EPG will need to be controlled to send pulses depending on the total fibre distance in order to satisfy the condition that there is only one light pulse traversing the fibre at a time. Moreover, 5 sub-carrier channels are created by using LTE-Advance (LTE-A) Carrier Aggregation (CA) technology, where each component carrier has a 20 MHz bandwidth and are spaced 22 MHz apart, forming an aggregated channel bandwidth of 108 MHz. The central frequency of the CA is 2 GHz so that each component carrier can directly feed a Radio head (RH). In order to directly modulate the laser diode, the multiplexing of the monitoring signal and the CA signal is done by an electrical power combiner where the transmission power of the CA signal is controlled to avoid laser clipping. The electrical spectrum of the combined monitoring and data signal is also shown in Fig. 6.14 where sub-carriers "a", "b" and "c" represent LTE-A test models E-TM 3.3, 3.2 and 3.1 respectively. These test models are used in order to measure the impact of the monitoring signal on different modulation formats. The backscattered light from the Fibre Under Test (FUT) is directed back to the OTDR device by two optical circulators and the fibre profile is traced. To measure the EVM, a VSG and a VSA are placed at the CO and OFN respectively.

### 6.4.1 Fibre Monitoring Results and Impact on Data Transmission

In Fig. 6.15 we present the effect of the OTDR peak current over different modulation formats and transmission powers. Note that the OTDR works with pulse bursts, therefore the EVM is not continuously affected by the monitoring signal and the EVM here is only considered when a burst of OTDR pulses is present. We can observe that by using higher transmission power for the data signal the penalty induced by the OTDR signal is reduced; similarly notice that under intense OTDR peak currents, the EVM of 64-QAM cannot be correctly detected.

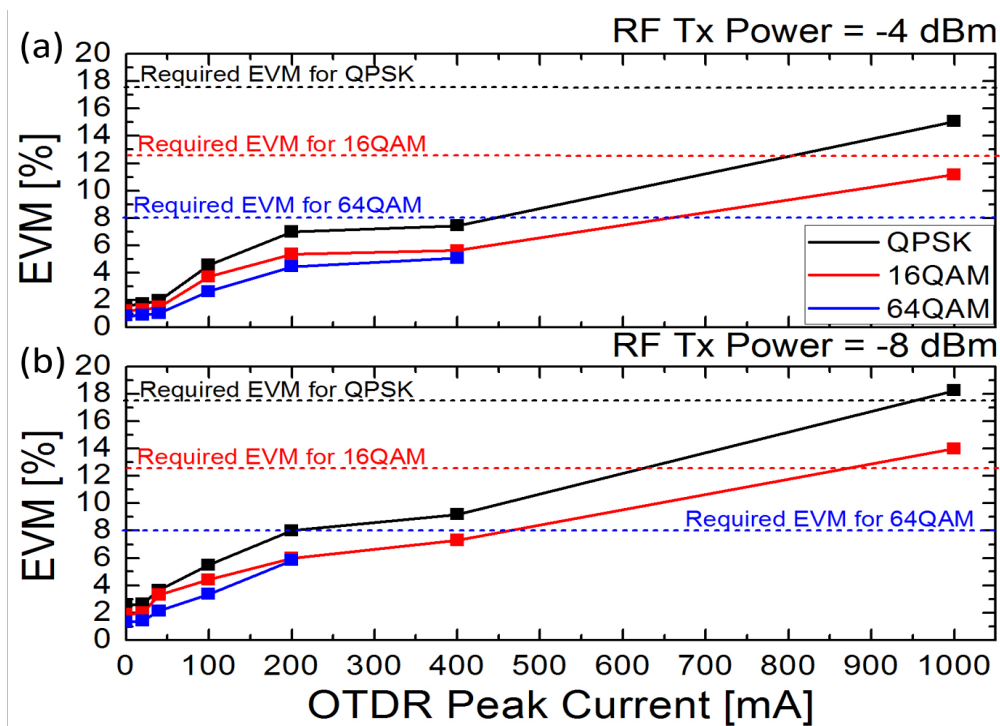


Figure 6.15: Measured EVM for QPSK, 16QAM and 64QAM under different system conditions. The data transmission power is set to a) -4 dBm and b) -8dBm. The required EVM percentages are shown for each modulation format.

Figure 6.16 shows the OTDR traces for different OTDR peak currents and transmission powers. The FUT used includes two fibre spools of 2.6 and 0.86 km respectively with a connector loss of  $\sim 0.5$  dB. The OTDR pulse widths are 100 ns and the measurement is averaged for 5 seconds in order to minimize impact on the data channels. The OTDR trace is degraded by the constant backscattered light coming from the average power of the data signal, thus only OTDR traces that can be distinguished from the noise floor and do not overpass the required EVM (as shown in Fig. 6.15) for each modulation format are shown. The backscattered signal affects the OTDR APD by adding a high

pass filter behaviour to the electric equivalent circuit. This behaviour hinders the DR estimation of in-service measurements. Even under these conditions the monitoring system is capable of localizing the fibre connector loss, since the spatial scale is not affected by the data signal. It is important to notice the trade-off between the EVM and the OTDR traces, e.g., it is not possible to generate an OTDR trace with 100 mA OTDR peak current when the transmission power is set to a value of -4 dBm (Fig. 6.16 a). On the other hand, the required EVM for 64-QAM is surpassed when the OTDR peak current is more than 200 mA and the transmission power is set to a value of -8 dBm (Fig. 6.16 b).

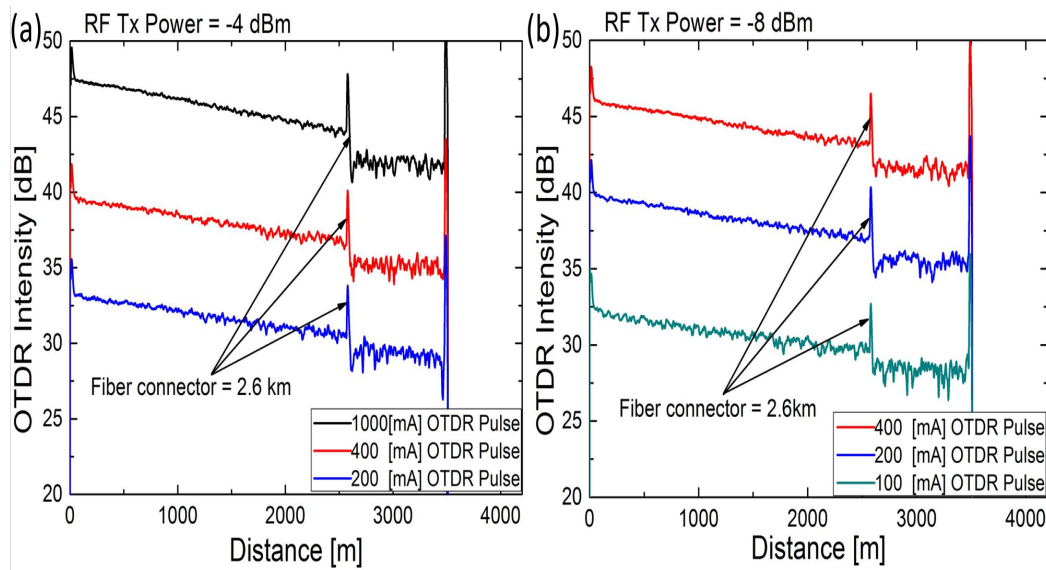


Figure 6.16: OTDR traces for different OTDR peak currents and Transmission Powers. The data transmission power is set to a) -4 dBm and b) -8 dBm. In a), the higher transmission power forces a higher minimum OTDR peak current (200 mA) for the return pulse to be seen. In b) only 100 mA is required.

We also evaluate the possibility of realizing offline OTDR monitoring using the BE-OTDR set-up presented. This is done by turning off the data signal and reducing the bias level of the LD to a minimum value. The resulting OTDR trace is shown in Fig. 6.17 where an induced loss of 11.6 dB was easily localized and quantified. A DR of  $\sim 24$  dB was achieved by using a 100 ns pulse width, a 1000 mA OTDR peak current and a 3 minute averaging time.

In this experiment we have experimentally demonstrated a low-cost BE-OTDR monitoring system for a-RoF systems transporting 5 subcarrier channels using LTE-A technology. The system is capable of in-service localization of fibre faults without surpassing the required EVM when a proper configuration is used. Furthermore, the system detects and quantifies fibre losses when

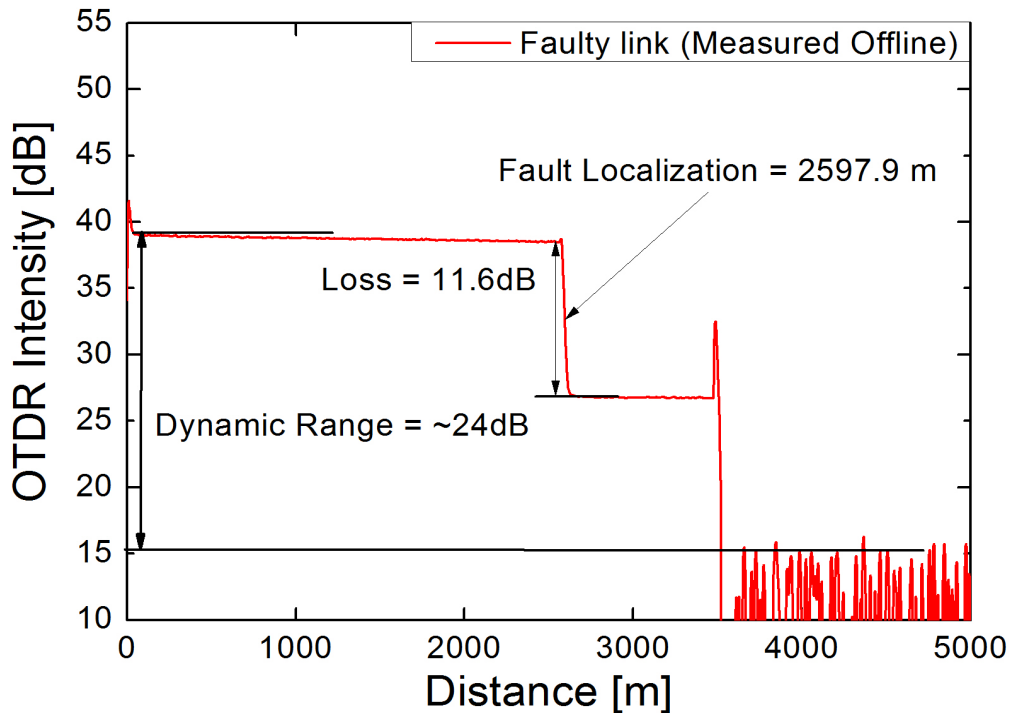


Figure 6.17: Offline BE-OTDR trace with induced loss and fault localization.

an offline measurement is performed; achieving 10 m spatial resolution and a DR of  $\sim 24$  dB. A demonstration video of the experiment was made by the Optoelectronics Laboratory - PUC-Rio [72].

## 6.5 Embedded Multiplexed AMCC and OTDR signal for Analogue Radio over Fibre Systems

In this experiment we experimentally demonstrate the possibility to embed three functionalities in a single optical transmitter: an Auxiliary Management and Control Channel (AMCC), an in-service BE-OTDR, and Long Term Evolution – Advanced (LTE-A) data transmission in MFH section of Radio Access Networks (RAN). The concept is tested based on the previous experiment demonstration. The OTDR and AMCC signals are time multiplexed without interfering with each other or affecting data transmission. The coexistence of the three functionalities is achieved through proper modulation index distribution across the AMCC, OTDR and LTE-A data signals. Furthermore, the monitoring is performed by an EPG, an oscilloscope and an APD; eliminating the commercial OTDR and reducing the total cost of implementation.

The transparent AMCC, that has been discussed and approved for applications in Next Generation Passive Optical Networks 2 (NG-PON2), is needed mainly to convey wavelength assignment and Operation Administration

Management (OAM) data [73, 74]. Recently, it has been used in various proof-of-concept experiments of digital fronthaul [75, 76], typically based on WDM-PON topologies. However, it could also be implemented in a-RoF systems which were studied in chapter 3. The immunity of a-RoF data to the AMCC can be assumed because of the spectral separation of the two signals, but, as shown in the results, there is a tradeoff between the laser linearity and the impact on the a-RoF data.

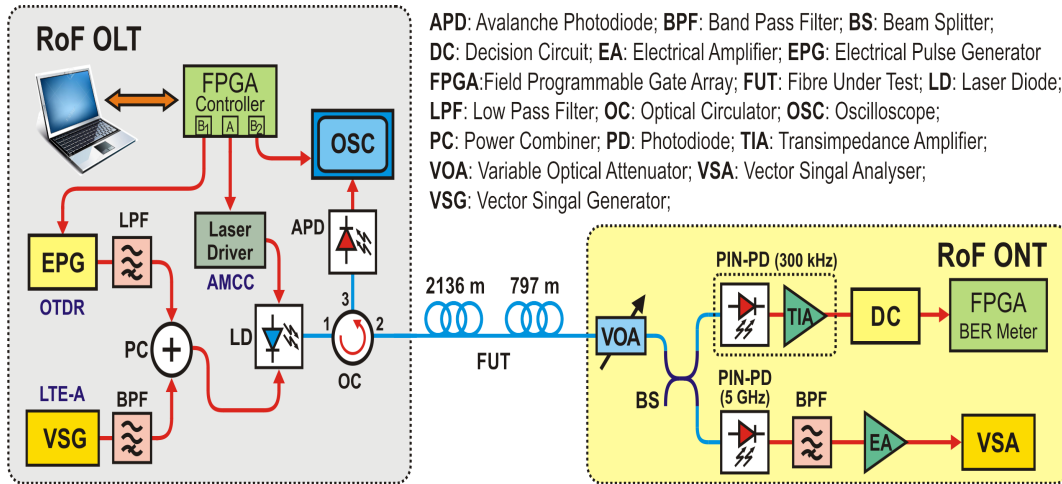


Figure 6.18: Embedded Multiplexed AMCC and OTDR signal for a-RoF.

Figure 6.18 shows the experimental setup of the proposed system where the RoF-Optical Line Termination (OLT) block diagram takes into account the OTDR, AMCC and a-RoF data transmission systems. A Field Programmable Gate Array (FPGA) is used in order to time multiplex the AMCC and OTDR signals, present at output ports “A” and “B1” respectively. The FPGA port “A” is connected to a variable electrical attenuator (Not shown in Fig. 6.18) that is used to control the modulation index of the AMCC signal. Later this is connected to a laser driver for direct modulation of the laser bias. Meanwhile, output port “B1” is used to trigger an EPG that generates OTDR pulses with different peak currents (500, 200 and 100 mA) but with the same pulse width of 100 ns. Note that we are employing the AMCC with baseband overmodulation where the bitrate is 115 kbps with a Non-Return-to-Zero (NRZ) ASK modulation format [73]. The time multiplexing of signals is performed by the FPGA as follows: the FPGA is connected to the computer and receives a 115 kbps Pseudo-Random Binary Sequence (PRBS) data stream, simulating the AMCC data. The data is grouped in packets of 32 bits and 3 bits are added for synchronism. The encapsulated packet of 35 bits is transmitted at 128 kbps as a burst in order to obtain the time required to multiplex the OTDR trigger pulses and make the system transparent to typical

AMCC operation. Every second, we transmit  $\sim 126$  kb ( $115 \cdot 35 / 32$ ) during the first  $\sim 983$  ms leaving  $\sim 17$  ms for the OTDR transmission, as shown in Fig 6.19. Note that in order to increase the AMCC data rate, it is mandatory to buffer 115 kb of data before transmitting. However downstream AMCC messages, as defined by ITU-T [74], are not time-sensitive, therefore this buffering has no impact on the overall system. In addition to the multiplexing, we also include a guard time before and after transmitting the OTDR trigger pulses to guarantee synchronization and that the OTDR signal will not interfere with the AMCC transmission. Fig. 6.19 shows the multiplexed AMCC and OTDR trigger signals at the output ports of the FPGA.

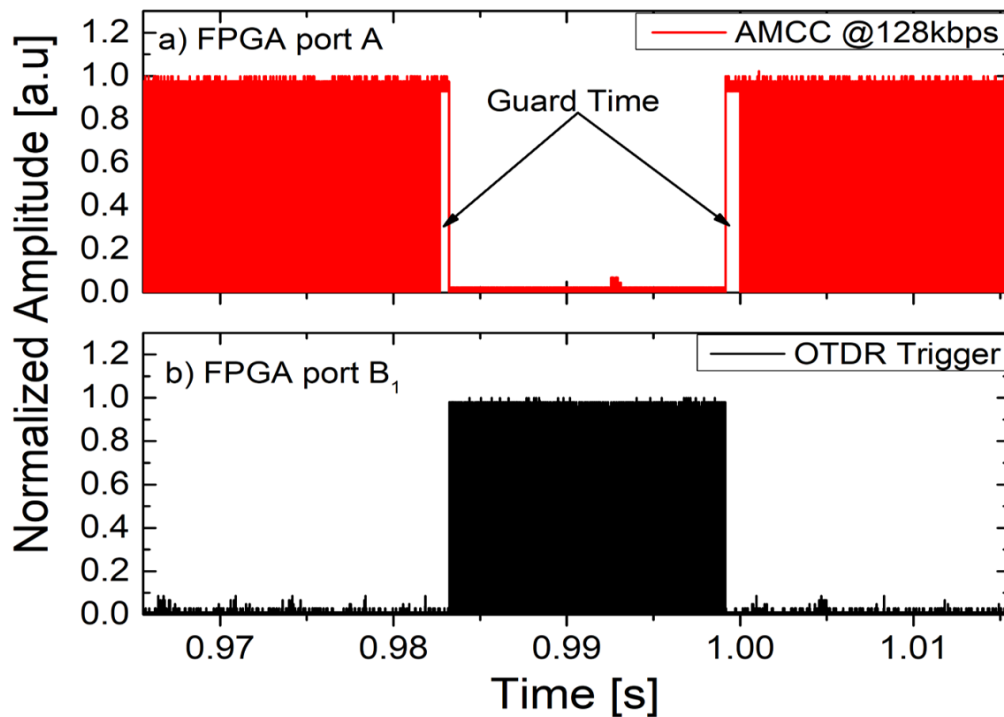


Figure 6.19: Outputs of the FPGA. a) shows the output of port A, the AMCC 128 kbps signal, while b) shows the output of port B, the OTDR trigger pulses. Both plots are zoomed to the 17 ms gap between AMCC signals where the 15.88 ms of OTDR triggers reside.

In this experiment we consider a maximum optical fibre length of 12 km; therefore, the time between two OTDR pulses is set to  $120 \mu\text{s}$  (roundtrip time for 12 km) which allows us to send  $\sim 132$  OTDR pulses between AMCC data streams. The electrical OTDR pulses generated by the EPG are later combined with the LTE-A a-RoF data signal by means of a power combiner. Here, the transmission power of the a-RoF signal is controlled in order to avoid laser clipping. A VSG is used to create three sub-carrier channels by using LTE-A Carrier Aggregation (CA) technology, where each component

carrier has a 20 MHz bandwidth, forming an aggregated channel bandwidth of 60 MHz. The central frequency of the CA is 1945 MHz so that each component carrier can directly feed a RH. Notice that it is possible to extend the total radio bandwidth of the a-RoF system to 5G bandwidth requirements (e.g.  $\sim 800$  MHz), but, when in-service operation, the total modulation index needs to be well distributed between the three functionalities. The resulting modulated optical signal is directed to an OC and transmitted through the FUT, composed of two (2136 and 797 m) standard single mode fibre spools. The same OC is used to direct the Rayleigh backscattering light to an APD, sending the electrical signal to the oscilloscope for data acquisition and signal processing. Synchronized OTDR trace acquisition is guaranteed by using the FPGA port “B2”, which triggers the oscilloscope at the same time that the OTDR pulse is generated in the EPG.

In the RoF-Optical Network Terminal (ONT), the optical received signal is divided across the AMCC and the LTE-A receivers by a BS. The LTE-A signal is recovered with a 5 GHz bandwidth PIN-PD, a BPF and an Electrical Amplifier (EA). The latter is connected to a VSA to measure the EVM, where the test model E-TM 3.1 is used. On the other hand, the AMCC signal is retrieved by a 300 kHz bandwidth PIN-PD, a Transimpedance Amplifier (TIA) and a decision circuit. An FPGA based BER meter was used to evaluate the AMCC data.

### 6.5.1

#### Fibre Monitoring Results and Impact on Data Transmission

The monitoring results and the impact on the data transmission are investigated by analyzing three different performance measurement indicators: the BER of the AMCC signal, the EVM of the LTE-A signal and the OTDR trace. We started by investigating the BER variation for different OTDR peak current pulses, when the AMCC, OTDR and LTE-A signals are transmitted simultaneously. The results are depicted in Fig. 6.20 for different ROP. We can observe that there is no appreciable AMCC BER penalty introduced by the OTDR signal, even when high OTDR peak currents are used. The impact of the LTE-A signal on the AMCC BER was measured and is also negligible.

In order to measure the impact of the OTDR signal on the LTE-A signal and the other way around, we select different laser bias currents to change the available modulation depth of the laser before laser clipping arises. This change affects the OTDR trace, since the backscattered light coming from the laser bias affects the APD of the OTDR, adding a High Pass Filter (HPF) behavior to the electric equivalent circuit as it was demonstrated in the previous section.

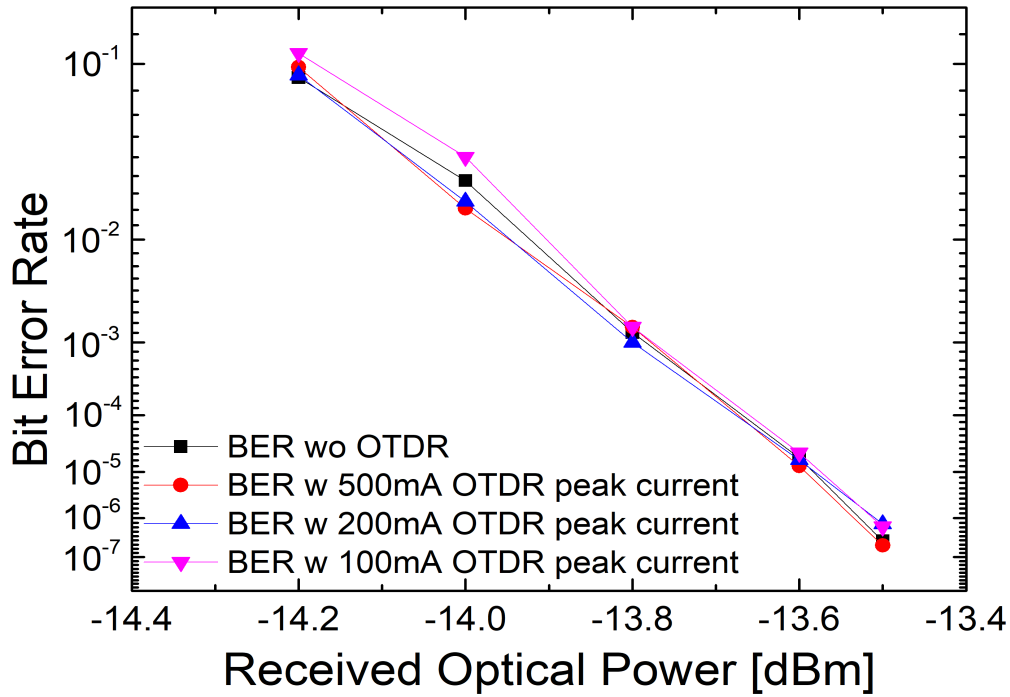


Figure 6.20: AMCC Bit Error Rate measurement with different OTDR peak currents.

In this experiment, the modulation amplitude of the LTE-A signal is increased as we increase the bias level of the laser. Note that the AMCC signal is not being transmitted in this case.

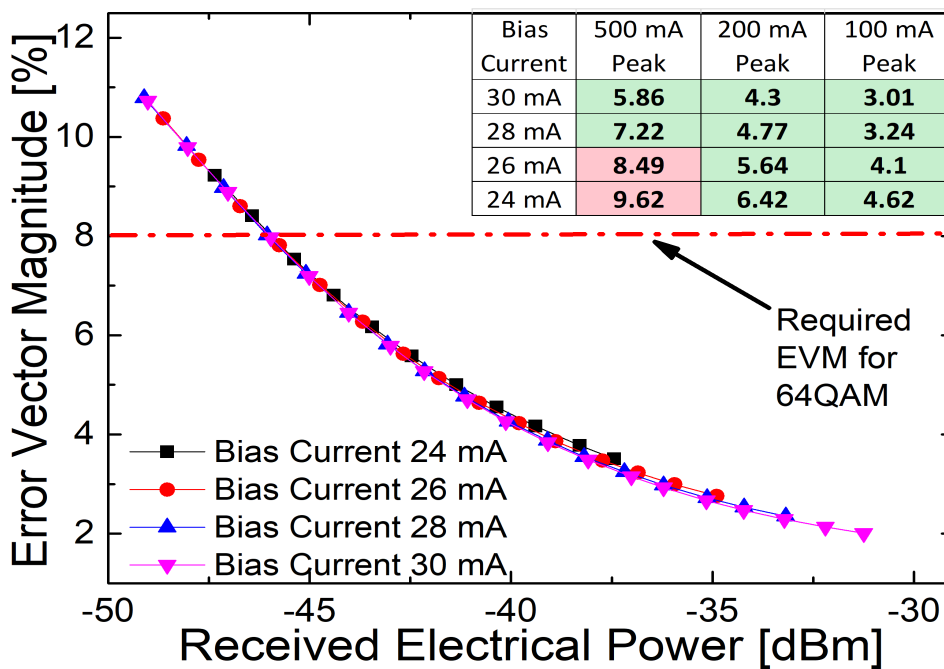


Figure 6.21: Error Vector Magnitude for different bias currents and OTDR peak currents.

Figure 6.21 depicts the EVM curve (measured in the middle channel) for different bias currents and LTE-A amplitude modulations. Here we can observe that the EVM improves with increasing Received Electrical Power (REP) and we obtain a higher REP while we increase bias and amplitude modulation. The REP is measured by the VSA. The EVM is measured by frames of 10 ms and is not a cumulative measurement, consequently during the experiment we noticed that the OTDR signal does not affect the EVM constantly, quite the opposite, it hardly appears in the measurement. This is logical since the pulse width used by the OTDR is 100 ns and we only send  $\sim 132$  pulses in one second transmission, so the probability of an OTDR pulse arriving at the PIN-PD is  $\sim 0.00132\%$ . Therefore, we add an inset table showing the measured EVM when an OTDR pulse arrives at the moment a measurement is occurring. In the table we can observe that only measurements with 500 mA peak OTDR pulses and low modulation bias (24, 26 mA) are above the required EVM level for 64QAM modulation. Note that EVM measurements in the inset table are obtained using the maximum REP for the different bias levels (e.g. for a 30 mA bias current we measure a REP of -31 dBm).

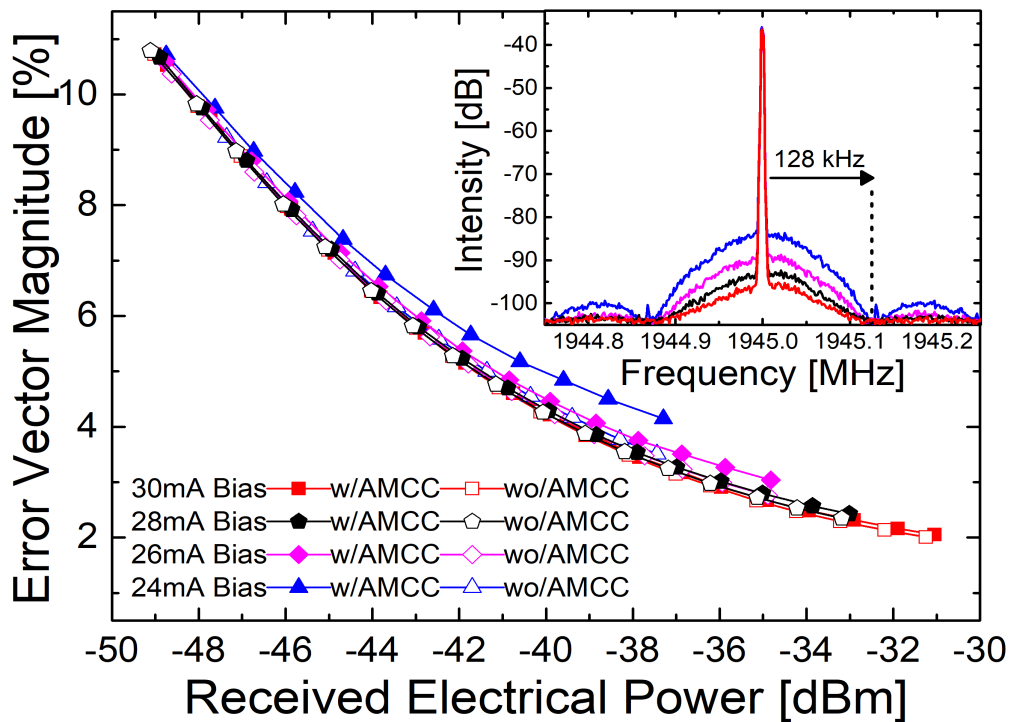


Figure 6.22: Error Vector Magnitude for different bias currents with and without AMCC signal.

Figure 6.22 shows the measured impact of the AMCC signal on the LTE-A signal. The measurement conditions are that the modulation amplitude of the AMCC signal is constant and modulation amplitude of the LTE-A signal

is increased while the laser bias is increased. Note that the total modulation amplitude never surpasses the laser threshold current but there is still a power penalty in the EVM curve when the AMCC signal is connected. This behavior is explained by the laser nonlinearity. Since at low bias, we modulate near to the laser threshold current and the laser nonlinearity up converts the low frequency signal of the AMCC to the 1945 MHz band of the LTE-A signal. This is shown in the inset of Fig. 6.22, where we are using a single tone for the purpose of showing the up converted signal (128 kHz AMCC bandwidth).

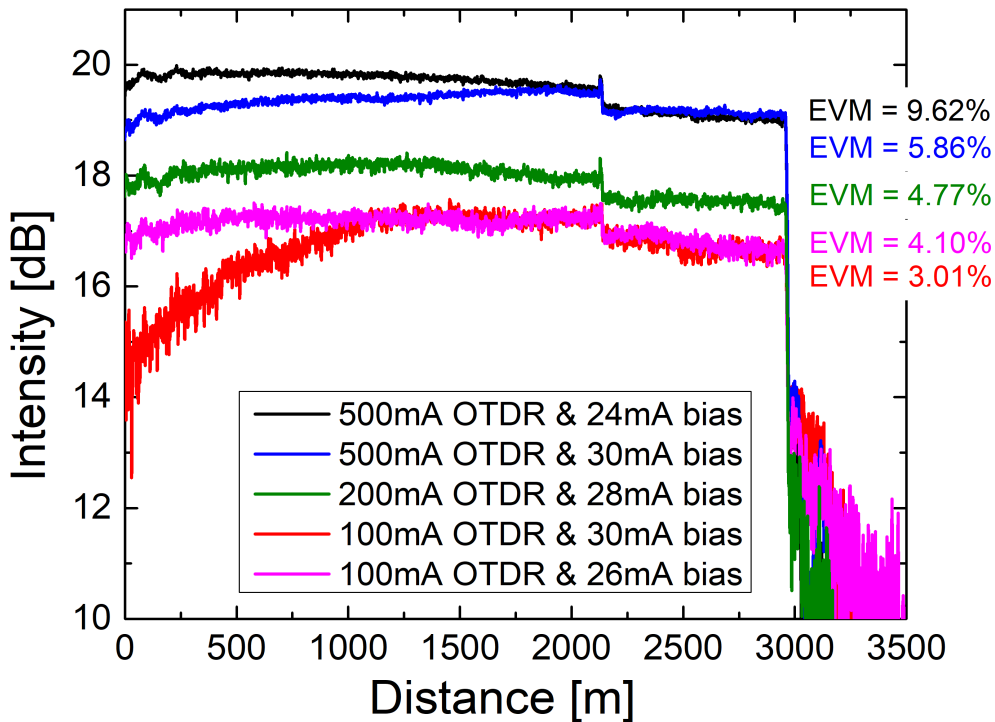


Figure 6.23: Different OTDR traces for different OTDR peak current pulses and different laser bias currents.

Finally, we evaluate the OTDR trace for different OTDR pulses and laser bias currents. Figure 6.23 shows the different OTDR traces obtained with 3 minute measurement times and 100 ns pulse widths. In this measurement we compare five different OTDR traces, where we show the worst and best cases of the EVMs shown in the inset table of Fig. 6.21 (i.e. the case where an OTDR pulse is affecting the measurement by arriving at the moment the measurement is taken).

By comparing the results obtained in these measurements, we can observe that the OTDR trace is affected by two different measurement conditions: the bias level of the laser, that causes the HPF behavior of the APD, contributing to the noise floor of the OTDR trace; and the peak amplitude of the OTDR current pulse, that is fundamental to the OTDR DR and also contributes

to the HPF behavior of the APD when different bias levels are used. Note that although the OTDR trace is distorted by the presence of the data signal transmission, the fault localization is preserved, as it is associated with a high frequency feature (step) and isn't filtered by the HPF characteristics. The best OTDR trace, in terms of DR, is obtained in the case where the lowest bias level (24 mA) and highest OTDR pulses (500 mA) are used, as is shown by the trace with EVM is 9.62%. The worst OTDR trace, in terms of DR, is obtained in the case where the highest bias level (30 mA) and lowest OTDR pulses (100 mA) are used, as is shown by the trace where the EVM is 3.01%. In these cases the EVM reveals the relationship between the OTDR trace and the bias level that can also be observed in the inset table of Fig. 6.21.

It is clear from comparison of the two OTDR traces with 30 mA biases (100 mA and 500 mA OTDR currents), that the HPF behavior is not only a contribution of the laser bias but a combination of the ratio between the laser bias and the OTDR pulse (i.e. by having a lower OTDR pulse current (100 mA) the HPF behavior is far more explicit in the OTDR trace than with a higher pulse current (500 mA) while the laser bias remains fixed). A comparison of the three middle of the road OTDR traces, where the EVMs are equal to 4.1%, 4.77% and 5.86%, as shown in Fig. 6.23, presents the tradeoff between the accuracy of the OTDR traces (that depends on the OTDR current pulse) and the EVM (that depends on the laser bias level and modulation amplitude).

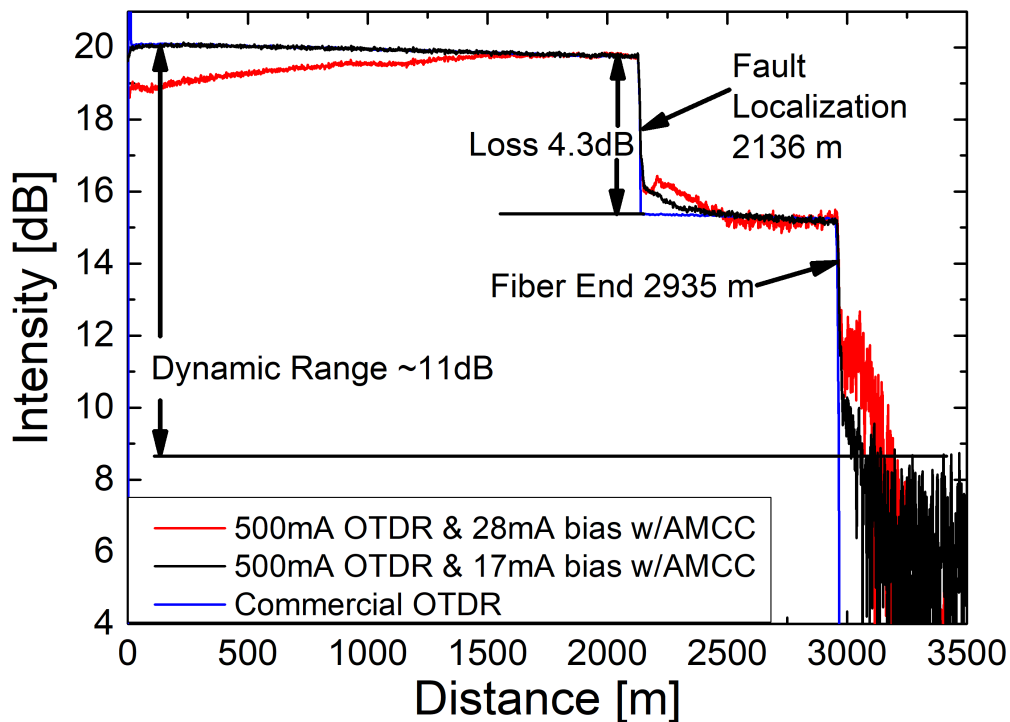


Figure 6.24: OTDR traces for a 4.3 dB induced loss.

Although it is very difficult to measure the DR because of the HPF behavior and the noise contribution of the laser bias, we perform a measurement with an induced loss to approximate the DR of our system. Fig. 6.24 shows the comparison between three OTDR traces where a 4.3 dB loss was induced between the two fibre spools. In the first OTDR measurement, the bias level was set to the threshold level of the laser (17 mA), where we can still transmit an error free AMCC signal. The second OTDR trace was measured with a bias level set to 28 mA, where the worst EVM is 7.22% and the AMCC channel is transmitting. In both cases the OTDR peak pulse current was set to 500 mA. The third OTDR trace was performed with a commercial OTDR (here the FUT is disconnected from the RoF-OLT and connected directly to the commercial OTDR). From Fig. 6.24 we can observe that fault localization is easily achieved by the three approaches. However, the noise contribution from the laser bias and the HPF behavior hinders the calculation of the real induced loss in the first two methods. Here we also measure a peak DR for our method to be a value of 11 dB. This measurement was done in the first (17 mA bias) OTDR trace since the HPF behavior and noise contribution of the laser bias are minimum when the bias is set to the threshold level. We also consider the peak noise after the HPF effects.

We experimentally demonstrated an optical transmitter with three embedded functionalities: AMCC data transmission, LTE-A data transmission and OTDR-based line monitoring. The system is capable of in-service localization of fibre faults without affecting the AMCC data and surpassing the required EVM level of the LTE-A signal when the proper modulation index distribution is applied across the three functionalities. Furthermore, the estimated OTDR DR is 11 dB and the spatial resolution is 10 m. The results showed the possibility of applying the presented concept to a-RoF systems with bandwidths corresponding to 5G requirements, provided that the total modulation index is properly distributed between the three functionalities.

## 7

# Conclusions

This thesis has presented information indicating that optical access networks will be needed in order to provide the capacity and requirements of the 5th generation mobile networks (5G). Furthermore, it is of great interest that a physical layer monitoring system is necessary in order to reduce the capital expenditure and operational expenditure of the system. Therefore, different monitoring systems were presented which provide in-service, rapid and detailed link evaluation while imposing minor additional costs and preserving high data signal quality.

Chapter 2 presented the legacy architectures of optical access networks, more specifically, passive optical networks and the convergence of mobile and fixed access networks by using an hybrid system.

Chapter 3 introduced radio over fibre technology and its use in mobile fronthaul systems. The motivation for using centralized radio access networks was described, followed by the theory of analogue and digital radio over fibre systems and the main differences and benefits of using them. Subcarrier multiplexing, in the context of mobile fronthaul systems combined with radio over fibre, was also presented.

Chapter 4 focused on the theory of optical time domain reflectometry. Furthermore, an overview of different monitoring systems that have been proposed in the literature was discussed. Here we focused our attention on WDM/PON monitoring systems and embedded monitoring systems.

In chapter 5, we presented our first monitoring system idea. We investigated the performance of a subcarrier channel in an SCM/WDM-PON system where the fibre monitoring signal is provided in the baseband of the same optical carrier as used for data transmission. The proposed system was simulated, using the commercial software VPI Photonics Transmission Maker, for 32 WDM channels, each of them transporting 8 subcarriers. The performance evaluation results have shown that with proper configuration the in-service baseband embedded monitoring signals have negligible impact on data transmission. This work has been presented and published by Villafani et al. [60].

In chapter 6, we presented our experimental results. Here we investigated different proposals by focusing on the reduction of costs and providing an

accurate and rapid monitoring while preserving the data signal quality. The experiments were chronologically presented.

Section 6.1 presented the baseband embedded OTDR with baseband data signals experiment. It was based on an optical combination of the monitoring and data signals. The monitoring and data signals were superimposed in the same frequency band and the results showed that data signal quality is spoiled by the monitoring signal.

Section 6.2 presented a baseband embedded OTDR with subcarrier multiplexed ASK digital signal experiment. It proposed subcarrier multiplexing as a solution for the frequency superposition of data and monitoring signals. Furthermore, the first proposed setup was enhanced in order to provide a better dynamic range for the OTDR trace, avoid coherent interference effects and provide a higher optical signal for data transmission. The results showed that the proposed technique achieves  $\sim 12$  dB dynamic range and 10 m spatial resolution. When in-service monitoring was performed, a 2.8 dB power penalty was introduced to the ASK data signal at a bit error rate of  $10^{-9}$ . The OTDR dynamic range suffered an additional penalty due to the constant Rayleigh back-scattered signal from the data optical carrier and, therefore, was lower than would be expected for conventional tuneable OTDR measurements. This work has been presented and published by Villafani et al. [77].

Section 6.3 presented a baseband embedded OTDR with Subcarrier Multiplexed LTE signal experiment. In this section a radio access technology was included in order to evaluate the impact of the monitoring system on the mobile data subcarrier. Furthermore, we enhanced our OTDR trace measurement by diminishing the coherent Rayleigh noise. The results showed that no data power penalty is introduced when in-service monitoring is performed. The proposition of combining data and monitoring signals in orthogonal polarization modes is imperative for the system's viable deployment in an SCM-PON environment. This work has been presented and published by Villafani et al. [77, 78].

Section 6.4 presented a baseband embedded OTDR with subcarrier multiplexed LTE-A signal electrically combined and directly modulated on the laser. In this experiment, the total cost of implementation and the number of devices were reduced by combining the monitoring and data signals electrically and using direct modulation. Furthermore, five subcarrier channels were created by using LTE-A carrier aggregation technology. The system was capable of in-service localization of fibre faults without surpassing the required EVM for different modulation formats when a proper configuration was used. Additionally, the system detected and quantified fibre losses when an offline

measurement was performed, achieving 10 m spatial resolution and a dynamic range of  $\sim 24$  dB. This work has been presented and published by Villafani et al. [79].

Section 6.5 presented the embedded multiplexed AMCC and OTDR signal for analogue radio over fibre systems. In this experiment we demonstrated an optical transmitter with three embedded functionalities: AMCC data transmission, LTE-A data transmission and OTDR-based line monitoring. The monitoring system was time multiplexed with the AMCC data by using a field programmable gate array. Furthermore, the monitoring was performed by an electrical pulse generator, an oscilloscope and an avalanche photodiode; eliminating the commercial OTDR and reducing the total cost of implementation. The system was capable of in-service localization of fibre faults without affecting the AMCC data or surpassing the required EVM level of the radio signal when a proper modulation index distribution was applied. Furthermore, the estimated OTDR dynamic range was  $\sim 11$  dB and the spatial resolution was 10 m. The results showed the possibility of applying the presented concept to a-RoF systems with bandwidths corresponding to 5G requirements, provided that the total modulation index is properly distributed between the three functionalities.

For future works we propose to improve the idea of the embedded multiplexed AMCC and OTDR. This can be done by using the fact that the bit length of the AMCC transmission is around  $\sim 8.5 \mu\text{s}$ . Considering this, we can send an OTDR pulse within an AMCC '1' bit without affecting the receiver decision and at the same time preserving the BER of the system. This needs to be implemented in an FPGA and we also need to verify the OTDR trace performance.

## Bibliography

- [1] DAT, P. T.; KANNO, A.; YAMAMOTO, N. ; KAWANISHI, T.. **5g transport and broadband access networks: The need for new technologies and standards**. In: ITU KALEIDOSCOPE: TRUST IN THE INFORMATION SOCIETY (K-2015), 2015, p. 1–8, Dec 2015.
- [2] METIS. **Metis deliverable d6.6, final report on the metis 5g system concept and technology roadmap**. [https://www.metis2020.com/wp-content/uploads/deliverables/METIS\\_D6.6\\_v1.pdf](https://www.metis2020.com/wp-content/uploads/deliverables/METIS_D6.6_v1.pdf), 2015.
- [3] METIS. **Metis deliverable d8.4, metis final project report**. [https://www.metis2020.com/wp-content/uploads/deliverables/METIS\\_D8.4\\_v1.pdf](https://www.metis2020.com/wp-content/uploads/deliverables/METIS_D8.4_v1.pdf), 2015.
- [4] 5GPPP. **5g ppp, view on 5g architecture**. <https://5g-ppp.eu/wp-content/uploads/2014/02/5G-PPP-5G-Architecture-WP-For-public-consultation.pdf>, 2016.
- [5] FIORANI, M.; MONTI, P.; SKUBIC, B.; MÅRTENSSON, J.; VALCARENGHI, L.; CASTOLDI, P. ; WOSINSKA, L.. **Challenges for 5g transport networks**. In: 2014 IEEE INTERNATIONAL CONFERENCE ON ADVANCED NETWORKS AND TELECOMMUNICATIONS SYSTEMS (ANTS), p. 1–6, Dec 2014.
- [6] METIS. **Metis deliverable d6.4, final report on architecture**. [https://www.metis2020.com/wp-content/uploads/deliverables/METIS\\_D6.4\\_v2.pdf](https://www.metis2020.com/wp-content/uploads/deliverables/METIS_D6.4_v2.pdf), 2015.
- [7] ITU-T. **G.984.1, gigabit-capable passive optical networks (gpon): General characteristics**. <http://www.itu.int/rec/T-REC-G.984.1-200803-I/en>, 2014.
- [8] 802.3, l. **Ieee standard 802.3, epon**. <http://standards.ieee.org/getieee802/802.3.html>, 2014.
- [9] CONSULTING, I.; RESEARCH. **Fttx market report**. <http://www.telecoms.com/files/2009/09/world-fttx-market-ideate200908.pdf>, 2009.

- [10] ITU-T. **G.987.1, 10-gigabit-capable passive optical networks (xg-pon): general requirements**. <https://www.itu.int/rec/T-REC-G.987.1/en>, 2010.
- [11] 802.3AV, I.. **10gb/s ethernet passive optical networks: Ieee p802.3av task force**. <http://www.ieee802.org/3/av/>, 2014.
- [12] ITU-T. **Spectral grids for wdm applications: Dwdm frequency grid. G.694.1**, <http://www.itu.int/rec/T-REC-G.694.1-201202-I/en>, 2012.
- [13] BANERJEE, A.; PARK, Y.; CLARKE, F.; SONG, H.; YANG, S.; KRAMER, G.; KIM, K. ; MUKHERJEE, B.. **Wavelength-division-multiplexed passive optical network (wdm-pon) technologies for broadband access: a review invited**. *J. Opt. Netw.*, 4(11):737–758, Nov 2005.
- [14] ITU-T. **G.989.1, 40-gigabit-capable passive optical networks (ng-pon2): General requirements**. <https://www.itu.int/rec/T-REC-G.989.1-201303-I/en>, 2013.
- [15] MAHLOO, M.; MONTI, P.; CHEN, J. ; WOSINSKA, L.. **Cost modeling of backhaul for mobile networks**. In: 2014 IEEE INTERNATIONAL CONFERENCE ON COMMUNICATIONS WORKSHOPS (ICC), p. 397–402, June 2014.
- [16] STEPHENS, W. E.; JOSEPH, T. R. ; CHEN, B. U.. **Analog microwave fiber optic communications links**. In: MICROWAVE SYMPOSIUM DIGEST, 1984 IEEE MTT-S INTERNATIONAL, p. 533–534, May 1984.
- [17] FIBER-SPAN. <http://www.fiber-span.com>. 2016.
- [18] FOXCOM. <http://www.foxcom.com>. 2016.
- [19] ICIRRUS. **icirrus deliverable 2.1, intelligent c-ran architecture**. <http://www.icirrus-5gnet.eu/wp-content/uploads/2016/02/D2.1-Intelligent-C-RAN-architecture.pdf>, 2015.
- [20] INSTITUTE, C. M. R.. **White paper v.3.0, c-ran the road towards green ran**. <http://labs.chinamobile.com/cran/wp-content/uploads/2014/06/20140613-C-RAN-WP-3.0.pdf>, Dec 2013.
- [21] ITU-T. **Radio-over-fibre (rof) technologies and their applications**. <https://www.itu.int/rec/T-REC-G.Sup55-201507-I/en>, 2015.

- [22] YANG, Y.; LI, F.; LIM, C. ; NIRMALATHAS, A.. **Radio-over-fiber technologies for future mobile backhaul supporting cooperative base stations**. In: MICROWAVE SYMPOSIUM DIGEST (IMS), 2013 IEEE MTT-S INTERNATIONAL, p. 1–3, June 2013.
- [23] OPATIC, D.. **Radio over fiber technology for wireless access**. [https://www.ericsson.com/hr/etk/dogadjanja/mipro\\_2009/12\\_1112\\_F.pdf](https://www.ericsson.com/hr/etk/dogadjanja/mipro_2009/12_1112_F.pdf), 2009.
- [24] JUNG, H. D.; LEE, K. W.; KIM, J. H.; KWON, Y. H. ; PARK, J. H.. **Performance comparison of analog and digitized rof systems with nonlinear channel condition**. IEEE Photonics Technology Letters, 28(6):661–664, March 2016.
- [25] NATHAN J. GOMES, PAULO P. MONTEIRO, A. G.. **NEXT GENERATION WIRELESS COMMUNICATIONS USING RADIO OVER FIBER**. Número 1. John Wiley & Sons, Ltd, 2012.
- [26] AKOS, D. M.; STOCKMASTER, M.; TSUI, J. B. Y. ; CASCHERA, J.. **Direct bandpass sampling of multiple distinct rf signals**. IEEE Transactions on Communications, 47(7):983–988, Jul 1999.
- [27] VAUGHAN, R. G.; SCOTT, N. L. ; WHITE, D. R.. **The theory of bandpass sampling**. IEEE Transactions on Signal Processing, 39(9):1973–1984, Sep 1991.
- [28] CPRI. **Cpri specification version 4.2: Common public radio interface (cpri); interface specification**. [www.cpri.info/downloads/CPRI\\_v\\_4\\_2\\_2010-09-29.pdf](http://www.cpri.info/downloads/CPRI_v_4_2_2010-09-29.pdf), 2010.
- [29] OBSAI. **Open base station architecture initiative: Bts system reference document, version 2.0**. [www.obsai.com/obsai/documents/public\\_documents/download\\_specifications](http://www.obsai.com/obsai/documents/public_documents/download_specifications), 2006.
- [30] LEE, K.; PARK, J. H. ; JUNG, H.. **Comparison of digitized and analog radio-over-fiber systems over wdm-pon networks**. In: 2013 INTERNATIONAL CONFERENCE ON ICT CONVERGENCE (ICTC), p. 705–706, Oct 2013.
- [31] NIRMALATHAS, A.; GAMAGE, P. A.; LIM, C.; NOVAK, D. ; WATERHOUSE, R.. **Digitized radio-over-fiber technologies for converged optical wireless access network**. Journal of Lightwave Technology, 28(16):2366–2375, Aug 2010.

- [32] HADDAD, A.; GAGNAIRE, M.. **Radio-over-fiber (rof) for mobile backhauling: A technical and economic comparison between analog and digitized rof.** In: OPTICAL NETWORK DESIGN AND MODELING, 2014 INTERNATIONAL CONFERENCE ON, p. 132–137, May 2014.
- [33] FAN, Y.; AIGHOBAHI, A. E.; GOMES, N. J. ; XU, K.. **Performance of commercial mimo access point in distributed antenna system with different fiber lengths.** In: MICROWAVE PHOTONICS (MWP) AND THE 2014 9TH ASIA-PACIFIC MICROWAVE PHOTONICS CONFERENCE (APMP), 2014 INTERNATIONAL TOPICAL MEETING ON, p. 17–20, Oct 2014.
- [34] PFEIFFER, T.. **Next generation mobile fronthaul architectures.** In: OPTICAL FIBER COMMUNICATIONS CONFERENCE AND EXHIBITION (OFC), 2015, p. 1–3, March 2015.
- [35] TANENBAUM, A.; WETHERALL, D.. **Computer Networks.** Número 4. Pearson, Boston, USA., 2012.
- [36] B. WILSON, Z. GHASSEMLOOY, I. D.. **Analogue Optical Fibre Communications.** Número 1. The Institution of Engineering and Technology, London, United Kingdom, 2007.
- [37] CHACINSKI, M.; DJUPSJOBACKA, A.; WESTERGREN, U.; SCHATZ, R.; FONJALLAZ, P. Y.; TIPSUWANNAKUL, E. ; UDVARY, E.. **400km transmission of stm-16 data on baseband and dvbt on 40ghz subcarrier.** In: TELECOMMUNICATIONS, 2008. ICT 2008. INTERNATIONAL CONFERENCE ON, p. 1–3, June 2008.
- [38] BRENDDEL, F.; ZWICK, T.; POËTTE, J. ; CABON, B.. **A novel technique for sideband stabilization in the presence of carrier phase noise in rof systems.** In: MICROWAVE CONFERENCE (EUMC), 2012 42ND EUROPEAN, p. 550–553, Oct 2012.
- [39] BRENDDEL, F.; ZWICK, T.; POËTTE, J. ; CABON, B.. **Pll-stabilized optical communications in millimeter-wave rof systems.** IEEE/OSA Journal of Optical Communications and Networking, 6(1):45–53, Jan 2014.
- [40] DERICKSON, D.. **Fiber Optic Test and Measurement.** Número 11. Prentice-Hall Inc., 1998.

- [41] ESMAIL, M. A.; FATHALLAH, H.. **Physical layer monitoring techniques for tdm-passive optical networks: A survey**. IEEE Communications Surveys Tutorials, 15(2):943–958, Second 2013.
- [42] URBAN, P. J.; GETANEH, A.; VON DER WEID, J. P.; TEMPORÃO, G. P.; VALL-LLOSERA, G. ; CHEN, J.. **Detection of fiber faults in passive optical networks**. IEEE/OSA Journal of Optical Communications and Networking, 5(11):1111–1121, Nov 2013.
- [43] K. YUKSEL, V. MOEYAERT, M. W.; MEGRET, P.. **Optical layer monitoring in passive optical networks (pons): A review**. In: 10TH ANNIVERSARY INTERNATIONAL CONFERENCE ON TRANSPARENT OPTICAL NETWORKS, 2008.
- [44] ESMAIL, M. A.; FATHALLAH, H.. **Physical layer monitoring techniques for tdm-passive optical networks: A survey**. In: IEEE COMMUNICATIONS SURVEYS AND TUTORIALS, 2013.
- [45] REN, T. Y.; GANG, S. Y.; CHIONG, T. P.; CHIN, T. T.; SHIEN, Y. K.; LENG, T. K. ; YEN, A. L. L.. **Development and characterization of tunable laser based optical time domain reflectometer**. In: 2011 2ND INTERNATIONAL CONFERENCE ON PHOTONICS, p. 1–3, Oct 2011.
- [46] URBAN, P. J.; VALL-LLOSERA, G.; MEDEIROS, E. ; DAHLFORT, S.. **Fiber plant manager: an otdr- and otm-based pon monitoring system**. IEEE Communications Magazine, 51(2):S9–S15, February 2013.
- [47] AMARAL, G. C.; GARCIA, J. D.; HERRERA, L. E. Y.; TEMPORÃO, G. P.; URBAN, P. J. ; VON DER WEID, J. P.. **Automatic fault detection in wdm-pon with tunable photon counting otdr**. Journal of Lightwave Technology, 33(24):5025–5031, Dec 2015.
- [48] SCHMUCK, H.; HEHMANN, J.; STRAUB, M. ; PFEIFFER, T.. **Embedded otdr techniques for cost-efficient fibre monitoring in optical access networks**. In: 2006 EUROPEAN CONFERENCE ON OPTICAL COMMUNICATIONS, p. 1–2, Sept 2006.
- [49] SCHMUCK, H.; STRAUB, M.; BONK, R.; HEHMANN, J. ; PFEIFFER, T.. **Embedded otdr measurement range extension for future metro-access networks employing in-line soas**. In: 2014 THE EUROPEAN CONFERENCE ON OPTICAL COMMUNICATION (ECOC), p. 1–3, Sept 2014.

- [50] EFFENBERGER, F. J.; MENG, S.. **In-band optical frequency domain reflectometry in pons.** In: OPTICAL FIBER COMMUNICATION/NATIONAL FIBER OPTIC ENGINEERS CONFERENCE, 2008. OFC/NFOEC 2008. CONFERENCE ON, p. 1–3, Feb 2008.
- [51] CHEN, W.; MULDER, B. D.; VANDEWEGE, J.; QIU, X. Z.; BAUWELINCK, J. ; BAEKELANDT, B.. **A novel technique for low-cost embedded non-intrusive fiber monitoring of p2mp optical access networks.** In: OPTICAL FIBER COMMUNICATION AND THE NATIONAL FIBER OPTIC ENGINEERS CONFERENCE, 2007. OFC/NFOEC 2007. CONFERENCE ON, p. 1–3, March 2007.
- [52] VANDEWEGE, J.; QIU, X. Z.; CHEN, W.; D. MULDER, B.; BAUWELINCK, J. ; BAEKELANDT, B.. **Low-cost non-intrusive fiber monitoring in a pon last drop.** In: OPTICAL COMMUNICATION (ECOC), 2007 33RD EUROPEAN CONFERENCE AND EXHIBITION OF, p. 1–2, Sept 2007.
- [53] MITCHELL, J. E.. **Integrated wireless backhaul over optical access networks.** volumen 32, p. 3373–3382, Oct 2014.
- [54] Vpi photonics, <http://www.vpiphotonics.com/Community/Forum/>. 2016.
- [55] SHADDAD, R. Q.; MOHAMMAD, A. B.; AL-HETAR, A. M. ; AL-GAILANI, S. A.. **A novel optical single-sideband frequency translation technique for transmission of wireless mimo signals over optical fiber.** In: 2012 IEEE 3RD INTERNATIONAL CONFERENCE ON PHOTONICS, p. 360–364, Oct 2012.
- [56] YANG, Y.; LI, F.; LIM, C. ; NIRMALATHAS, A.. **Converged fiber-wireless access networks for next generation mobile backhaul enabling comp.** In: 2013 IEEE INTERNATIONAL CONFERENCE ON COMMUNICATIONS WORKSHOPS (ICC), p. 890–894, June 2013.
- [57] Vpi transmissionmaker optical systems user’s manual. May 2014.
- [58] LIGHTWAVE, I.. **Wdm dfb fiber optic source modules.** [http://assets.newport.com/webDocuments-EN/images/79800F\\_Fiber\\_Optic\\_Source\\_Module\\_IX.pdf](http://assets.newport.com/webDocuments-EN/images/79800F_Fiber_Optic_Source_Module_IX.pdf), May 2015.
- [59] ENABLANCE. **Athermal 100 ghz wavelength division multiplex/demultiplexer.** [http://www.enablance.com/technologies/wp-content/uploads/2013/07/Datasheet\\_OCSD\\_AWG\\_Athermal\\_100GHz.pdf](http://www.enablance.com/technologies/wp-content/uploads/2013/07/Datasheet_OCSD_AWG_Athermal_100GHz.pdf), May 2015.

- [60] VILLAFANI, D.; ALMEIDA, R.; URBAN, P.; COSTA, J.; VON DER WEID, J.; CHEN, J.. **Scm/wdm-pon with in-service baseband embedded {OTDR} monitoring**. Optics Communications, 356:250 – 255, 2015.
- [61] AGRAWAL, G. P.. **Fiber-Optic Communication Systems**. John Wiley & Sons, second edition, 2002.
- [62] PROJECT, O.. **Oase project d5.1: Overview of methods and tools**. <http://www.ict-oase.eu/index.php?page=120&>, 2015.
- [63] HUI, R.; O’SULLIVAN, M.. **Chapter 4 - Fiber Optic Measurement Techniques**. Academic Press, Boston, 2009.
- [64] ANRITSU. **Otdr access master mt9083c**. <http://www.anritsu.com/en-GB/Products-Solutions/Products/MT9083C2.aspx>, 2015.
- [65] LEE, D.; YOON, H.; KIM, P.; PARK, J.; PARK, N.. **Optimization of snr improvement in the noncoherent otdr based on simplex codes**. Journal of Lightwave Technology, 24(1):322–328, Jan 2006.
- [66] NASEEM, A.; MEHMOOD, H.; MUHAMMAD, S. S.; ABBAS, S. A.. **Composite coding scheme for otdr snr enhancement**. In: TELECOMMUNICATIONS (CONTEL), PROCEEDINGS OF THE 2011 11TH INTERNATIONAL CONFERENCE ON, p. 321–324, June 2011.
- [67] SHIMIZU, K.; HORIGUCHI, T.; KOYAMADA, Y.. **Characteristics and reduction of coherent fading noise in rayleigh backscattering measurement for optical fibers and components**. Journal of Lightwave Technology, 10(7):982–987, Jul 1992.
- [68] VILLAFANI, D.. **Supervisão de redes ópticas passivas WDM-PON**. M.S. thesis, Dept. Elect. Eng., PUC-Rio Univ., Rio de Janeiro, RJ, Brazil, 2013.
- [69] HERRERA, L. E.; CALLIARI, F.; GARCIA, J. D.; DO AMARAL, G. C.; VON DER WEID, J. P.. **High resolution automatic fault detection in a fiber optic link via photon counting otdr**. In: OPTICAL FIBER COMMUNICATION CONFERENCE, p. M3F.4. Optical Society of America, 2016.
- [70] VILLAFANI, D.; VON DER WEID, J. P.; URBAN, P. J.. **Tuneable otdr measurements for wdm-pon monitoring**. In: MICROWAVE OPTOELECTRONICS CONFERENCE (IMOC), 2013 SBMO/IEEE MTT-S INTERNATIONAL, p. 1–5, Aug 2013.

- [71] 3GPP. **3gpp ts 36.521-1 v. 11.2.0, lte; evolved universal terrestrial radio access (e-utra); user equipment (ue) conformance specification; radio transmission and reception; part 1:conformance testing, release 11.** [http://www.etsi.org/deliver/etsi\\_ts/136500\\_136599/13652101/11.02.00\\_60/ts\\_13652101v110200p.pdf](http://www.etsi.org/deliver/etsi_ts/136500_136599/13652101/11.02.00_60/ts_13652101v110200p.pdf), 2013.
- [72] OPTOELECTRONICS-LABORATORY-PUC-RIO. Available at: <https://www.youtube.com/watch?v=AdaAvsfFaaQ>. 2016.
- [73] ITU-T. **G.989.2 amendment 1, 40-gigabit-capable passive optical networks 2 (ng-pon2): Physical media dependent (pmd) layer specification.** <https://www.itu.int/rec/T-REC-G.989.2-201412-I/en>, 2016.
- [74] ITU-T. **G.989.3, 40-gigabit-capable passive optical networks (ng-pon2): Transmission convergence layer specification.** <https://www.itu.int/rec/T-REC-G.989.3-201510-I/en>, 2015.
- [75] NAKAGAWA, G.; SONE, K.; ODA, S.; YOSHIDA, S.; AOKI, Y.; TAKIZAWA, M. ; RASMUSSEN, J. C.. **Tuneable otdr measurements for wdm-pon monitoring.** In: ECOC 2016; 42ND EUROPEAN CONFERENCE ON OPTICAL COMMUNICATION, 2013.
- [76] YOSHIMA, S.; KATSUMATA, T.; MIURA, H.; NOGUCHI, Y.; NAGASAWA, A.; SUZUKI, N. ; NODA, M.. **Experimental investigation of an optically-superimposed amcc in 100 gb/s coherent wdm-pon for 5g mobile fronthaul.** In: ECOC 2016; 42ND EUROPEAN CONFERENCE ON OPTICAL COMMUNICATION, 2016.
- [77] VILLAFANI, D. R.; HERRERA, L. E. Y.; DO AMARAL, G. C.; URBAN, P. J. ; VON DER WEID, J. P.. **Experimental demonstration of scm-pon monitoring with baseband embedded otdr.** In: 2017 FIBER AND INTEGRATED OPTICS (FIO), 2016.
- [78] VILLAFANI, D.; HERRERA, L.; AMARAL, G.; WEID, J. P. V. D. ; URBAN, P.. **Experimental demonstration of scm-pon monitoring with baseband embedded otdr.** In: 2016 INTERNATIONAL WORKSHOP ON FIBER OPTICS IN ACCESS NETWORK (FOAN), 2016.
- [79] VILLAFANI, D.; HERRERA, L.; URBAN, P. J. ; VON DER WEID, J. P.. **Low-cost embedded otdr monitoring for direct modulation analog**

**radio over fiber.** In: MICROWAVE OPTOELECTRONICS CONFERENCE (IMOC), 2017 SBMO/IEEE MTT-S INTERNATIONAL, 2017.